

THESIS FOR MASTER OF SCIENCES IN NANOSCIENCES

C-CINA  
Biozentrum  
University of Basel

---

# Structural Analysis of Mitochondria in the Context of Parkinson's Disease

---

**Patrick Lattner**

May 13, 2018



## Abstract

The objective of this Master's Thesis was to isolate mitochondria from differentiated LUHMES cell lines and investigate their interaction with oligomeric and fibrillar alpha-synuclein ( $\alpha$ -Syn) on a structural basis by using cryo electron tomography. The background of this work was the pathogenesis of the neurodegenerative Parkinson's disease, which is still vastly unknown. The cellular death of neurons in the substantia nigra, which is the main symptom of the disease, seems to be related to different processes involving  $\alpha$ -Syn and the death of mitochondria. Upon investigating the interaction of mitochondria and oligomeric or fibrillar  $\alpha$ -Syn in the absence of any other cellular influences the intention was to find new evidence or some confirmation of the in vivo and in vitro findings. However, the mere isolation of mitochondria from differentiated LUHMES cells was a new area and has proven to be more difficult than expected. Therefore this Master's Thesis mainly investigates suitable methods to isolate mitochondria from differentiated LUHMES cells. Protocols were successfully developed to isolate mitochondria using either nitrogen cavitation or dounce homogenisation together with differential centrifugation. Cryo electron microscopy was used to obtain images of isolated mitochondria. Nevertheless, the method has to be optimized and further investigations are needed to improve the results. Based on the here developed protocols to isolate mitochondria from differentiated LUHMES cells, future experiments concerning the interaction of  $\alpha$ -Syn and isolated mitochondria may be conducted.

Patrick Lattner *Structural Analysis of Mitochondria in the Context of Parkinson's Disease* University of Basel  
Center for Cellular Imaging and NanoAnalytics (C-CINA)  
May 13, 2018

SUPERVISORS:

Prof. Dr. Henning Stahlberg  
Dr. Thomas Braun

## Acknowledgements

I would like to thank Prof. Dr. Henning Stahlberg and Dr. Thomas Braun for the supervision during my Master's Thesis and the possibility of working in the C-CINA. The work environment was warm and welcoming and beside a lot of freedom on how to conduct my experiments I was motivated to go on with new ideas.

Especially I would like to thank Andrej Bieri. He has introduced me to the equipment and helped me especially in the beginning with new ideas and approaches or with cultivating the cells. Concerning the cultivation of cells I also want to thank Rosmarie Suetterlin for her help with the LUHMES cells and introducing me to the art of cultivating cell.

Furthermore I want to thank Kenneth Goldie and Mohamed Chami for their help with the cryo EM and Carola Alampi for the help with the Spirit EM.

For the fixation of samples I want to thank Christel Genoud from the Friedrich-Miescher Institute and Cinzia Tiberi from the Bio EM lab of the C-CINA for their help. Especially Cinzia helped me a lot and showed me how to fixate my sample, embedding it in agarose and preparing ultrathin sections for the EM.

From the Max Plank Institute of Biophysics I would like to thank Prof. Dr. Werner Kühlbrandt, who agreed to share his time and expertise concerning the purification of mitochondria. From his group I especially want to thank Niklas Klusch and Lea Dietrich for their inputs about the purification. Although the mitochondria I isolated at the MPI with Niklas were from single-celled organism and in a much larger amount present than my LUHMES cells, I gained some valuable insight for a successful purification. Additionally, Lea Dietrich was able to give me new tips and tricks on purifying mitochondria from brain tissue as well as on obtaining suitable cryo grids.

For proofreading my Master's Thesis I also want to thank Raphael Pachlatko, who made sure I didn't overlook grave mistakes in logic or grammar.

Finally I would like to thank all the other people from the C-CINA for the good atmosphere and the continuous support during my Master's Thesis.

# Contents

<b>1</b>	<b>Introduction</b>	<b>1</b>
<b>2</b>	<b>Influence of Mitochondria in PD</b>	<b>3</b>
2.1	MPTP and Rotenone Model of PD and Involvement of Complex I . . . . .	3
2.2	Oxidative Stress and Complex I Deficiency Induced Apoptosis . . . . .	4
2.3	Influence of $\alpha$ -Syn on Mitochondria . . . . .	4
2.4	Influence of $\alpha$ -Syn on the Morphology of Mitochondria . . . . .	7
<b>3</b>	<b>Purification of Mitochondria</b>	<b>9</b>
3.1	LUHMES Cell Line . . . . .	9
3.2	Methods to Purify Mitochondria . . . . .	10
3.2.1	Homogenisation . . . . .	11
3.2.2	Viability of Mitochondria . . . . .	13
<b>4</b>	<b>Material and Methods</b>	<b>14</b>
4.1	LUHMES Cell Line . . . . .	14
4.2	SH-SY5Y Cell Line . . . . .	14
4.3	HEK 293FT Cell Line . . . . .	14
4.4	Isolation Buffers . . . . .	14
4.5	Isolation Using Magnetic Beads . . . . .	15
4.6	Negative Stain . . . . .	15
4.7	On-Grid Gold-Labeling . . . . .	15
4.8	MitoTracker Orange . . . . .	15
4.9	Dot-Blot . . . . .	16
4.10	Cryo Electron Microscopy . . . . .	16
4.11	Sample Fixation . . . . .	16
4.12	Centrifugation . . . . .	17
<b>5</b>	<b>Results</b>	<b>18</b>
5.1	Sonication . . . . .	18
5.2	Potter-Elvehjem Homogenisation . . . . .	22
5.3	Dounce Homogenisation . . . . .	23
5.4	Nitrogen Cavitation . . . . .	37
<b>6</b>	<b>Discussion</b>	<b>45</b>
6.1	Increase in Cell Count . . . . .	45
6.2	Resilience of Differentiated LUHMES Cells . . . . .	45
6.3	Adaptions of Protocol . . . . .	46
6.4	Nitrogen Cavitation and Dounce Homogenisation Show Success . . . . .	48
6.5	Dounce Homogenisation shows large Variance . . . . .	50
6.6	PTA vs UA for Negative Stain . . . . .	50
6.7	On-Grid labelling shows little Results . . . . .	50
6.8	Cryo Electron Microscopy . . . . .	51
6.9	Membrane Potential and Mitochondria Viability . . . . .	51
6.10	Magnetic Bead Isolation . . . . .	52
<b>7</b>	<b>Conclusion</b>	<b>53</b>
<b>8</b>	<b>Outlook</b>	<b>54</b>

## List of Figures

1	Schematic overview of a selection of PD related apoptosis mechanisms. . . . .	5
2	Schematic overview of a selection of PD related $\alpha$ -Syn and mitochondria interactions. . . . .	8
3	Schematic of the used protocol . . . . .	12
4	EM pictures of UA negative stained sonicated differentiated and undifferentiated LUHMES cells. Crude mitochondria sample and percoll purified sample. . . . .	19
5	EM pictures of UA negative stained crude mitochondria fractions with on-grid 5 nm Au-bead labelling against VDAC from differentiated LUHMES cells. . . . .	21
6	Cryo EM pictures of curde mitochondria pellets obtained by sonnicator based homogenisation of HEK 293FT cells. . . . .	22
7	EM pictures of UA negative stained crude mitochondria fractions of dounce homogenizer based isolation from differentiated LUHMES cells (pestle B). . . . .	24
8	Cryo EM and negative stain (UA) EM pictures of the crude mitochondria fractions of dounce homogenizer based isolation from HEK 293FT cells (pestle B). . . . .	25
9	Fluorescent microscope pictures of MitoTracker orange treated crude mitochondria pellets of differentiated LUHMES cell obtained by dounce homogenisation. . . . .	26
10	EM pictures of UA negative stained crude mitochondria fractions of dounce homogenizer and magnetic bead based isolation from HEK 293FT cells. . . . .	27
11	Dot-blot against VDAC of different steps during differential centrifugation based purification of mitochondria from differentiated LUHMES cell homogenate (both pestles). . . . .	28
12	EM pictures of ultra-thin sections (200 nm) from glutaraldehyde fixated crude mitochondria pellets obtained by dounce homogenizer based isolation from undifferentiated LUHMES cells. . . . .	29
13	Dot-blot of the crude mitochondria fractions of dounce homogenizer based isolation from differentiated LUHMES cells (gentle strikes). . . . .	30
14	Cryo EM and negative stain (UA) EM pictures of the crude mitochondria fractions of dounce homogenizer based isolation from differentiated LUHMES cells (gentle strikes). . . . .	31
15	EM pictures of ultra-thin sections (200 nm) from para-formaldehyde and glutaraldehyde fixated and agarose embedded crude mitochondria pellets obtained by dounce homogenizer based isolation from differentiated LUHMES cells (reduced, gentle strikes). . . . .	33
16	Dot-blot, cryo EM and Au-bead labelled negative stain (UA) EM pictures of the crude mitochondria fractions of dounce homogenizer based isolation from differentiated LUHMES cells (pestle A). . . . .	35
17	EM pictures of ultra-thin sections (200 nm) from para-formaldehyde and glutaraldehyde fixated and agarose embedded crude mitochondria pellets obtained by dounce homogenizer based isolation from differentiated LUHMES cells (pestle A). . . . .	36
18	Schematic procedure of differential centrifugation and obtained dot-blot of nitrogen cavitation based homogenisation and differential centrifugation isolation of differentiated LUHMES cells (sample one). . . . .	38
19	Cryo and UA negative stained EM pictures of the crude mitochondria fractions of nitrogen cavitation based isolation from differentiated LUHMES cells (sample one). . . . .	39
20	Schematic procedure of differential centrifugation and obtained dot-blot of nitrogen cavitation based homogenisation and differential centrifugation isolation of differentiated LUHMES cells (sample two). . . . .	40

21	On-grid 5 nm Au-bead (anti mouse and protein A) labelled negative stained EM pictures of the crude mitochondria fractions of nitrogen cavitation based isolation from differentiated LUHMES cells (sample two). . . . .	42
22	Cryo EM pictures of the crude mitochondria fractions of nitrogen cavitation based isolation from differentiated LUHMES cells (sample two). . . . .	43
23	EM pictures of ultra-thin sections (200 nm) from para-formaldehyde and glutaraldehyde fixated and agarose embedded crude mitochondria pellets obtained by nitrogen cavitation based isolation from differentiated LUHMES cells (sample two). . . . .	44
24	Schematic of the developed dounce homogeniser based isolation protocol . . . . .	47
25	Literature results of mitochondria in cryo-EM. . . . .	49

# 1 Introduction

Parkinson's disease (PD) is aside from Alzheimer's disease (AD), Huntington's disease (HD) and Amyotrophic lateral sclerosis (ALS), one of the most prominent neurodegenerative diseases and affects roughly 0.3% <sup>[1][2]</sup> of the total world population and around 1-1.8% of the people over 60 years <sup>[1][3][4][5][6]</sup>. The risk of PD increases with age and leads in its course of disease to the rather selective loss of dopaminergic neurons in the *substantia nigra* (SN) <sup>[7][8][9][10]</sup>, a subregion in the midbrain that plays an important role in movement. This leads to the known symptoms, such as trembling, slowness of movements and loss of balance <sup>[1][6][9]</sup>. Also the occurrence of so called *Lewy bodies* or *Lewy neurites* is an known, however not necessary <sup>[11]</sup>, indicator of PD. <sup>[12]</sup> Lewy bodies are large aggregates composed mainly of lipids and *alpha-synuclein* ( $\alpha$ -Syn), an abundant protein in the brain that accounts for approximately 1% of total protein mass there. <sup>[13]</sup>

However, the molecular mechanism of the neurodegeneration, as well as the spreading of the degeneration through the body and the cause of the disease are still unclear and a matter of debate. There are some known pathways that can trigger PD, such as genetic mutations of certain genes, such as the  $\alpha$ -Syn gene SNCA <sup>[14]</sup>, overexpression of wild type (wt)  $\alpha$ -Syn causing the familial form of PD, <sup>[12][15]</sup> or environmental factors, e.g. neurotoxins like Rotenone or MPP+ <sup>[12]</sup>. But a lot of researches only highlight spot-wise interactions or sometimes even show different results. <sup>[7]</sup> An overview is therefore hard to obtain and it is still likely that some individual diseases with similar symptoms or related pathogenesis are contained in the term PD, rendering a further comparison even more difficult. But on the other hand this would explain the vast amount of different information.

So far, the literature shows different suggestions and possible relations between the findings, where the connection of  $\alpha$ -Syn and mitochondria seem to be of particular importance. One of the most recent hypothesis on how PD is caused is a prion-like propagation of  $\alpha$ -Syn, which leads to its aggregation and formation of  $\alpha$ -Syn oligomers and/or fibres. <sup>[6][7][16]</sup> It is further assumed that these oligomers and fibres can cluster and form Lewy bodies <sup>[17]</sup>, which is consistent with the electron microscopy (EM) findings of fixated, delipidated and air dried human brain samples of PD patients as well as the high  $\alpha$ -Syn concentration found in Lewy bodies. <sup>[6][10]</sup> Additionally, an abnormally high  $\alpha$ -Syn concentration is present in the dopaminergic neurons of PD patients, which is – like the presence of Lewy bodies or Lewy neurites – considered a hallmark of the disease. <sup>[7][18]</sup> Therefore,  $\alpha$ -Syn seems to be one of the most prominent proteins of interest for PD, similar to Amyloid  $\beta$  or Tau for AD.  $\beta$ - and  $\gamma$ -Syn on the other hand do not seem to be involved with PD so far <sup>[14][16]</sup> and the role of the Lewy bodies during the disease is still unknown, such as whether they have a contribution to cellular toxicity or are just a side product. However, the process of the actual neuronal degeneration is not included in this hypothesis so far. Experiments with neurotoxins like Rotenone or N-methyl-4-phenyl-1,2,3,6-tetrahydropyridine (MPTP) gave rise to another hypothesis early on, where mitochondrial dysfunction and oxidative stress are the cause of neuronal death and therefore lead to the pathogenesis of PD. The literature generally agrees that both  $\alpha$ -Syn and mitochondria are essential to the progression and function of PD, although the exact process still remains unclear.

This work aims to investigate the interaction of mitochondria with  $\alpha$ -Syn oligomers and fibrils. Therefore, mitochondria were isolated from Lund Human Mesencephalic (LUHMES) cell cultures. Incubation with  $\alpha$ -Syn oligomers and fibrils followed by structural analysis of the superstructure of the mitochondria by cryo EM and comparison with untreated isolated mitochondria were planned. This would further clarify the interactions between  $\alpha$ -Syn and mitochondria as well as provide a basis to further work with pure mitochondria without the influence of other organelles. However, due to problems purifying the mitochondria, this work merely focuses on the different methods and problems of purifying mitochondria from LUHMES cell lines.

## 2 Influence of Mitochondria in PD

### 2.1 MPTP and Rotenone Model of PD and Involvement of Complex I

Mitochondria are, due to the respiratory chain reaction, a major source of reactive oxygen species (ROS) like superoxide anions and hydrogen peroxide.<sup>[19]</sup> However, they are also very sensitive towards oxidative stress and since neuronal cells in general have a high energy demand they are therefore especially sensitive to mitochondrial dysfunctions.

The idea of the involvement of mitochondria in the PD pathogenesis came up at the end of the 20th century mainly due to neurotoxins like Rotenone<sup>[20][21]</sup> and N-methyl-4-phenyl-1,2,3,6-tetrahydropyridine (MPTP), which inhibit the electron transport chain at Complex I (NADH-ubiquinone oxidoreductase), leading to the same syndromes as PD and which therefore often serve as a model for investigating the disease.<sup>[9][14][20][21]</sup>

MPTP is a metabolite which results in N-methyl-4-phenylpyridinium (MPP<sup>+</sup>) after selective uptake into dopaminergic neurons present in the substantia nigra.<sup>[6][20][21]</sup> After uptake MPP<sup>+</sup> is concentrated in the mitochondrial matrix, resulting in an interruption of oxidative phosphorylation by inhibiting Complex I, which subsequently leads to cell death.<sup>[10][12][22]</sup> However, beside the Complex I inhibition, MPP<sup>+</sup> also seems to meddle with the vesicular dopamine and causes overproduction of ROS.<sup>[23]</sup>

Additionally, Schildknecht et al. (2013)<sup>[13]</sup> has shown that MPP<sup>+</sup> seems to reduce the mitochondrial mobility along the neurites in a LUHMES based experiment. Rotenone on the other hand is a naturally occurring pesticide with high affinity to the Complex I of the respiratory chain. It is the classic Complex I inhibitor and competes with MPP<sup>+</sup> in the binding site in Complex I.<sup>[24]</sup> In contrast to MPTP it can cross the membranes in the brain easily due to its lipophilic character.<sup>[21]</sup>

Such PD models showed that indeed a systematic defect in Complex I of the respiratory chain causes PD and that dopaminergic neurons of the substantia nigra are especially sensitive to this Complex I defects.<sup>[12][21]</sup> Betarbet et al. (2000)<sup>[25]</sup> has shown this selectivity in Rotenone experiments, where Complex I in other brain parts was also inhibited, but only the substantia nigra neurons degenerated.

Interestingly, other tissue from PD patients such as platelets, fibroblasts, muscle, nigral and non-nigral brain show a reduced Complex I activity.<sup>[10][20]</sup> This was also proven by Ana Navarro et al. (2009)<sup>[1]</sup> where she showed that significant mitochondrial dysfunction with oxidative damage also occurs in the human frontal cortex (as well as reduced O<sub>2</sub> uptake and Complex I activity). However, at the same time the mass of mitochondria increased, which most likely is a response of the frontal cortex to compensate the loss of ATP production.<sup>[1]</sup> These results therefore correlate with the PD model of Betarbet et al. (2000)<sup>[25]</sup> and support the selectivity of substantia nigra neuron degeneration.

These findings and models strongly suggest a major role of the mitochondria and especially of the Complex I of the respiratory chain in PD. Additionally the selectivity for the substantia nigra neuronal degeneration is shown here. The important role of the mitochondria is further supported by findings that many of the mutated nuclear genes responsible for the familial forms of PD (PINK1, Parkin, DJ-1, LRRK2) either affect directly or indirectly the mitochondria.<sup>[10][12][14]</sup>



## 2.2 Oxidative Stress and Complex I Deficiency Induced Apoptosis

In almost all  $\alpha$ -Synucleinopathies, meaning neurodegenerative diseases with  $\alpha$ -Syn involvement, mitochondrial proteins and the respiratory chain are affected, where for PD especially the electron transfer and expression of subunits of Complex I of the respiratory chain is disturbed, which further supports the MPTP and Rotenone based model. [1][9][10][12][14] According to said model the catalytic activity in the electron transport chain is lost due to oxidation of the subunits of the complex (oxidative stress) [20] or faulty expression of the subunits. In contrast to Complex I, Complex II-V seemed not to be severely affected. [9] Andreas Bender et al. (2006)[26] showed that there is a high level of mitochondrial DNA (mtDNA) deletion in the substantia nigra of PD patients. Substantia Nigra neurons have a high oxidative capacity and oxidative stress may lead to mtDNA deletion. [26] And since 7 out of 46 subunits of Complex I are coded by mtDNA as well as the mtDNA-encoded subunit to assemble the subunits of the complex, Complex I activity can be impaired by genetic defects in either the mtDNA or the DNA of the other 39 subunits.[9] An impaired ATP production will lead to a loss of the membrane potential of the mitochondria and the formation of more ROS, resulting in oxidative stress, energy depletion and ultimately in cell death.[10][20] The cell death is therefore due to a mitochondria-dependent apoptosis pathway, where Cytochrome c release into the cytosol and the pro-apoptotic protein Bax play key roles.[10][18][27][28] Experiments by Kumar et al. (2016)[18] with PD inducing pesticide (Maneb and Paraquat) co-exposed mice showed that Cytochrome c and  $\alpha$ -Syn co-localize in the midbrain of the mice and form a complex. Originally this would delay apoptosis induction triggered by free Cytochrome c, which is therefore a protective mechanism for the cell. However, Cytochrome c acts as peroxidase in the cytoplasm, due to oxidation or cleavage of a methionine residue by cytoplasmic enzymes, and leads to peroxidase induced protein radical formation. In return  $\alpha$ -Syn radicals could be produced, leading to oligomerization of  $\alpha$ -Syn and further biological effects such as propagation (prion-like) or cellular toxicity. [7][18]

This finding supports the theory of Wallace (2005) [29], which connects ageing with increased PD risk. He postulates that due to the ROS production in mitochondria as a byproduct, the mtDNA can be damaged or altered over the years.[30] This in return can lead to a higher risk of mitochondrial dysfunction, which will lead to apoptosis as mentioned above. Results of Brandt et al. (2017)[30] showed an increased ROS production and decreased respiratory activity in aged fruit flies. Multiple mtDNA transfer experiments from PD tissue [26][31][32] showed a possible dependence of the observed Complex I deficiency on mtDNA alteration.

Further, Bender et al. (2006)[26] showed that a high mtDNA deletion in dopaminergic neurons is associated with a decrease of Cytochrome c oxidase activity (Complex IV), which is a key enzyme within the respiratory chain, causing mitochondrial functional defects such as ROS production.

Together, these findings show that PD related loss of respiratory chain functions in mitochondria can lead to apoptosis, where mainly Complex I deficiency and Cytochrome c release are the important factors. All the mentioned interactions are schematically shown as overview in figure 1.

## 2.3 Influence of $\alpha$ -Syn on Mitochondria

The question remains how  $\alpha$ -Syn, which is proven to be a major player in PD, is related to mitochondrial dysfunction. Kumar et al. (2016)[18] have suggested a radical formation due to the Cytochrome c peroxidase function, as mentioned above, but since this Master's Thesis is focused on the interaction of  $\alpha$ -Syn and mitochondria, some further interactions are worth mentioning.

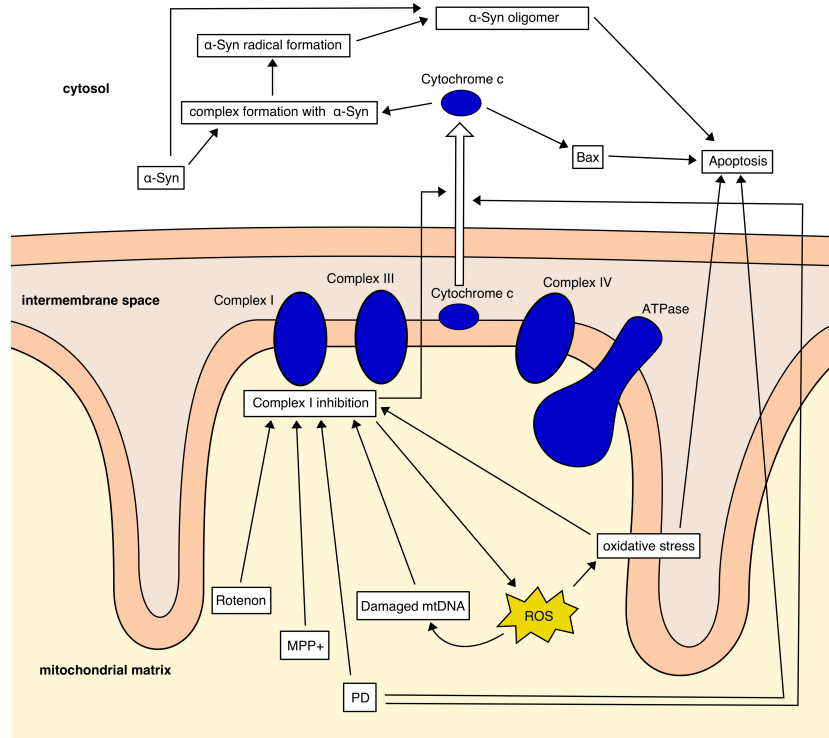


Figure 1: Schematic overview of the literature results about MPP<sup>+</sup> and Rotenone, as well as oxidative stress and their connections to apoptosis, which are mentioned in the chapters 2.1 MPTP and Rotenone Model of PD and Involvement of Complex I and 2.2 Oxidative Stress and Complex I Deficiency Induced Apoptosis. It is to note that the white boxes are not necessarily place specific in this schematic but rather for visualizing connections (e.g. Complex I inhibition has not to take place in the mitochondrial matrix).

$\alpha$ -Syn is predominantly localized in the cytosol [8][12] and therefore it was a long time assumed that it only indirectly interacts with mitochondria. But several studies have recently shown that there seems to be a prominent interaction between  $\alpha$ -Syn and mitochondria, especially with the mitochondrial membrane. [10][33][34] The N-Terminus of the protein contains multiple lysines and because of them binds to the negatively charged lipid membrane. [14][35] However,  $\alpha$ -Syn has specific binding preferences due to the affinity to different lipid-head groups and lipid chain structures, namely acidic phospholipid cardiolipin (CL). [14][35] Interestingly,  $\alpha$ -Syn can change its structure upon binding to the mitochondrial membrane and has the ability to cluster artificially produced liposomes containing CL in the form of intermediate oligomers (but not as monomers or fibrils), as shown by Nakamura et al. (2011)[14].  $\alpha$ -Syn accumulation, and pathological aggregation to oligomers, can lead to problems with dopamine release [7], which could be related to the artificial liposome model and therefore also vesicle clustering. Additionally,  $\alpha$ -Syn seems to prefer the mitochondrial membrane over other membranes like the endoplasmic reticulum, [12][14][16] and also associates with the inner mitochondrial membrane of human dopaminergic neurons (containing more CL than the outer membrane [14]), causing inhibition

of the Complex I, similar to MPP<sup>+</sup> or Rotenone toxicity. [12][17] In vitro studies of Banerjee et al. (2010)[8] on isolated rat brain mitochondria with recombinant human  $\alpha$ -Syn showed indeed a loss of phosphorylation capacity and a transmembrane potential loss, but no significant effect of  $\alpha$ -Syn on the respiratory chain complexes. Interestingly, Li et al. (2007)[33] have shown that for dopaminergic (and other  $\alpha$ -Syn positive) mouse neurons  $\alpha$ -Syn is present on the outer mitochondrial membrane, whereas Devi et al. (2008)[34] showed a predominant affinity of  $\alpha$ -Syn to the inner mitochondrial membrane in a human system. Still, most studies agree on an inhibitory effect of  $\alpha$ -Syn on the oxidative phosphorylation and an increase in oxidative stress. [17]

In contrast to the seemingly negative effect of  $\alpha$ -Syn, Ludtmann et al. (2016)[16] have shown a positive interaction of unfolded, monomeric  $\alpha$ -Syn and the subunit  $\alpha$  of the ATPase within the mitochondria of cortical and mid-brain neurons as well as of glyca cells in mice brains. Deficiency of  $\alpha$ -Syn leads to a lower ATPase efficiency and a lower ATP level.

Rostovtseva et al. (2015)[17] conducted studies of the voltage dependent ion channel (VDAC) of rat liver mitochondria in vitro which revealed an interaction of monomeric  $\alpha$ -Syn with VDAC that result in a reversible blockage of the channel as well as the possible translocation of  $\alpha$ -Syn through VDAC. A subsequent yeast experiment also showed a dependence of  $\alpha$ -Syn toxicity on VDAC1.

Devi et al. (2008)[34] have also shown that the N-terminal 32 amino acids of human  $\alpha$ -Syn contain a mitochondrial targeting signal, which allows accumulation of the wild type protein in human dopaminergic neurons, where they reduce the Complex I activity and increase ROS production. Their experiments showed a constitutive presence of  $\alpha$ -Syn in the mitochondria of the substantia nigra, the striatum, and the cerebellum of normal human brains. For PD human brains the  $\alpha$ -Syn accumulation and decreased Complex I activity in the substantia nigra were significant. [14] Further experiments in vivo and in vitro showed indeed an association of  $\alpha$ -Syn with Complex I. For the translocation into the mitochondria a channel is necessary [34], which correlates with the VDAC findings of Rostovtseva et al. (2015)[17]. The experiments of Devi et al. (2008)[34] further showed that the inhibition of Complex I (but not of the other complexes of the respiratory chain) is concentration dependent. It also seems that the localisation to the inner mitochondrial membrane is in some cases increased with higher  $\alpha$ -Syn expression.[14] Other studies support concepts where specifically aggregated  $\alpha$ -Syn is able to induce a Cytochrome c release, leading to apoptosis, [7][10] which would be more along the line of the prion-hypothesis of  $\alpha$ -Syn. Furthermore it has been found that the mitochondrial membrane can be permeabilized by oligomeric  $\alpha$ -Syn. [7]

In LUHMES cell based experiments with MPP<sup>+</sup> Stefan Schildknecht et al. (2013)[13] has shown that there seems to be an interaction between  $\alpha$ -Syn and MPP<sup>+</sup>, where a knockdown of  $\alpha$ -Syn decreased the toxicity of MPP<sup>+</sup>. This finding is consistent with results on dopaminergic mice neurons of Dauer et al. (2002)[36] and Klivenyi et al. (2006)[37].

In conclusion, these findings suggest that  $\alpha$ -Syn can selectively enter mitochondria and accumulate on the inner membrane. Interactions with VDAC was also reported, which to some degree could explain the translocation to the inner mitochondrial membrane. There,  $\alpha$ -Syn seems to interact with Complex I of the respiratory chain which inhibit oxidative phosphorylation and leads to oxidative stress in a concentration dependent manner. For PD patients, this accumulation in the substantia nigra and the decrease of Complex I activity were high. Oligomerized  $\alpha$ -Syn leads to increased Cytochrome c release and membrane permeabilization, which ultimately leads to apoptosis.

## 2.4 Influence of $\alpha$ -Syn on the Morphology of Mitochondria

Fusion and fission of mitochondria occur on a constant frequency. This process is fundamental to exchange mitochondrial genome and maintain a functional respiratory activity. With in vivo experiments with Purkinje cells in mouse brains Chen et al. (2007)<sup>[38]</sup> has shown that absence of mitochondrial fusion leads to impaired respiratory complex activity and defects in the inner membrane structure, as well as a loss of mtDNA nucleotides. Additionally, the distribution of mitochondria within the neurons are disturbed.

Rotenone and MPP<sup>+</sup> also induce mitochondrial fission, besides interfering with Complex I of the respiratory chain. <sup>[10]</sup> PINK1 (mitochondrial kinase) and Parkin (mitochondrial binding protein), both PD-related proteins <sup>[12]</sup>, both seem to regulate mitochondrial fusion and fission, therefore controlling the mitochondrial morphology. <sup>[10][12]</sup> Both proteins are major components of the mitophagy pathway. <sup>[19]</sup>

Fragmentation of mitochondria, meaning exaggerated fission, occurs if  $\alpha$ -Syn is overexpressed in vitro <sup>[12]</sup>. Experiments on HeLa cells transfected with human wt  $\alpha$ -Syn of Nakamura et al. (2011)<sup>[14]</sup> showed a reduction of length, perimeter and area of mitochondria as well as an increase of mitochondrial fragments per cell, however, there was no significant morphological alteration of other organelles – such as the endoplasmatic reticulum – meaning the effect is specific for mitochondria. Fragmentation and disordered cristae were observed with enlarged intermembrane space in vitro (transfected HeLa) as well as in vivo (midbrain neurons of transgenic mice). However, they also showed that despite high fragmentation the membrane potential remained normal and no superoxide increase was observed for 24 hours. However, after 48 hours, the respiration decreased and cell death increased. Nakamura et al. (2011)<sup>[14]</sup> additionally has shown that the fission is Drp1 <sup>1</sup> independent and needs a direct interaction of  $\alpha$ -Syn and the mitochondria. The effect of mitochondrial morphology therefore could contribute to the neuronal degeneration.

Experiments of Menges et al. (2017)<sup>[19]</sup> have shown the formation of so called mitospheres (spherically shaped and hyperpolarized mitochondria) as a special kind of mitochondrial fragmentation due to induced oxidative stress in neurogliome cells and LUHMES cell cultures. This fission is Drp1 dependent and leads to reduced mitochondrial activity and enhanced apoptosis, but not via Parkin-related mitophagy.  $\alpha$ -Syn indeed seems to prevent this fragmentation into mitospheres and therefore the following apoptosis, suggesting a protective function during oxidative stress.

In vivo  $\alpha$ -Syn also seems to alter the mitochondrial morphology, as Lee et al. (2006)<sup>[39]</sup> showed in mice brain overexpressing the human A53T mutant  $\alpha$ -Syn, where a subset of mitochondria of the spinal cord and the brainstem cells were shrunk or swollen. However, the effects vary and a common denominator has yet to be found. <sup>[12]</sup> An interesting question is how and if physiological concentrations of  $\alpha$ -Syn have an influence on mitochondrial dynamics.

Considering the effect of ageing, for which mostly mitochondrial dysfunction appears responsible, and which is related to higher ROS production, ultrastructure and function experiments of mitochondria in mouse and *D. Melanogaster* of Brandt et al. (2017)<sup>[30]</sup> have shown a link between the inner membrane architecture and the functional decrease. Since the oxidative phosphorylation is also responsible for the shape of the inner membrane and therefore the cristae of the mitochondria, oxidative damage and respiratory dysfunction may influence the superstructure of the mitochondrial inner membrane. Davies et al. (2012)<sup>[40]</sup> showed for example in a yeast model a morphological change of the cristae due to faulty ATP-synthase assembly. Therefore a possible  $\alpha$ -Syn effect onto the respiratory chain could also lead to morphological changes of mitochondria in the brain.

<sup>1</sup>DRP+: Protein normally responsible for mitochondrial division

In conclusion,  $\alpha$ -Syn seems to have an specific interaction with mitochondria with significant morphological alterations, whereby it can cause fragmentation if highly concentrated as well as disordered cristae (Nakamura et al. (2011)<sup>[14]</sup>) which lead to increased cell death. Also mutated forms of  $\alpha$ -Syn seem to have an effect on the mitochondrial morphology. Influence on the respiratory chain may in turn influence the morphology of the inner mitochondrial membrane (cristae). On the other hand Menges et al. (2017)<sup>[19]</sup> showed a protective function of  $\alpha$ -Syn during oxidative stress fragmentation. However,  $\alpha$ -Syn clearly seems to interact with the mitochondria (be it with the membrane, Complex I or VDAC) and influences the morphology of mitochondria. All the mentioned interactions of  $\alpha$ -Syn and the mitochondria are schematically shown as a simplified overview in figure 2.

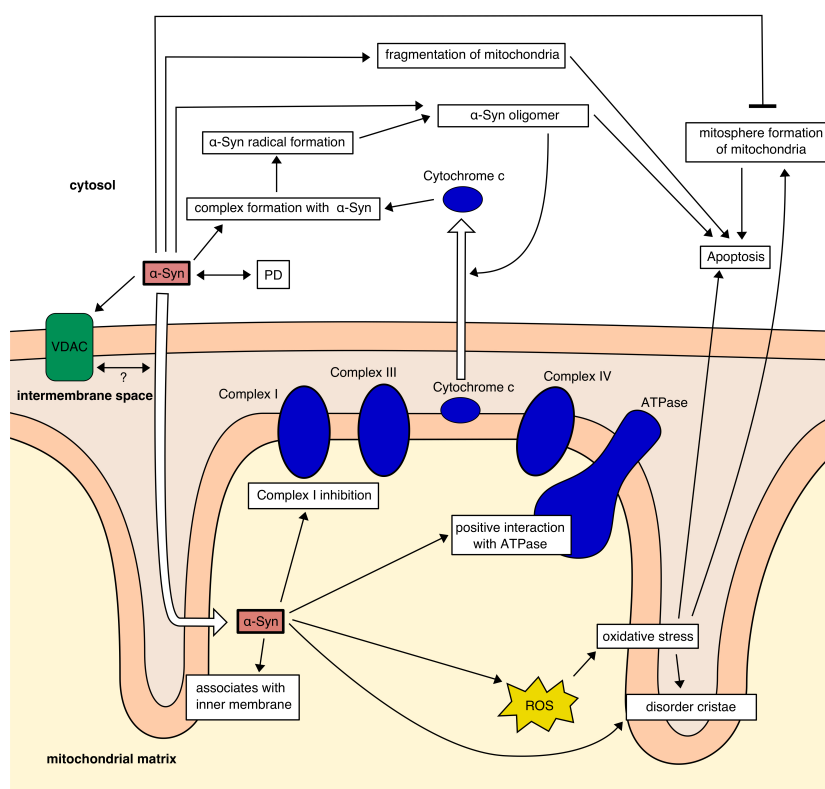


Figure 2: Schematic overview of a selection of PD related  $\alpha$ -Syn and mitochondria interactions from literature, which are mentioned in chapter 2.3 **Influence of  $\alpha$ -Syn on Mitochondria** and 2.4 **Influence of  $\alpha$ -Syn on the Morphology of Mitochondria**. It is to note that the white boxes as well as the red  $\alpha$ -Syn box are not necessarily place specific in this schematic but rather for visualizing connections (e.g. Complex I inhibition has not to take place in the mitochondrial matrix). Additionally the connections do not have to be direct.

### 3 Purification of Mitochondria

#### 3.1 LUHMES Cell Line

For the experiments conducted in this work Lund Human Mesencephalic (LUHMES) cells were chosen. As a conditionally-immortalized neuronal precursor cell line <sup>[13]</sup> they have several advantages compared to tissue samples, be it in reproducibility of experiments or acquisition of samples. Since they can be indefinitely cultured, similar to HeLa cells, there is no need for human brain samples, which are more difficult to obtain. However, in contrast to the HeLa cell line, which originates from cervical cancer cells, the LUHMES cell line originates from the mesencephalon, where also the substantia nigra is located. Upon shutting down the myc transgene with a differentiation medium they can be differentiated into post-mitotic, dopaminergic neurons. <sup>[6][13][19]</sup> Degeneration of cells similar to PD can be observed if they are treated with the neurotoxins MPP<sup>+</sup>, methamphetamine, paraquant or Rotenone <sup>[13]</sup> and they are well suited for PD models.

For experiments with whole cells multiple factors could influence the experiments as species and cell type <sup>[12]</sup>. Yeast for example has different behaviour concerning  $\alpha$ -Syn release than SH-SY5Y cells. <sup>[7]</sup> Also expression levels of e.g.  $\alpha$ -Syn can be cell type dependent. <sup>[14]</sup> The most commonly used model so far are therefore transgenic mice and LUHMES cell cultures. Nevertheless some models seem to have flaws. Li et al. (2007)<sup>[33]</sup> and Devi et al. (2008)<sup>[34]</sup> for example showed that the presence of  $\alpha$ -Syn on mitochondria is different in mice than in humans. Lee et al. (2016)<sup>[39]</sup> has shown in transgenic A53T <sup>2</sup> mice that there was no remarkable change in the substantia nigra, but for neocortex, brainstem and spinal cord, while Van der Puten et al. (2000)<sup>[41]</sup> has shown a lack of transgene expression in the substantia nigra par compact of transgenic A53T mice. Therefore it makes sense to stick to the closest model possible, like the LUHMES cell lines.

Mitochondria themselves are evolutionarily well preserved organelles, and as mentioned before, the mtDNA is an important factor for the pathology of PD <sup>[9][26][31][32]</sup> as well as the presence of  $\alpha$ -Syn within the mitochondria <sup>[12][17]</sup>. A considerable part of the mitochondrial proteins are stored in the cellular DNA, as for example for the Complex I of the respiratory chain. Therefore, the mitochondria could very well have slight differences between species and cell types. As a consequence of these slight differences not SH-SY5Y, as a human neuroblast cell line derived from bone marrow, was taken but rather LUHMES cells, as a cell line directly derived from the midbrain and therefore closest related to the dopaminergic neurons of the substantia nigra.

In contrast to studies in whole cells, studies on isolated mitochondria have some advantages as for example they are able to show a direct interaction of a certain element ( $\alpha$ -Syn fibrils/oligomers in our case) with mitochondria, meaning without any (or at least strongly reduced) secondary or indirect interactions of other proteins. <sup>[42][43]</sup> Additionally, the experimental conditions can be precisely controlled. <sup>[44]</sup> However, there are also some major disadvantages. For example, are the mitochondria affected by the isolation step and normal mitochondrial interactions are disrupted by isolation. Due to the selection method of isolation, which is by organelle mass in differential centrifugation, the outcome can be biased, as for example swollen mitochondria have a lower density than normal ones. <sup>[43]</sup> However, since no specially treated or pathologic cells were used here the biasing of mitochondria is not important for us. Also the amount of cells or tissue to end up with a satisfying amount of mitochondria is a problem, as well as the rapid drop of membrane potential, as soon as they are isolated and the problem of storage (aliquoting, since freezing/thawing cycle may injure the mitochondria further).

<sup>2</sup>A53T mutation: Mutation in the human  $\alpha$ -Syn gene, causing familial parkinson

### 3.2 Methods to Purify Mitochondria

There are several different methods for Mitochondrial purification, one of which is the differential centrifugation. <sup>[27][43][45][46]</sup> For this purification, the cells will be broken up and homogenized in the presence of a suitable buffer. Afterwards the homogenate consisting of different cellular organelles and compartments will be centrifuged in different steps to obtain a pellet consisting ideally mostly out of mitochondria, the so called crude mitochondria pellet. For brain tissue for example, differential centrifugation of the homogenate removes the unbroken cells, the nuclei and further cytosolic material, however it is still contaminated with synaptosomes and myeline.<sup>[45]</sup> Additional gradient centrifugation steps (with sucrose <sup>[45][47]</sup>, glycerol,<sup>[48]</sup> Percoll<sup>[45][46][49][50][51]</sup> or kit based <sup>[52]</sup> gradients) can therefore be used to further purify the crude mitochondria pellet. The basic schematic of this process is shown in figure 3, representing the parameters mostly used in this work for purifying mitochondria out of LUHMES cells. Since a sucrose gradient exposes the mitochondria to a hypertonic environment, a Percoll gradient is much better suited and leads to a higher respiratory activity of the sample. <sup>[27][45]</sup> Alternatively, a purification by magnetic beads is also possible, as shown by Franko et al. (2013)<sup>[53]</sup> and Hornig-Do et al. (2009)<sup>[44]</sup> which purified mitochondria from mouse liver tissue and from HEK/HeLa, respectively, using 50 nm magnetic microbeads, which were conjugated to anti TOM22 <sup>3</sup> antibodies and isolated by a magnetic field using a MACS separator.

What sounds simple at first glance is actually not that easy and mostly quite vague. <sup>[42]</sup> There are four important factors that play a major role in these isolation and purification steps. The most important factor is the cell type. depending on the sample (tissue or cell culture) the methods for homogenisation vary greatly and the same goes for the different cell type. While for example yeast or plant cells (like potatoes or spinach leaves) can actually be homogenized with a simple kitchen blender (huge amount of cells and in general quite robust cell type) <sup>[54]</sup> other samples have to be treated more carefully, which leads to the second important step: The homogenisation. The main goal here is to break up the cells without harming the mitochondria. Depending on the rigidity and amount of cells the method has to be adjusted. Plant cells, bacteria and yeast for example need more drastic methods to break up than neuronal cell lines or brain samples. Tissue samples can generally be treated more crudely, since if only a small part of the cells break up it is more than enough to purify mitochondria (high wet-weight) while at the same time reducing the risk of overhomogenisation, whereas for cell lines a method should be chosen to maximize the amount of fragmented cells without overhomogenizing the sample. Overhomogenisation refers to the process of damaging more mitochondria than breaking up intact cells. <sup>[49]</sup> This is mainly caused by the repetitive shear force exhibited upon the suspension. Therefore, the amount of sample plays an important role, since more sample allows a lower degree of homogenisation to yield a suitable outcome and reducing the overhomogenisation risk. The third factor, which is also based on the tissue/cell type, are the buffer used during the isolation protocol. Depending on the composition of the buffer, the mitochondria can be damaged or altered (swelling and disruption of mitochondria) which is especially problematic if structural based methods of analysis are the long term goal. The fourth factor are the different centrifugation steps (in differential centrifugation) to purify the homogenate and at the same time minimizing the loss of isolated mitochondria.

<sup>3</sup>TOM22: Component of the translocase of the outer mitochondrial membrane (TOM)

### 3.2.1 Homogenisation

There are several different methods for breaking up the cells and the different protocols vary from lab to lab, be it in the method used (dounce homogenizer, Potter-Elvehjem homogenizer, etc) or the handling (like number of strikes with pestles).<sup>[53]</sup>

The most commonly used system in literature are the Potter-Elvehjem <sup>[27][28][30][42][46][47][52]</sup> and the dounce homogenizer <sup>[45][50][53][55]</sup>. The cells are broken up due to two shear forces during the homogenisation: one caused by the up-and -down movement and one (for the Potter-Elvehjem) caused by the rotation of the pestle.<sup>[56][57]</sup> In fact a lot of people using the Potter-Elvehjem homogenizer tend to attach the pestle to a drill, which leads to a more consistent rotation.<sup>[42][46]</sup> In contrast to the Potter-Elvehjem homogenizer, the dounce homogenizer is a more gentle method for purifying mitochondria from softer tissue and cell suspensions, without the rotational shear force.<sup>[55]</sup> However, since the classic homogenisation by Potter-Elvehjem or dounce homogenizer requires different forces for distinct cell types/tissues <sup>[53]</sup> and the process is generally based on empirical parameters, extensive experience is needed and reproducibility is difficult.<sup>[53][57]</sup> Excessive force during homogenisation can alter mitochondrial properties, therefore the downward stroke should be slow and the upward should not lead to a gap between pestle and homogenate.<sup>[45]</sup> However, the pestle used (pestle A with 0.0035-0.0065 in clearance or pestle B with 0.0010-0.0030 in clearance for dounce homogenizer) as well as the number of strikes and the speed of the strikes (and therefore the force) vary greatly from protocol to protocol.

Beside the pestle there are also other methods for homogenisation. Cell lysis buffer, as used in certain kits such as from thermo scientific (Mitochondria Isolation Kit for Tissue), or enzymatic digestion of cell walls, as used by Davies et al. (2012)<sup>[40]</sup>. However, there is always a danger of affecting the mitochondria, therefore cell wall digestion is only an option for experiments with e.g. *Saccharomyces cerevisiae*, as used by Davies et al. (2012)<sup>[40]</sup>. For Tissue samples, shredder-techniques as the PCT shredder can be used as shown by Gross et al. (2011)<sup>[57]</sup> with rat kidney and skeletal muscles. There are even freezing and thawing cycles suggested by an invitrogen mitochondria isolation kit. However, the risk of damaging mitochondria in this process is especially for cultured cells simply too high. Furthermore, syringes with differently sized needles can be used to exhibit shear forces to break up cells, either alone or in combination with a pestle, as shown by Hornig-Do et al. (2009)<sup>[44]</sup> and Lampl et al. (2015).<sup>[42]</sup>

The probably most gentle method of homogenisation however is the nitrogen cavitation, which is best suited for cell cultures.<sup>[56][57]</sup> For this method, a nitrogen pressure of 1500 psi is applied onto the cell suspension within a pressure chamber for 20 min.<sup>[57]</sup> The nitrogen diffuses into the cells and upon rapid decompression gas bubbles are formed within the cell, causing them to rupture without harming the mitochondria.<sup>[49][51][56][57]</sup> In contrast to the classic pestle based homogenisation, this method has no repetitive damage of the cells, which is the main problem of overhomogenisation for the Potter-Elvehjem or dounce based methods.<sup>[49][56]</sup> Additionally, it is more reproducible than the other methods and yield a better respiratory control ratio.<sup>[49]</sup>

The use of different kits normally boils down to either lysate buffer (MITOISO2 from Sigma mitochondria isolation kit for cultured cells from abcam or mitochondrial isolation kit for tissue/cultured cells from thermo scientific) or a dounce homogenizer usage (mitochondrial isolation kit for tissue/cultured cells from thermo fisher) which again is cell type specific. Therefore, and because of the low use of kits in literature, no kit was used here.



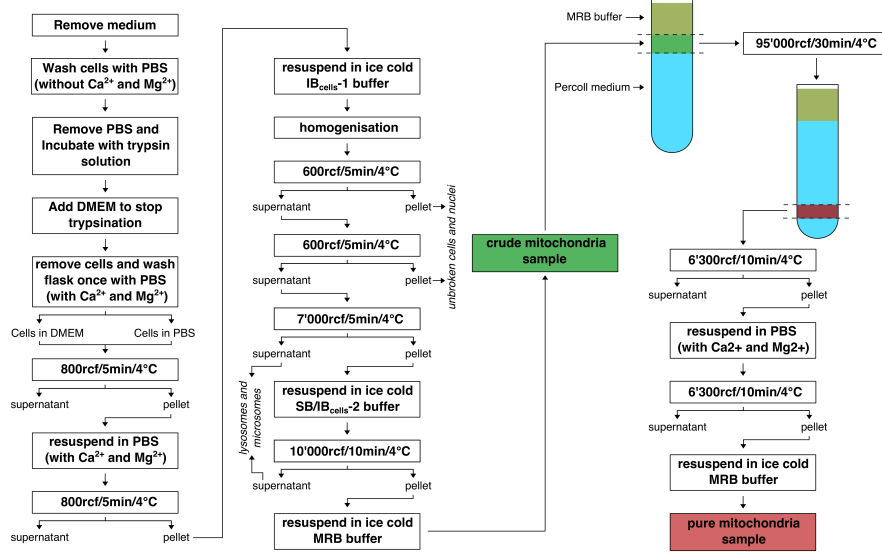


Figure 3: Schematic of the protocol predominantly used here, which based on the protocol of Wieckowski et al. (2009)<sup>[46]</sup> for HeLa and MEF cells. Crude mitochondria fraction shown in green, pure mitochondria fraction shown in red. For the mentioned buffer see table 1 in section Material and Methodes. **rcf** stands for relative centrifugal force and can be translated as *g*-force.

In this work several different methods for breaking up the cells were used, such as sonication, Potter-Elvehjem and dounce homogenizer and nitrogen cavitation. The protocol of Wieckowski et al. (2009)<sup>[46]</sup> for mouse embryonic fibroblast (MEF) and HeLa cells was chosen as template, due to its focus on cell culture and little deviation from other protocols using cultured cells, as Frezza et al. (2007)<sup>[27]</sup> and Lampl et al. (2015)<sup>[42]</sup>. Figure 3 shows the workflow used here. The protocol is focused on isolation of mitochondria associated membranes (MAMs), however, pure mitochondria are also produced here and hence the protocol can also be used for purifying mitochondria. It is to mention that mitochondria cannot be stored over long periods of time, therefore they were frozen in liquid nitrogen and stored at  $-20^{\circ}\text{C}$ . Multiple freezing and thawing cycle, however, damage the mitochondria. In combination with relatively low sample concentrations this resulted in the need of repeating mitochondria purifications if a process failed, e.g. preparation of cryo grids.

For breaking up the cells by nitrogen cavitation the same protocol as used by Tibor et al. (2005)<sup>[49]</sup> for breaking up neurons and astrocytes in cell cultures was taken. The following differential centrifugation of the homogenate was again based on the protocol of Wieckowski et al. (2009)<sup>[46]</sup>.

An additional method for purification of homogenized mitochondria by magnetic bead coupling was tried, however without much success.

### 3.2.2 Viability of Mitochondria

There are four different methods used for estimating the viability of mitochondria after isolation: immunoblotting (western blot)<sup>[28][44][46][47][49][50][53][54][56][57]</sup>, measuring respiratory activity by oxygen consumption (using a Clark-type oxygen electrode)<sup>[27][30][45][49][50][53][56][57]</sup>, using a fluorescent probe to measure the membrane potential via tetramethylrhodamineethyl ester (TMRE) detection<sup>[42]</sup> or investigating the mitochondrial superstructure using transmission electron microscopy (TEM).<sup>[27][30][40][49][52][53][57]</sup>

Despite the usable results of western blots, the best method to estimate mitochondrial injuries is to measure the oxygen consumption of the isolated mitochondria.<sup>[43]</sup> However, a Clark-type oxygen electrode is a highly specialized and Complex Instrument with a low throughput and therefore other methods as the TMRE use are easier and faster to use.<sup>[42]</sup>

In this work MitoTracker orange was used, which is similar to TMRE - a fluorescent dye that stains mitochondria in dependence of their membrane potential - as well as immunoblotting against the mitochondria specific protein VDAC<sup>[50][57]</sup> to verify the presence of mitochondria in the final sample.

Due to the fundamental interest on mitochondrial structure in this work, an additional fixation protocol was used here as well as negative staining of the final sample with uranyl acetate (UA) and phosphotungstic acid (PTA). Also cryo EM was used to obtain information of untreated, isolated LUHMES mitochondria. For the negative stain EM an additional on-grid Au-labelling protocol was used to locate the mitochondria. However, this method did not show a consistent result.

## 4 Material and Methods

### 4.1 LUHMES Cell Line

LUHMES cells were plated in 43 µg/mL poly-L-ornithine (PLO)- 1 µg/mL Fibronectin coated T75 or T175 nunclon cell culture flasks. The cells were cultered at 37.0°C and 5.0% CO<sub>2</sub> in proliferation medium containing 2 mM L-Glutamine (L-Gln), 1% N-2 supplement and 40 ng/mL fibroblast growth factor (FGF) in advanced DMEM/F12. For differentiation the proliferation medium was removed and differentiation medium containing 2 mM L-Glutamine (L-Gln), 1% N-2 supplement, 1 mM cAMP, 1 µg/mL Tetracycline and 2 ng/mL glial cell line-derived neurotrophic factor (GDNF) in advanced DMEM/F12 was added. 48 hours after medium change the cells were ready for mitochondria isolation.

### 4.2 SH-SY5Y Cell Line

SH-SY5Y cells were plated in T75 or T175 nunclon cell culture flasks. The cells were cultered at 37.0°C and 5.0% CO<sub>2</sub> in proliferation medium containing 1% non-essential amino acid solution (NEAA) and 2.25% fetal calf serum (FCS) in DMEM/F-12 GlutaMAX supplement.

### 4.3 HEK 293FT Cell Line

HEK 293FT cells were plated in T75 or T175 cell culture flasks. The cells were cultered at 37.0°C and 5.0% CO<sub>2</sub> in proliferation medium containing 1% G418 (Genecticin), 1% GlutaMAX, 1% non-essential amino acid solution (NEAA), 1% Sodium pyruvate and 1% fetal calf serum (FCS) in DMEM, high glucose media.

### 4.4 Isolation Buffers

Different buffer were used during the course of experiments, as shown in the table 1. If not further noted, the buffer were used as shown in figure 3. All buffers were aliquoted and stored at -80°C.

Table 1: List of different buffers used during the experiments.

<i>Starting buffer (SB)/Isolation buffer 2 (<math>IB_{cells} - 2</math>)</i>	225 mM mannitol, 75 mM sucrose, 30 mM Tris-HCl (pH 7.43)
<i>Isolation buffer 1 (<math>IB_{cells} - 1</math>)</i>	225 mM mannitol, 75 mM sucrose, 0.1 mM EGTA 30 mM Tris-HCl (pH 7.43)
<i>Mitochondria resuspending buffer (MRB)</i>	250 mM mannitol, 5 mM HEPES (pH 7.4) 0.5 mM EGTA (pH 7.51)
<i>Mitochondria resuspending buffer - special (MRBs)</i>	350 mM sucrose, 0.5 mM EGTA, 5 mM HEPES (pH 7.40 at 10°C)
<i>Isolation buffer - special (IBs)</i>	350 mM succrose, 1.5 mM EGTA, 30 mM Tris-HCL, 0.3% bovine serum albumin (BSA; pH 7.65 at 7.4°C)
<i>Freezing buffer (FB)</i>	350 mM threalose, 5 mM HEPES, 0.5 mM EGTA
<i>Percoll medium (PM)</i>	225 mM mannitol, 25 mM HEPES, 1 mM EGTA, 30% Percoll

### 4.5 Isolation Using Magnetic Beads

Biotinylation was conducted by changing the buffer of anti VDAC (mouse) antibody to PBS, using a Zeba Desalting column, and adding ten times molar excess of PC-Biotin-NHS ester (photocleaveable biotin reagent) to the antibody. The mixture was incubated for 1 h at RT while gently mixing. Excess crosslinker were removed with a Zeba desalting column. The biotinylated antibody was added to the homogenate as well as Dynabeads MyOne streptavidin T1 (1  $\mu$ m). The mixture was incubated for 1-12 h at 4°C while gentle mixing. For the process of isolation of mitochondria, an amount of approximately 5  $\mu$ L of the antibody-homogenate mixture was aspirated into a capillary of a magnet bead protein isolation setup for separating proteins with magnetic beads. The conjugated Dynabeads were tapped in a magnetic field and washed with 200  $\mu$ L MRB at a speed of 20  $\mu$ L/min for several minutes. The obtained bead plug was exposed to UV light for approximately 10 min. An amount of 3  $\mu$ L of the mixtures was eluted onto a carbon film coated TEM Cu grid, followed by negative staining (UA). The isolation by magnetic beads presented in this Master's Thesis was done in collaboration with Claudio Schmidli.

### 4.6 Negative Stain

A carbon-Cu-grid for TEM (400/200 mesh) was exposed to an air plasma for 20 s (glow discharge). The glow discharged grid was incubated with the sample for roughly 1-2 min, followed by a three-time wash of the grid with MRB. Afterwards, the grid was incubated with negative stain (2%UA or 2% PTA), once for 5 s and once for 20 s followed by drying on air (after blotting away the excess staining). The grids were investigated using the Tecnai Spirit electron microscope operating at an accelerating voltage of 80 kV.

### 4.7 On-Grid Gold-Labeling

For all steps the grid was placed on top of approximately 10  $\mu$ L drops, which were placed onto a paraffin foil. The carbon-Cu-grid (400 mesh) were 20 s glow discharged and incubated with sample for 5 min (the grid was placed on top of drop), followed by a 10 min wash with 1% BSA-MRB. Afterwards the grids were incubated for 1 h with a primary antibody (1:200 anti VDAC (rabbit) in 0.5% BSA-MRB), followed by two times 5 min washes with 0.5% BSA-MRB. Subsequently the grids were incubated for 1 h with a secondary antibody (1:20 protein A 5 nm Au-beads conjugate; 1:40 anti rabbit (goat) 5 nm Au-beads from BBI solution or from Sigma), followed by three time 10 min washes with MRB. Following negative staining (without glow discharge and washing) with UA or PTA was done as mentioned above. The grids were investigated using the Tecnai Spirit electron microscope operating at an accelerating voltage of 80 kV.

### 4.8 MitoTracker Orange

A Stock solution of 1 mM MitoTracker orange in DMSO was prepared and stored at -20°C. It is to note that during the whole work with MitoTracker orange the solution needed to be protected from light to avoid bleaching.

For the incubation with cells, the medium was removed and 50 nM Mitotracker orange in medium was added and incubated at culture condition for 20-30 min.

For the incubation of isolated mitochondria, the resuspended crude mitochondria pellet was incubated in a 500  $\mu$ M MitoTracker orange MRB solution for 60-75 min at RT. Afterwards, the sample was centrifuged (10 000 g for 10 min at 4°C) and the pellet was resuspended in MRB. The contact of the sample with light was reduced as much as possible. Readout of the results was done using an Axiophot fluorescent phasecontrast microscope from Zeiss.

## 4.9 Dot-Blot

Approximately 0.4  $\mu$ L sized drops of different samples were placed on a marked nitrocellulose membrane. The membrane was afterwards incubated for 1 h in 3% BSA in TBS (10 mM Tris pH 7.5, 150 mM NaCl in H<sub>2</sub>O) as a blocking buffer, followed by two times 10 min washes with TBS T/T (20 mM Tris pH 7.5, 500 mM NaCl, 0.05% (v/v) Tween 20, 0.2% (v/v) Triton X-100 in H<sub>2</sub>O) and 10 min wash with TBS. Afterwards the membrane was incubated for 1 h in a primary antibody solution (1:5'000 anti VDAC (rabbit/mouse) in 10 mL blocking buffer), followed by two times 10 min washes with TBS T/T and a 10 min wash with TBS. Subsequently the membrane was incubated for 1 h in a secondary antibody solution, while being protected from light (1:3'000 anti rabbit/mouse (donkey) 800 nm IR dye from LI-COR in 10 mL 10% (w/v) milk powder in TBS). The membrane was four times 10 min washed with TBS T/T. All steps were done at RT on a shaker (primary and secondary antibody incubation was also done over night at 4°C). Readout of the results was done using a 9120 Odyssey infrared imaging system from LI-COR.

## 4.10 Cryo Electron Microscopy

Cryo EM grid preparation was done using a EM grid plunger from Leica at -180°C Ethane cup temperature and 80% air humidity. The samples were investigated using the Tecnai T12 electron microscope (operating at an accelerating voltage of 120 kV) or the FEI Talos F200X (operating at an accelerating voltage of 200 kV).

## 4.11 Sample Fixation

*Fixation protocol used by Christer Genoud from the Friedrich Miescher Institute for the results shown in figure 12:*

The obtained crude mitochondria pellet was immersed in fixative **A** (2% para-formaldehyde (PFA) and 2.5% glutaraldehyde in 0.1 M cacodylate buffer pH 7.4) for formaldehyde fixation or in fixative **B** (1.5% glutaraldehyde in 0.1 M cacodylate buffer pH 7.4) for glutaraldehyde fixation. The following wash of the sections was done in cacodylate buffer (0.1 M, pH 7.4). Postfixation was done in 1% osmium tetroxide in cacodylate buffer (0.1 M, pH 7.4) for 1 h. Afterwards, the sections were washed three times 5 min with H<sub>2</sub>O. Dehydration was done in graded ethanol series (1x50%; 1x70%; 1x90%; 1x95%; 3x100% each for 5 min). The sample was embedded in embed 812 resin in rotational vials. An increasing amounts of resin was added to the section in 100% ethanol. Afterwards the sample was incubated in a 1:1 Ethanol - Embed812 solution for 30 min, followed by a incubation in 100% Embed812 for 30 min. Afterwards the solution was replaced with fresh resin and incubated over night while rotating. The resin was again replaced with fresh one and polymerized at 60°C for 48 h. The staining was done with UA and lead citrate.

*Fixation protocol used for the results shown in figure 15:*

The crude mitochondria pellet was centrifuged (10 000 g, 10 min, 4°C), the supernatant removed, a fixative added (2% PFA and 2.5% Glutaraldehyde in 0.15 M Cacoodylate buffer (0.15 M Cacoodylate 2 M CaCl<sub>2</sub> pH 7.2)), the pellet gently loosened (not dispersed) and incubated for 2 h

at 4°C. Afterwards the sample was again centrifuged (10 000 g, 10 min, 4°C), the fixative was removed and storage buffer was added (1% PFA in 0.15 M Cacoolydate buffer). In this condition the sample was stored at 4°C over several days.

The storage buffer was removed and the sample washed three times 10 min with 0.15 M Cacoolydate buffer at 4°C. The pellet was embedded in 4% Agarose (low melting point) on ice and afterwards cut in small pieces again embedded (the work has to be done quick to minimize the direct exposure of the pellet to air). The obtained Agarose-blocks were washed 10 min with 0.15 M Cacoolydate buffer at 4°C and postfixed in reduced osmium (1% osmium tetroxide and 1.5% KFeCN in 0.15 M Cacoolydate buffer) for 30 min at 4°C, followed by a quick wash with H<sub>2</sub>O at 4°C and 1% osmium tetroxide (in H<sub>2</sub>O) incubation for another 30 min at 4°C. The blocks were washed four times 5 min with H<sub>2</sub>O at 4°C. En block staining was preformed with 1% UA for 1 h at 4°C in the dark. The blocks were washed four times 5 min with H<sub>2</sub>O at 4°C, followed by dehydration in graded ethanol series (1x50%; 1x70%; 1x90%; 3x100% each for 5 min; until 90% ethanol at 4°C, afterwards RT). Following solvent transition was done with propylene oxide (three time 5 min at RT). Resin (23.5% Poly/Bed 812; 28.1% dodecenylsuccinic anhydride (DDSA); 25.8% nadic methyl anhydride (NMA); 2.6% 2,4,6-tris(dimethylaminomethyl)phenol (DMP 30)) infiltration was done by incubating the blocks in a 1:1 propylene oxide – resin solution for 1 h, followed by 100% resin Epon 812 incubation over night in rotational vials. The resin was replaced with fresh one and polymerized at 60°C for 48 h.

The obtained blocks were cut in sections and evaluated by light microscopy. Upon finding suitable sections, ultra thin sections (200 nm) were prepared and placed on carbon film coated TEM Cu grids with slot. The grids were stained with 6% UA in the dark for 8 min, washed four times with H<sub>2</sub>O and dried on air (after blotting away the excess staining). The same procedure was repeated with lead citrate (1 min incubation). The grids were investigated using the Tecnai Spirit electron microscope operating at an accelerating voltage of 80 kV.

*Fixation protocol used for the results shown in figures 17 and 23:*

The crude mitochondria fraction was centrifuged (10 000 g, 10 min, 4°C), the supernatant was removed and the fixative was added (2% PFA and 2.5% Glutaraldehyde in in HEPES).

The rest of the fixation protocol was conducted as for the sample shown in figure 15 (as described above) with some slight changes. Instead of one wash of 10 min between embedding and post fixation two washes of 10 min were done. Also an additional ethanol dehydration step (1x30% ethanol for 5 min at 4°C) was added and instead of propylene oxide during transition and infiltration of resin acetone was used. The resin infiltration was done in an 1:2 acetone - resin solution for 4 h instead of a 1:1 solution for 1 h.

## 4.12 Centrifugation

For the Percoll based purification at 95 000 g and 6300 g a Optima L-80 XP Ultracentrifuge from Beckman Coulter was used with a SW40Ti rotor from Beckman and 12.5 mL open top tubes at 27 400 rpm (95 000 g) respectively a 70Ti rotor from Beckman and 26.9 mL quickseal tubes at 7800 rpm (6300 g). Acceleration and deceleration was set to 4 and 7, respectively (arbitrary units of the Optima L-80 XP Ultracentrifuge). For all other purposes a centrifuge 5415 R from Eppendorf or a Labofuge 400R Heraeus from Function Line was used.

## 5 Results

### 5.1 Sonication

A UP200ST (200 W, 26 kHz) from Hielscher was used to homogenize the cell suspension in the cold room (4°C). Counting of living and dead/damaged cells was done by using Trypan Blue solution from Sigma and counting chambers (Neubauer Improved) from Laboroptik as well as an Axiovert 40C inverted light microscope from Zeiss.

In a first experiment with undifferentiated LUHMES cells, a single 10 pulse sonication (Amplitude (A) 100%; Power (P) 80 W; pulse time/s (C) 30%; time [s] (T) 10) approximately 60% of the cells were dead (data not shown) but not completely obliterated, since the dead cells were still seen as more or less whole, blue dyed cells. The suspension was centrifuged at 7000 g for 10 min at 4°C and the cell pellet was again sonicated (two additional steps; A: 100%, P: 80 W respectively 88 W, C: 20%, T: 10) to avoid damaging of possible mitochondria after the first 3 s of pulses.

Interestingly, a sonication at similar conditions (A: 100%, P: 110 W, C: 30%, T: 12) with differentiated LUHMES cells showed only few up to no dead cells (data not shown). It is worth mentioning that although the power could be increased for the sonication, the display didn't show the chosen amount during the pulse but only a fraction (20-25 W peak). Nevertheless it took two more sonication steps (A: 100%, P: 110 W, C: 30% respectively 50%, T: 12 respectively 10) meaning 8.6 second of pulses to reach around 70% dead cells. The change appeared suddenly after the third sonication step (not gradually over all 3 steps).

Negative stain (UA) of the crude mitochondria pellet isolated of undifferentiated (or differentiated) LUHMES cells homogenized in that way showed mostly no intact structure that reminds of mitochondria or vesicular objects, as seen in figure 4 **A** and **B**. These structures could come from destroyed mitochondria or cellular debris that was not removed during differential centrifugation. Generally there were not a lot of structures and most remembered more of cellular debris than vesicles.

Further Percoll based purification, as suggested by Wieckowski et al. (2009)<sup>[46]</sup>, of the undifferentiated and differentiated LUHMES samples showed a huge contamination of Percoll and some vesicles of 200-500 nm size, as shown in figure 4 **C** and **D**. Those structures could be mitochondria (range of 200-500 nm) but also other vesicles, such as liposomes, of similar size. Although it is not possible to identify mitochondria by negative stain, mainly due to the collapse of structure because of the massive salt concentration and the so caused drying, it is at least possible to estimate the amount of cellular debris and presence of potential mitochondria or mitochondria like structures. However, for a mitochondria the structures shown in figure 4 **C** and **D** seem to be empty and one would expect to see more membrane-folding due to the cristae. Additionally the final sample had a very low concentration of cellular structures of any kind and during the Percoll purification no pellet or mitochondria band in the Percoll was visible. Additional increase of concentration by repeating of the last step and resolving of the (not visible) pellet in a lower volume yield no different results than already shown (except a higher Percoll contamination). It should be noted, that after the Percoll centrifugation step (95 000 g, 30 min) a sedimentation of Percoll at the bottom of the tube was observed, which was not described in the protocol. Since the mitochondria band was not visible it is likely that a significant part of the sedimented Percoll was subtracted with the guessed (since not visible) mitochondria band, explaining the heavy Percoll contamination.

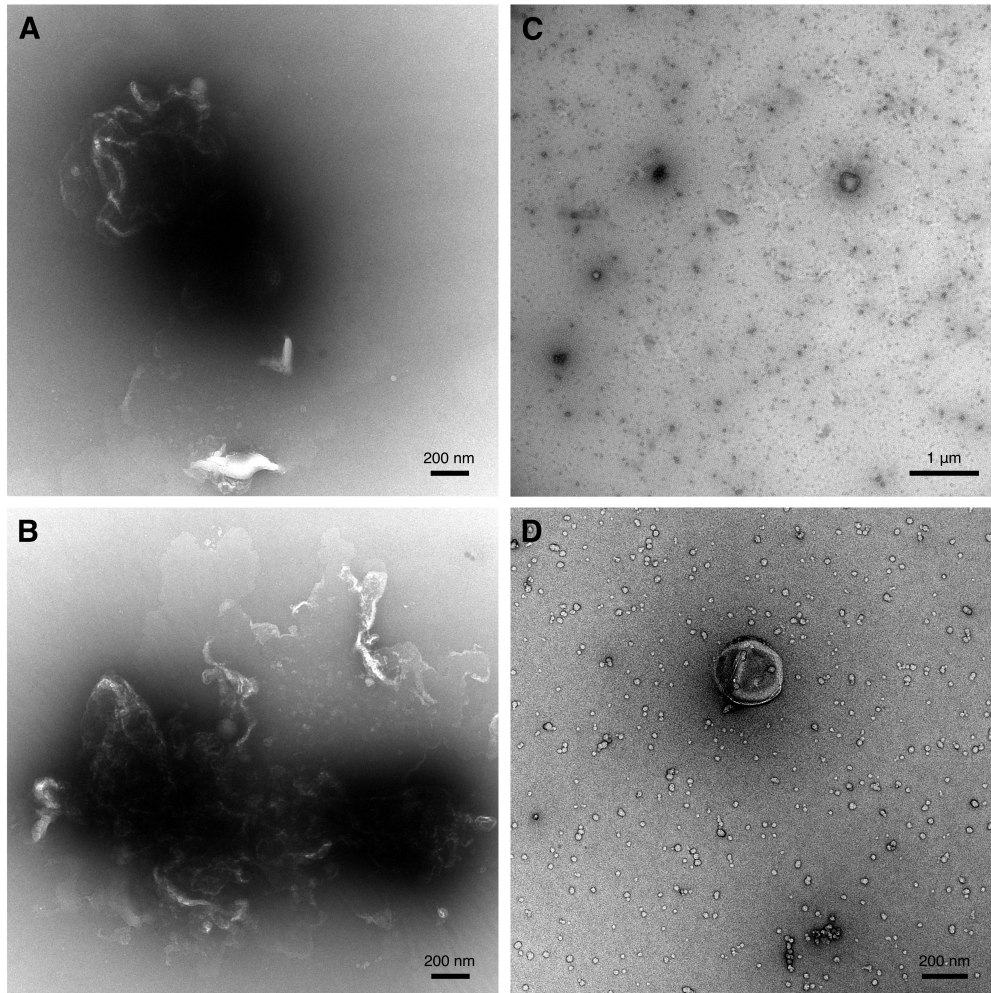


Figure 4: EM pictures of UA negative stained curde mitochondria samples as well as percoll purified samples. **A** and **B**: Crude mitochondria sample after homogenisation of differentiated (**A**) and undifferentiated (**B**) LUHMES cells using sonication. Pictures showing typical structures found after negative staining. There were no significant differences between differentiated and undifferentiated samples in negative stain. **C** and **D**: Purified mitochondria fraction of differentiated (**C**) and undifferentiated (**D**) LUHMES after whole protocol with sonication and Percoll purification. **C** shows still some cell debris in the upper right corner. Percoll was still present in the samples, as visible in both pictures (granular beads of silicate with same size, well seen in **D**). Also some vesicular structures of 200-500 nm were visible. Samples had a low concentration of possible mitochondria structures and looked similar for differentiated and undifferentiated LUHMES cells.



In a second experiment of homogenizing differentiated LUHMES cells using sonication, again multiple sonication steps (five, all around A: 100%, P: 110 W, C: 50%, T: 15) meaning 37.5 s of pulses were needed to reach approximately 80% dead cells in the suspension (data not shown). As before during the first 3 steps (meaning the first 22.5 s) only a slight reduction of living cells was observed until the numbers suddenly dropped in the next 15 s. Negative stain showed no significant difference to the undifferentiated LUHMES cell grids in sight of structures observed or their amount. On-grid 5 nm Au-labelling against VDAC (anti rabbit and protein A) however showed no labelling of any structures, that could represent mitochondria as visible in figure 5 **A-D** (Au-beads exemplary indicated by red arrows). Free gold particles were also floating around. The same goes for most of the cellular debris found by Au-labelling and negative staining. However, some fuzzy structures, as seen in figure 5 **E** and **F** showed a weak labelling with Au-beads conjugated to protein A (circled in red). Interestingly this structures do not resemble mitochondria at all as they were expected. Nevertheless, since the Au-beads conjugated to protein A did not label all structures this suggests that the structure shown in figure 5 **E** is a damaged mitochondria.

The homogenisation of three T175 cell culture flasks of HEK 293FT cells took only two sonication steps (A: 100%, P: 100 W, C: 30%, T: 15 and A: 100%, P: 120 W, C: 50%, T: 20) with a total of 14.5 s of pulses to kill over 90% of the cells. The crude mitochondria fraction was incubated with 500 nM MitoTracker orange and purified with Percoll as suggested by Wieckowski et al. (2009)<sup>[46]</sup>. As expected a Percoll sedimentation took place after the 95 000 g centrifugation (again no mitochondria band formed). Above the Percoll pellet the layers were separated in four fractions à 1 mL plus the rest (supernatant) to investigate where the mitochondria are located. All fractions showed small particles, which emitted visible fluorescent light upon stimulation. For the two fractions closest to the Percoll pellet also bigger, round particles were visible. However, upon negative staining of the obtained four fractions with UA nothing was found aside from some dirt and Percoll, whereby the Percoll contamination was highest in the fraction closest to the pellet (data not shown). In the remaining fractions the Percoll contamination was more or less equally distributed.

Cryo EM of the crude mitochondria pellets (without MitoTracker orange) showed predominately multi-laminar structures and vesicles of different sizes but nothing resembling a mitochondria, as shown in figure 6.

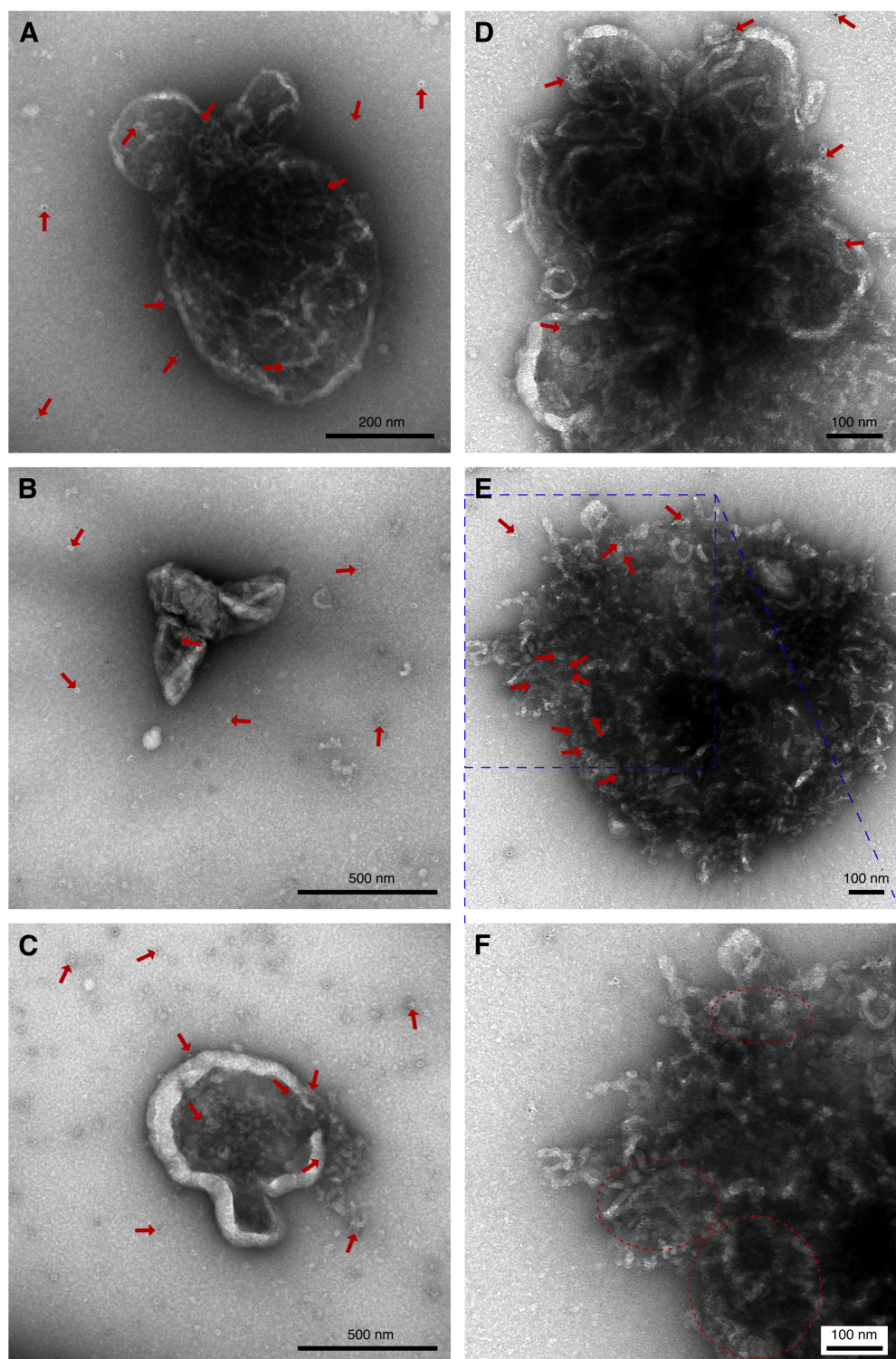
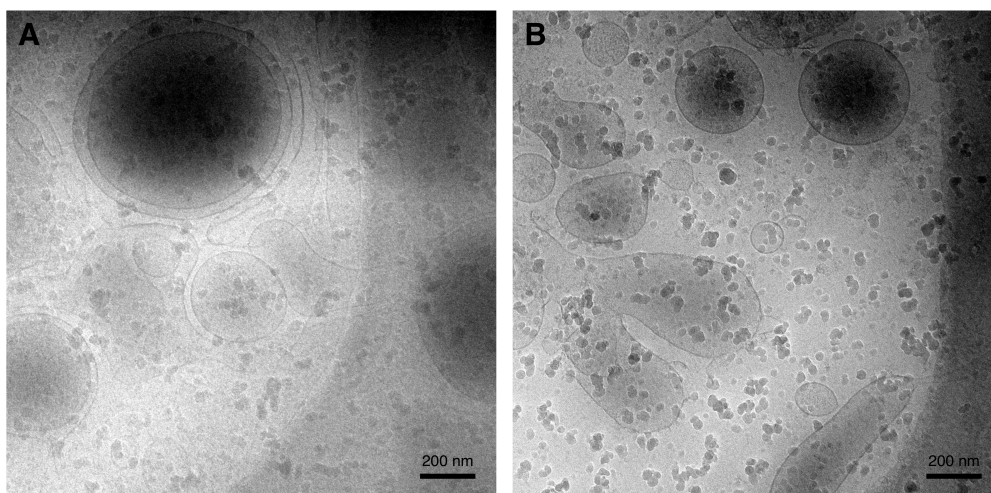


Figure 5: EM pictures of UA negative stained crude mitochondria fractions with on-grid 5 nm Au-bead labelling against VDAC from differentiated LUHMES cells. **A** and **B** 1:200 anti VDAC (rabbit) and 1:10 anti rabbit Au-beads; **C** 1:200 anti VDAC (rabbit) and 1:20 anti rabbit Au-beads; **D-F** 1:200 anti VDAC (rabbit) and 1:40 protein A Au-beads. **A-D** showing possible mitochondrial structures. Red arrows indicate some Au-beads. Au-beads were randomly distributed and showed no specific labelling of the structures. **E** showing a fuzzy structure, seemingly labelled with Au-beads. **F** showed a magnification of **E** (blue dotted square) with areas of increased, visible Au-beads marked with red dotted circles.



*Figure 6: Cryo EM pictures of crude mitochondria pellets obtained by sonicator based homogenisation of HEK 293FT cells. Multiple liposome like vesicles of several 100 nm and membranes visible, as well as multi-laminar vesicles but no mitochondria. Some of the vesicles were rather thick (dark) but do not seem to have cristae-like internal structures. The image shows a high density of surface contamination of the grid.*

## 5.2 Potter-Elvehjem Homogenisation

The use of a 15 mL Potter-Elvehjem homogenizer (glass-teflon) needed over 200 strikes to destroy approximately 60% (control every 50 strikes) of the undifferentiated LUHMES cells grown in a coated T75 culture flask (data not shown). Counting of living and dead/damaged cells was done by using Trypan Blue solution from Sigma and counting chambers (Neubauer Improved) from Laboroptik as well as an Axiovert 40C inverted light microscope from Zeiss. After the first 50 strikes some smaller compartments than the cells were visible, however, the number of living cells was only slightly reduced and the next 150 strikes showed not much change.

Attaching a GSR14, 4V-LI professional screwdriver from Bosch to increase the rotational shear forces and stabilize the number of rounds per minute did not considerably decrease the amount of living cells (after additional 60 strikes with screwdriver no significant increase in dead cells was visible, data not shown).

The use of SH-SY5Y as a different cell line showed, similar to the LUHMES cell line, after 150 strikes still a high amount of living cells (approximately 50%). After the first 50 strikes there was a significant decrease of living cells and an appearance of a large amount of smaller compartments. However, the next 100 strikes only marginally decreased the number of living cells. Upon mounting of the screwdriver from Bosch as for the LUHMES cells, the number of living cells dropped after 60 additional strikes. Nevertheless the amount of living cells remained in the magnitude of 40-50% (data not shown).

### 5.3 Dounce Homogenisation

Differentiated LUHMES cells were homogenized using only the tight (B) pestle of the 15 mL dounce homogenizer. Cellcount of dead cells was done every 25-50 strikes using Trypan Blue solution from Sigma and counting chambers (Neubauer Improved) from Laboroptik as well as an Axiovert 40C inverted light microscope from Zeiss. An amount of 150 rather rough strikes were needed to reduce the amount of living cells by approximately 70-80%. It should be noted that after the first control the amount of smaller compartments visible (considerably smaller than the cells and of approximately similar size) was massively increased and continued to increase slightly over the course of homogenisation. Negative stain (UA) of the crude mitochondria fraction showed a mixture between cellular debris and vesicle like structures, for which some were in the range of 200-500 nm and could be mitochondria. A selection of those structures are shown in figure 7 **A-D**, and seem to resemble the ones found for the sonicated samples before (shown in figure 5 **A-C**). Some of the structures seemed damaged and fuzzy as in figure 7 **E** shown. Others appear to have no internal membrane structure like liposomes, as in figure 7 **C** indicated by blue arrows.

Following on-grid labelling with 5 nm gold-beads (anti rabbit) as done for the sonicated samples showed no kind of specific targeting for any of those structures, as seen in figure 7 **F** and **G** (Au-beads exemplary indicated by red arrows). Neither for possible mitochondria like structures as in figure 7 **F** nor for a structure that appeared to be a vesicle or liposome with no internal membrane structure as in figure 7 **G**. Interestingly some fuzzy structures showed labelling, as visible in 7 **H**, which is a similar finding as for the sonicated samples (see figure 5 **F**). Based on the labelling of those structures it is possible that these are ruptured mitochondria.

Preparation of cryo EM grids led to the formation of thick ice on the grid. Only a few spots had suitable thin ice for cryo EM. Liposomal structures and vesicles of different size were found but no structures that resemble mitochondria (data not shown).

Further purification with Percoll as suggested by Wieckowski et al. (2009)<sup>[46]</sup> showed nothing but Percoll and some dirt (negative stain of the purified mitochondria fraction), which was not surprising, since during the whole procedure no pellet or mitochondria band was observable (data not shown).

Identical experiments with HEK 293FT cells, which were also homogenized using only the tight (B) pestle of the 15 ml dounce homogenizer, showed a similar behaviour, although the number of pestle strikes was slightly more effective (125 strikes for 80-90% dead cells). Negative stain results (UA) of the crude mitochondria fraction however showed many vesicular structures, as visible in figure 8 **A** and **B**. There was still some cellular debris visible and some vesicular structures were too big to be mitochondria, but the amount of possible mitochondrial structures (size of 200-500 nm with possible collapsed cristae inside) was significantly bigger, compared to the differentiated LUHMES experiments so far. Cryo EM results of the crude mitochondria fraction however showed mainly multi laminar liposome-like structures, as shown in figure 8 **C** and **D**, where the ice of the grids was not too thick. **D** also shows a structure that could resemble the fuzzy structures shown in figures 7 **H** or 5 **E** and **F**. This structure could either be a damaged mitochondria or simply a membrane cluster.

Similar to the differentiated LUHMES cells the further purification using Percoll resulted in no visible mitochondria band or pellet and negative stain (UA) results of the pure mitochondria fraction showed again nothing but some Percoll contaminations.



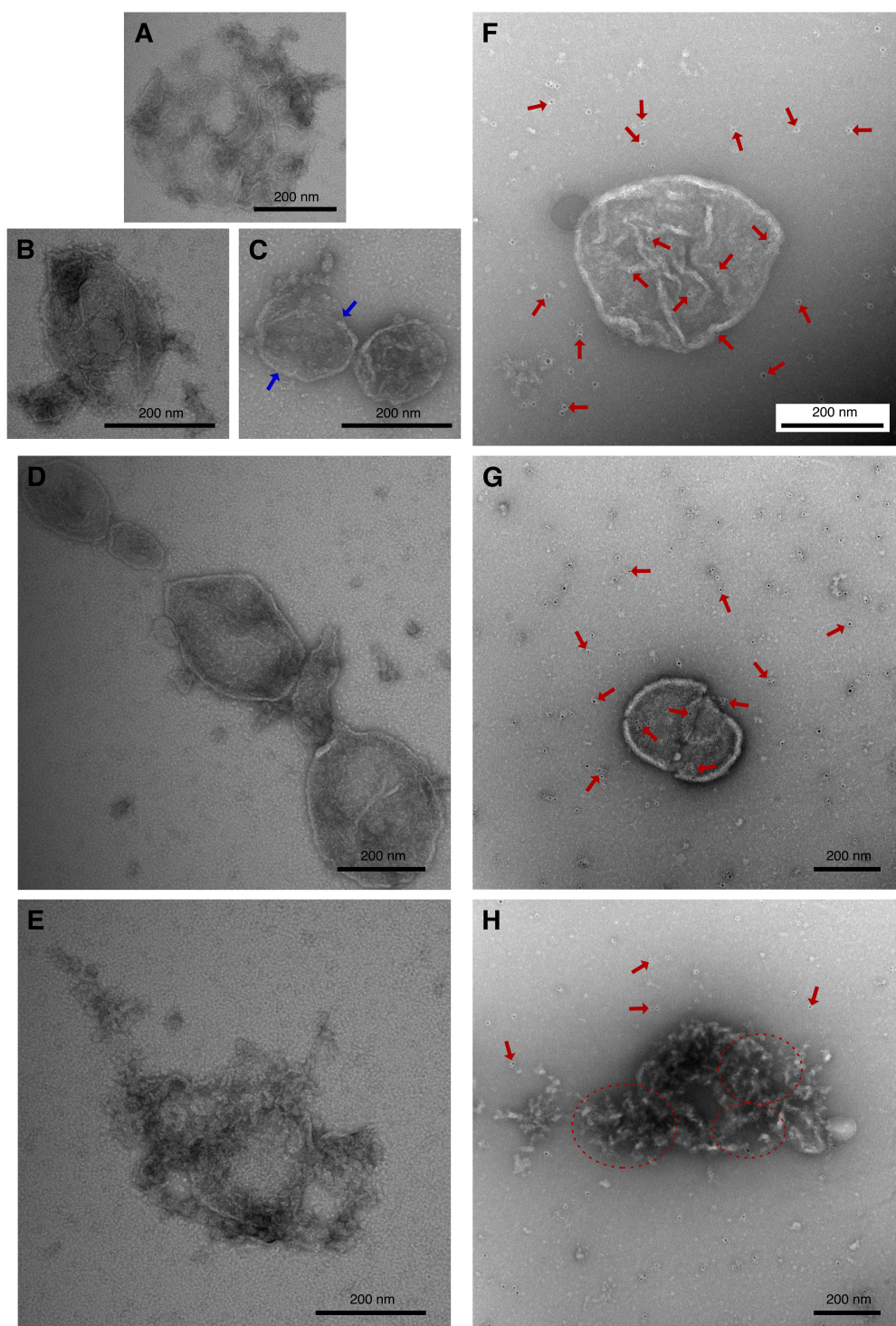


Figure 7: EM pictures of UA negative stained crude mitochondria fractions of dounce homogenizer based isolation from differentiated LUHMES cells. Only tight (B) pestle used. **A-D** show example of some possible mitochondria structures together with vesicles without internal membrane structures (**C**, indicated by blue arrows). **E** showed a fuzzy structure that could represent a ruptured mitochondria. **F-H** 1:200 anti VDAC (rabbit) and 1:10 anti rabbit 5 nm Au-beads. Beads exemplary marked with red arrows. **F** and **G** examples for non-labeled structures (**F** for structures that were regarded as possible mitochondria like structures in negative stain and **G** for possibly liposome or a similar vesicle structures). **H** fuzzy structure that shows labelling (red circles for area with large amount of beads) and therefore could be a burst mitochondria, similar to the sonicator based results.

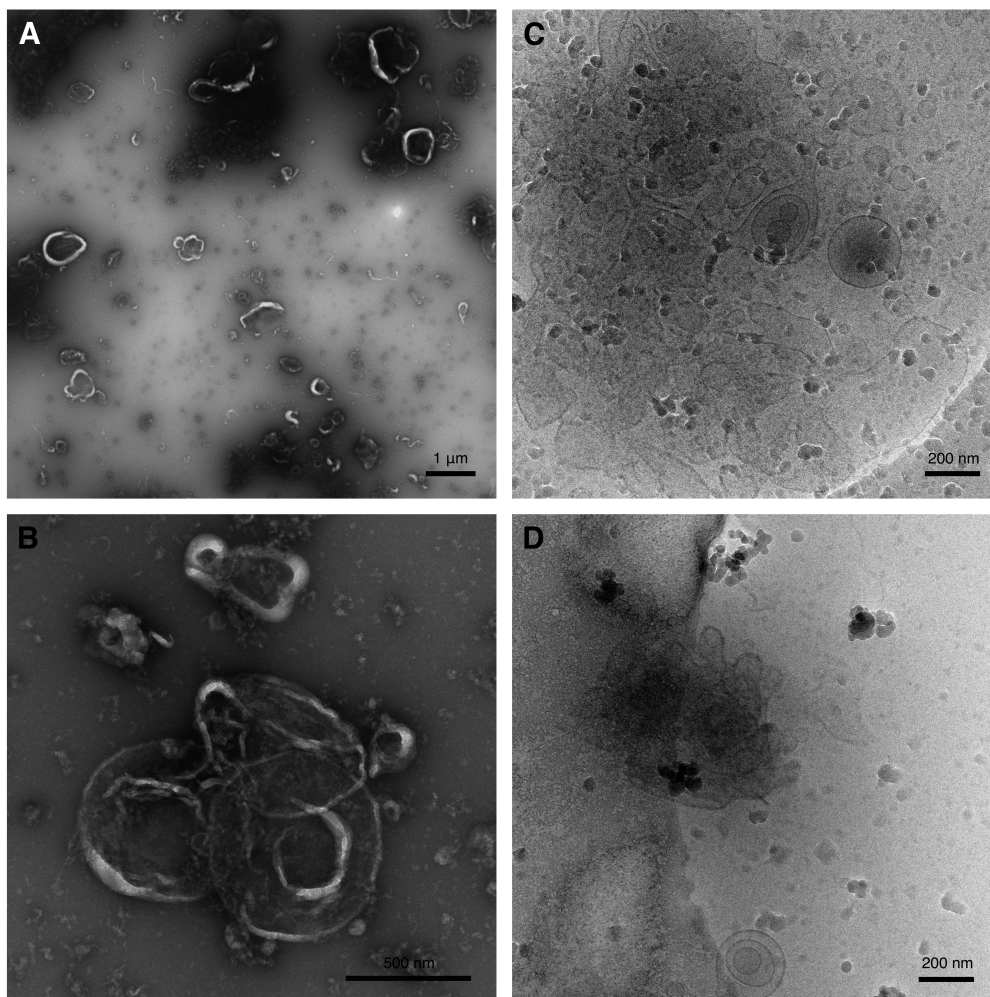
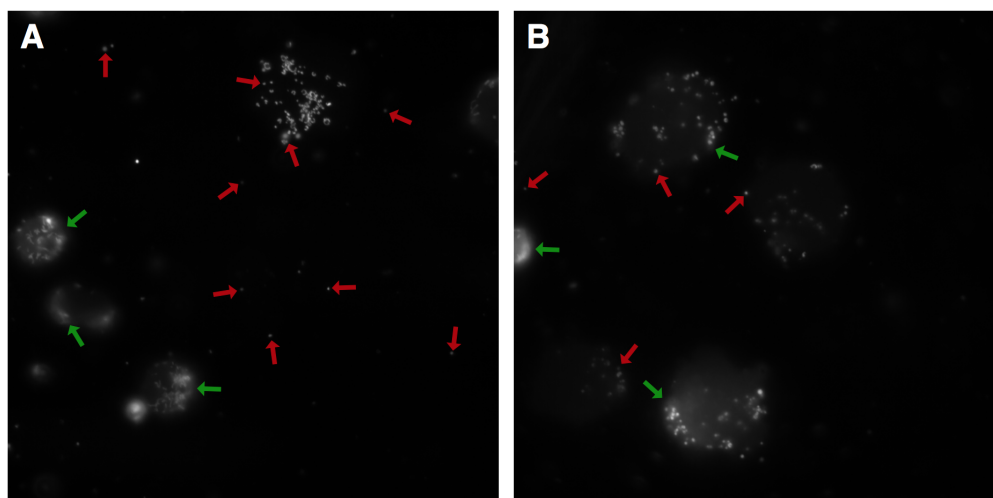
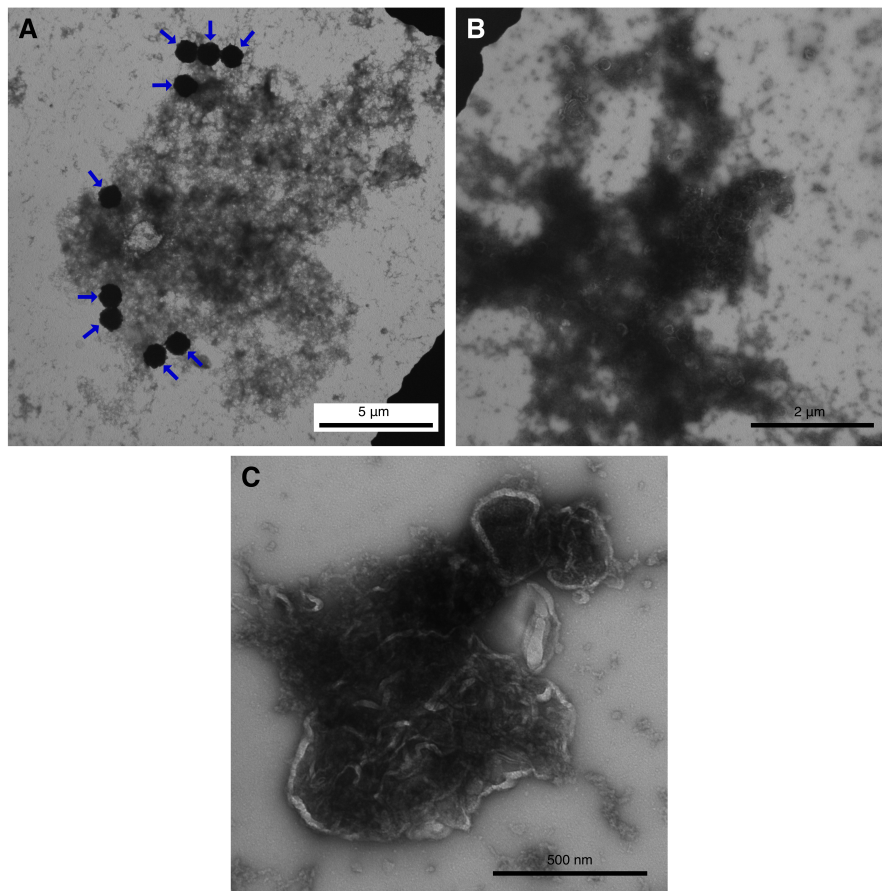


Figure 8: Cryo EM and negative stain (UA) EM pictures of the crude mitochondria fractions of dounce homogenizer based isolation from HEK 293FT cells. Only tight (B) pestle used. **A** overview of the large amount of vesicular structures and **B** showing a possible mitochondria structure found, similar to the ones found for differentiated LUHMES cells shown in figure 7. **C** and **D** showing cryo EM results of the crude mitochondria samples. In **C** multiple liposome like vesicles are visible and sometimes multi laminar vesicles but no mitochondria like structure. The lower part of **D** shows another multi laminar vesicle while in the upper part a fuzzy structure is visible, which seems to consist of multiple membranes and resembles the structures found in negative stain for 7 H. Samples showed heavy ethane contaminations.

Upon incubation of the crude mitochondria samples with MitoTracker orange, nearly everything in the HEK 293FT samples was glowing (data not shown). This is either due to a too high concentration of the MitoTracker, although the background was relatively normal, or a high concentration of mitochondria in the sample. One of the differentiated LUHMES cell cultures was also incubated with MitoTracker orange, however, before homogenisation. Interestingly this method allowed to track the presence of mitochondria in the pellets during each step of the differential centrifugation by the naked eye (due to the high concentrations there; crude mitochondria pellet had a slight reddish colour in the end). The fluorescent microscope results of MitoTracker orange shown in figure 9 **A** and **B** indicate the presence of mitochondria within the crude mitochondria fraction (exemplary shown by red arrows). At the same time whole cells or cell-remains seem to be still present, as indicated by the green arrows. It should be noted that the spots are blurry, since the sample was still moving. This is also the reason why no other MitoTracker orange data is shown in this report. The free mitochondria were moving most of the time rather fast for the camera, therefore they are often not well visible in figure 9 **A**. Another reason for the lower emission of fluorescent light of the free mitochondria, could be a lower labelling by the MitoTracker. This is likely, since isolated mitochondria show a decrease in membrane potential and therefore become less attractive for the MitoTracker. Also fast bleaching due to the light reduced the signal rapidly, hence up to no free mitochondria were seen in **B** anymore. Mitochondria inside or around cells seemed nevertheless more stained, therefore more healthy (still relatively high membrane potential) than the free ones. Additional gentle pressure on the glass-slide was enough to let the cells or cell-remains burst and free the mitochondria. For better pictures the sample would have to be fixated, but since the MitoTracker was only used as a control and not as final result, no such procedure was done here.



*Figure 9: Fluorescent microscope pictures ( $\times 100$  magnification) of MitoTracker orange treated crude mitochondria pellets of differentiated LUHMES cell obtained by dounce homogenisation. Only tight (B) pestle used. Red arrows indicate exemplary mitochondria and green arrows indicate still present cells or cell-remains. Mitochondria present within the cellular remains or around them seemed to emit more light than the free ones. The stronger signal is caused by stronger staining and therefore the mitochondria, which are still within the cellular remains, possess a higher membrane potential than the free ones. The observed cell remains burst when gentle pressure is applied onto the glass-slide.*



*Figure 10: EM pictures of UA negative stained crude mitochondria fractions of dounce homogenizer and magnetic bead based isolation from HEK 293FT cells. **A** shows overview with stained meshwork of cellular debris and magnetic beads (1 µm, indicated by blue arrows) still attached to the sample. In **B** the meshwork of membranes and vesicles is visible and **C** shows a more separated vesicle structure that could represent a mitochondria. However, most of the potential mitochondria structures were still attached to the meshwork shown in **B**.*

A different purification method aside from differential centrifugation was also tested with HEK 293FT, homogenated in the same way as described above. For this isolation method, reminding of the purification method used by Franco et al. (2013)<sup>[53]</sup> or the isolation kit of invitrogen/Dynal (magnetic isolation of pure, intact human mitochondria), the protocol to isolate proteins from solutions with magnetic beads and the magnet bead protein isolation setup was used. For this 1 µm magnetic beads were coupled via a photocleavable biotin linker to VDAC antibodies. The beads were able to attach to mitochondria and the mitochondria-bead mixture should have been able to separate from the homogenate. The beads were cleaved off again by UV light and the purified mitochondria placed on a TEM grid and negatively stained with UA. However, as shown in figure 10 **A** and **B** the mixture mainly consisted of large scale clusters of different membranes and cellular compartments that stuck together. Even some of the magnetic beads (indicated by blue arrows) were still attached to the meshwork. Already during the washing procedure of the isolated mitochondria bound to the beads in the capillary of the setup



they seemed to have formed a plug. There were some more or less separated structures found that could be mitochondria, as seen in 10 C. However, it is visible in 10 B that most of the vesicular structures were trapped in the meshwork. It is possible that the magnetic beads and the mitochondria formed a dense cross-linked network like a polymer and trapped the cellular debris, forming the observed plug. The washing step therefore could even have damaged the structures due to the pressure applied onto the plug. In that case this method will not work in this setup. Upon a second try with HEK 293FT homogenized cells, the outcome did not change (still huge meshwork with beads partially still attached). Therefore this method was not further pursued.

The usage of the looser pestle (A) before the tighter one (B) during homogenisation of differentiated LUHMES cells showed no significant difference, although after an amount of 25-30 strikes already some cells died in differentiated LUHMES cell suspensions.

Nevertheless, further isolation experiments of differentiated LUHMES cells using pestle A and B, as well as using MitoTracker orange were able to reproduce the MitoTracker orange presence in the pellets during differential centrifugation, as well as in the crude mitochondria pellet in the end. Additional dot-blot experiments against VDAC confirmed the presence of mitochondria within the crude pellet and track the relative concentration along the differential centrifugation, as shown in figure 11 (two different intensities of 800 nm illumination of dot-blot). It is visible that the highest concentration is in the final pellet ( $\epsilon$ ) followed by the homogenate ( $\alpha$ ) and pellet of unbroken cells and nuclei ( $\beta$ ), which was to be expected. The supernatant after removing the unbroken cells and nuclei ( $\beta^+$ ) has a relatively low signal, which can be explained by the low concentration of mitochondria in the supernatant (in contrast to the high concentrated crude mitochondria pellet for example). The two supernatants at 7000 g and 10 000 g have the lowest till barely present relative concentration ( $\gamma$  and  $\delta$ ), which is to be expected, since the mitochondria should be mostly in the pellet in these steps (nevertheless, this shows a slight loss of mitochondria during those centrifugation steps).

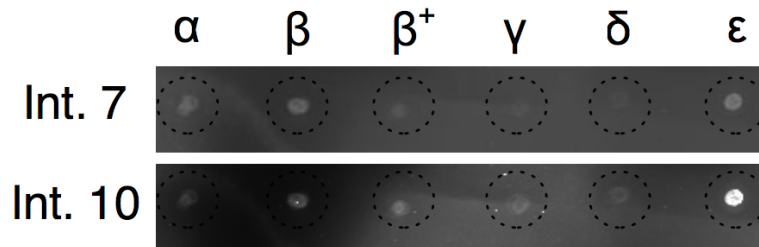


Figure 11: Dot-blot against VDAC of different steps during differential centrifugation based purification of mitochondria from differentiated LUHMES cell homogenate. Both pestles were used for homogenization. Two different 800 nm illumination intensity results shown (intensity 7 and intensity 10; arbitrary units of the Odyssey infrared imaging system).  $\alpha$ : homogenate;  $\beta$ : pellet of unbroken cells and nuclei;  $\beta^+$ : supernatant of pellet of unbroken cells and nuclei, containing mitochondria;  $\gamma$ : Lysosome and microsome supernatant;  $\delta$ : supernatant of 10 000 g centrifugation;  $\epsilon$ : crude mitochondria pellet after resuspension with MRB.  $\epsilon$  shows strongest signal (especially at intensity 10) indicating a high concentration of mitochondria in the crude mitochondria fraction.  $\alpha$  and  $\beta$  show second highest concentration as to be expected (homogenate possess mitochondria and unbroken cells as well).  $\beta^+$  shows some concentration of mitochondria as expected. The signal is weaker as for the final pellet because the mitochondria are more diluted.  $\gamma$  and  $\delta$  show weak signal, which indicates a certain loss of mitochondria during these steps

Figure 12 **A-C** show ultra-thin section (200 nm) results of a crude mitochondria pellet which was fixated with formaldehyde and glutaraldehyde, respectively. The crude mitochondria pellet was obtained by homogenizing undifferentiated LUHMES cells with both pestles and following the differential centrifugation protocol as normal. As seen in figure 9 **A** there are some free mitochondria (indicated by red arrows), but free cells can be recognized as well. With exception of the nucleus and the mitochondria, the other cellular organelles as well as the plasma membrane seem to be missing. The cytoplasm is still present around the nucleus and the mitochondria, which are located within the cytoplasm (indicated by green arrows, **B**) look different than the free ones, which are not surrounded by the cytoplasm (indicated by red arrows, **C**). The free mitochondria seem to be swollen and the cristae shows round structures instead of the more ordered, lamellar structures observed for the ones still surrounded by cytoplasm. This observation correlates with the more or less intact cells found by MitoTracker orange (figure 9). These results are to some degree surprising, since the centrifugation after homogenisation is supposed to get rid of nuclei and unbroken cells.

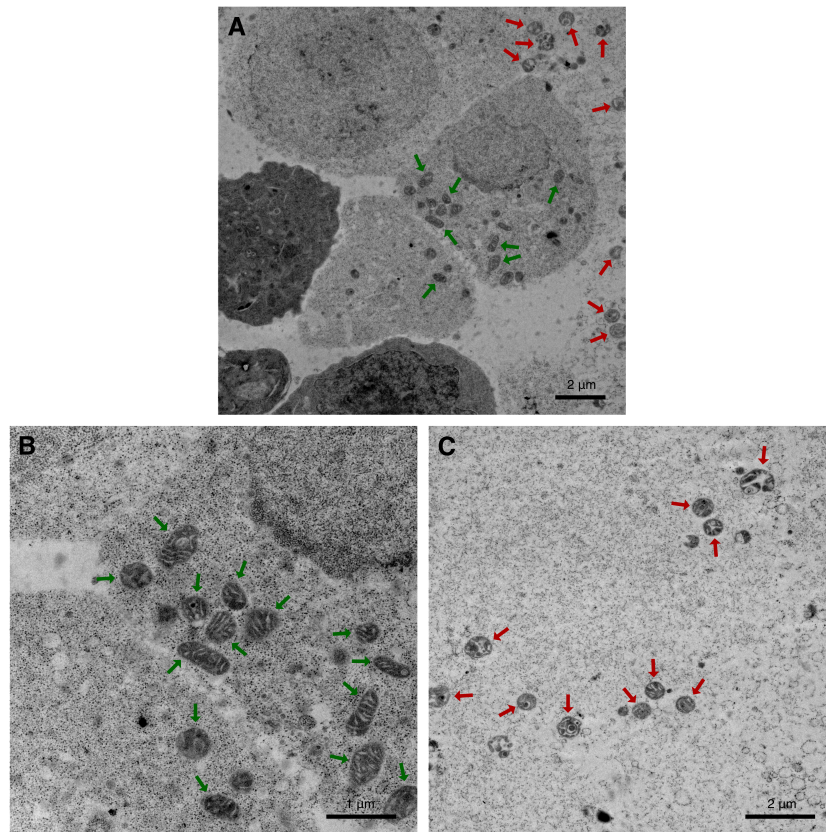


Figure 12: EM pictures of ultra-thin sections (200 nm) from glutaraldehyde fixated crude mitochondria pellets obtained by dounce homogenizer based isolation from undifferentiated LUHMES cells. Both pestles were used for homogenization. **A** showing overview with free mitochondria (indicated with red arrows) and mitochondria still surrounded by cytoplasm (indicated with green arrows) of present cells, which do not possess any membrane or organelles anymore but a nucleus. **B** shows a selection of mitochondria within cytoplasmic environment (green arrows), **C** shows a selection of free mitochondria (red arrows)

Up to this point the homogenisation was usually done by a rather harsh pestle movement (this means active pushing and pulling of the pestle). However, due to the improved risk of overhomogenisation, this was changed and the pestle was barely pushed for the next homogenisation of differentiated LUHMES cells (gently with two finger). Also the centrifugation after homogenisation was increased to three times 800 g at 4°C to get rid of the unbroken cells and the cellular debris. As hallmark the normal centrifugation force used to spin-down cell suspension (800 g) was taken. Due to the reduction of pestle-force, 40 strikes with pestle A and 150 with pestle B were only able to reduce the amount of living cells by 20-30%. However, to avoid further overhomogenization the protocol was continued at this point. While a dot-blot monitoring the progress during the following differential centrifugation clearly indicates a strong signal for the crude mitochondria fraction, as seen in figure 13  $\epsilon$ , the negative stain results in figure 14 **A** and **B** as well as the cryo EM results **C** and **D**, show the same or similar results as for the samples before. This means for negative stain, that a considerably large amount of cellular debris was visible, as well as some structures that could represent mitochondria, which is shown in figure 14 **A**. But at the same time there were also vesicular structures visible that are too big (around 2  $\mu\text{m}$  in diameter) to be mitochondria, as shown in figure 14 **B** (indicated with blue arrows) and could be e. g. nuclei or giant vesicles, which are despite increased centrifugation force of the homogenate still present in the crude mitochondria fraction. For cryo EM similar as the other samples means thick ice and a lot of vesicular structures, remembering of liposomes as seen in an small overview in figure 14 **C**. Additionally some cellular debris is visible as blurry structures. **D** shows a more detailed view, revealing liposome-like structures (lower right corner) and some tubular double membrane structure, which could be decorated at some points with proteins (red arrows). Those structures could probably be a part of the endoplasmatic reticulum (ribosomal decoration) and would show an additional contamination of the crude mitochondria pellet. Nevertheless, no mitochondrial structure was found within the part where the ice wasn't too thick. The rest of the dot-blot showed a similar tendency as in figure 11. The signal of the crude mitochondria fraction (figure 13  $\epsilon$ ) was the brightest, indicating a concentration of mitochondria in the final fraction.  $\alpha$  and  $\beta$  were again showing signals, whereas for  $\gamma$  and  $\delta$  up to no signal is seen as expected.  $\beta^+$  showed a signal, but due to the relatively high dilution only a weak one.  $\theta_1$ - $\theta_3$  (MRB, SB and MRB without mannitol and sucrose) were negative controls and as expected showed no signal.

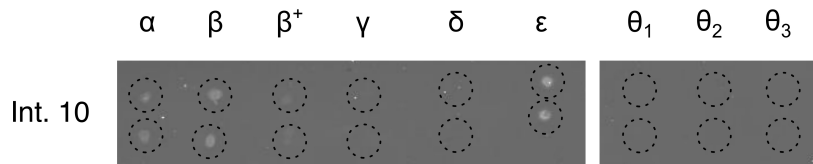


Figure 13: Dot-blot of the crude mitochondria fractions of dounce homogenizer based isolation from differentiated LUHMES cells. Both pestle were used for homogenization with gentle strikes.  $\alpha$ : homogenate;  $\beta$ : pellet of unbroken cells and nuclei;  $\beta^+$ : supernatant of pellet of unbroken cells and nuclei, containing mitochondria;  $\gamma$ : Lysosome and microsome supernatant;  $\delta$ : supernatant of 10 000 g centrifugation;  $\epsilon$ : crude mitochondria pellet after resuspension with MRB;  $\theta_1$ : MRB (with mannitol and sucrose);  $\theta_2$ : SB ;  $\theta_3$ : MRB (without mannitol and sucrose).  $\epsilon$  shows strongest signal indicating a high concentration of mitochondria in the crude mitochondria fraction.  $\alpha$  and  $\beta$  show second highest concentration as to be expected (homogenate possess mitochondria and unbroken cells as well).  $\beta^+$  shows some concentration of mitochondria but due to the relative high dilution a weaker one than  $\epsilon$ .  $\gamma$  and  $\delta$  show no visible signal at all, as well as  $\theta_1$ - $\theta_3$  which were negative controls.

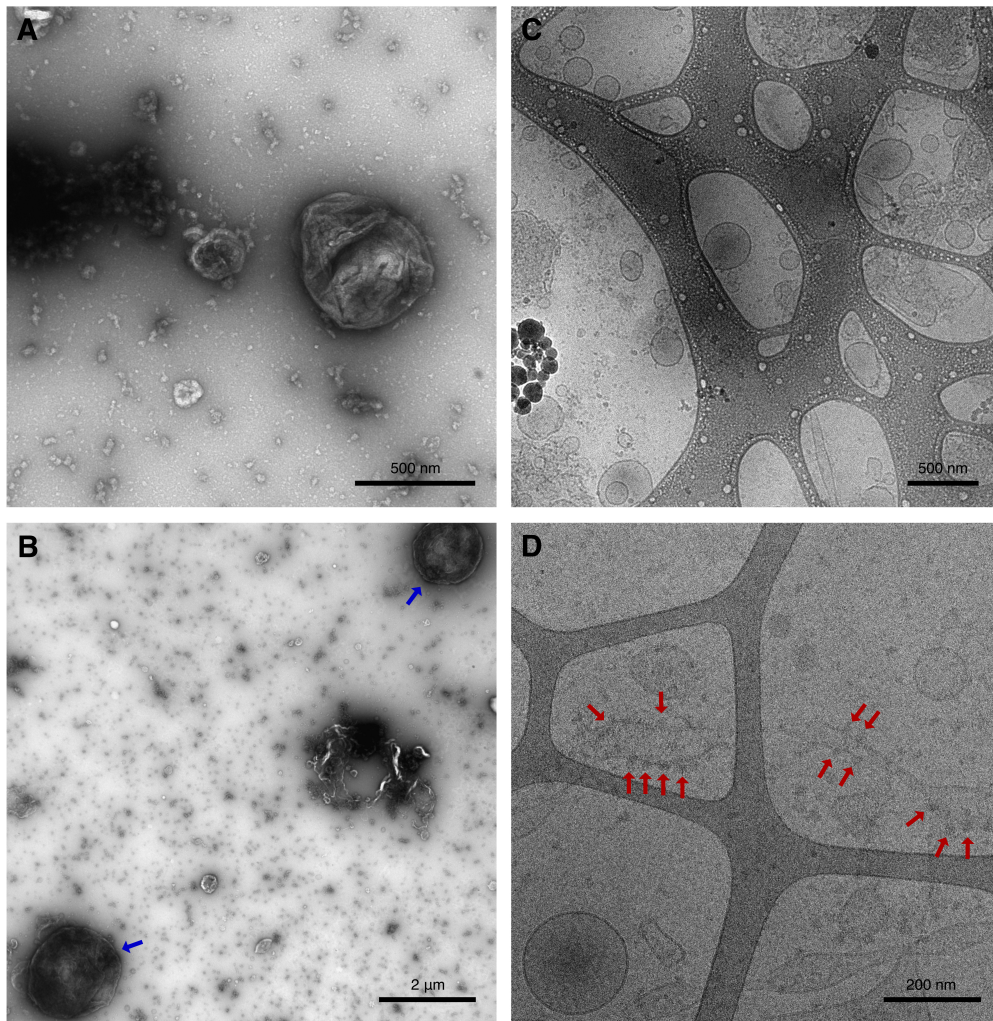


Figure 14: Cryo EM and negative stain (UA) EM pictures of the crude mitochondria fractions of dounce homogenizer based isolation from differentiated LUHES cells. Both pestle were used for homogenization with gentle strikes. **A** and **B** show negative stain (UA) EM pictures of the crude mitochondria fraction. Similar results as for all other samples so far. Possible mitochondria structures in **A** with cell debris and structures that are with 2  $\mu\text{m}$  too big to be mitochondria and could instead be e. g. nuclei (indicated with blue arrows). **C** shows a small cryo EM overview with different sized liposome-like vesicles and membrane structures but no mitochondria structures. Picture showed some electron beam damage as seen on the carbon. In **D** a more detailed view is shown with a liposome-like structure in the left lower corner and a possible ribosomal structure (tubular membrane structure, possibly decorated with proteins, as indicated by red arrows). However, no mitochondrial structure was found.



The fixated sample shown in figure 15 was obtained by homogenizing only with pestle B for 20 moderate strikes, which was enough to reduce the amount of living cells by around 50% and following the differential centrifugation protocol as normal. The obtained pellet was fixated with para-formaldehyde and glutaraldehyde and embedded with agarose. It is clear from figure 15 **A** that there are still a lot of cellular compartments around and some mitochondria are still stuck in the cytoplasm of more or less intact cells (**C**) or cellular compartments (**D**). The isolated mitochondria (**A** and **B**, indicated with red arrows) are often swollen or even destroyed (indicated with blue arrows). Compared to the free mitochondria the ones surrounded by cytoplasm look very elongated and with twisted cristae but still not very healthy. Interestingly there seem to be rather big differences, if **C** and **D** are compared. While **C** resembles more the isolated mitochondria as the ones found in 12, the two seen in **D** resemble more the textbook fixated mitochondria found in intact cells. Also some so called *ghosts*, empty vesicles as in **B**, are visible. Those could very well represent the liposome-like structures found by cryo EM. Generally the mitochondria look more damaged and twisted than for the undifferentiated LUHMES cell ones in figure 12 and there are a lot of different vesicles and cellular compartments in the pellet left for which only a fragment appear to be mitochondria. The amount of disrupted mitochondria could be caused by an increased swelling due to osmotic pressure or by the procedure of fixation and embedding.

Another sample was done using a combination of pestle and syringe. 10 B pestle strikes and 5 cycles of pulling in the homogenate with 18 G - 1.5 inch syringes and pushing out with 26 G - 1 inch syringes similar to the method used by Lampl et al. (2015)<sup>[42]</sup> were done. Negative stain (UA and PTA) as well as cryo EM showed similar results compared to before.

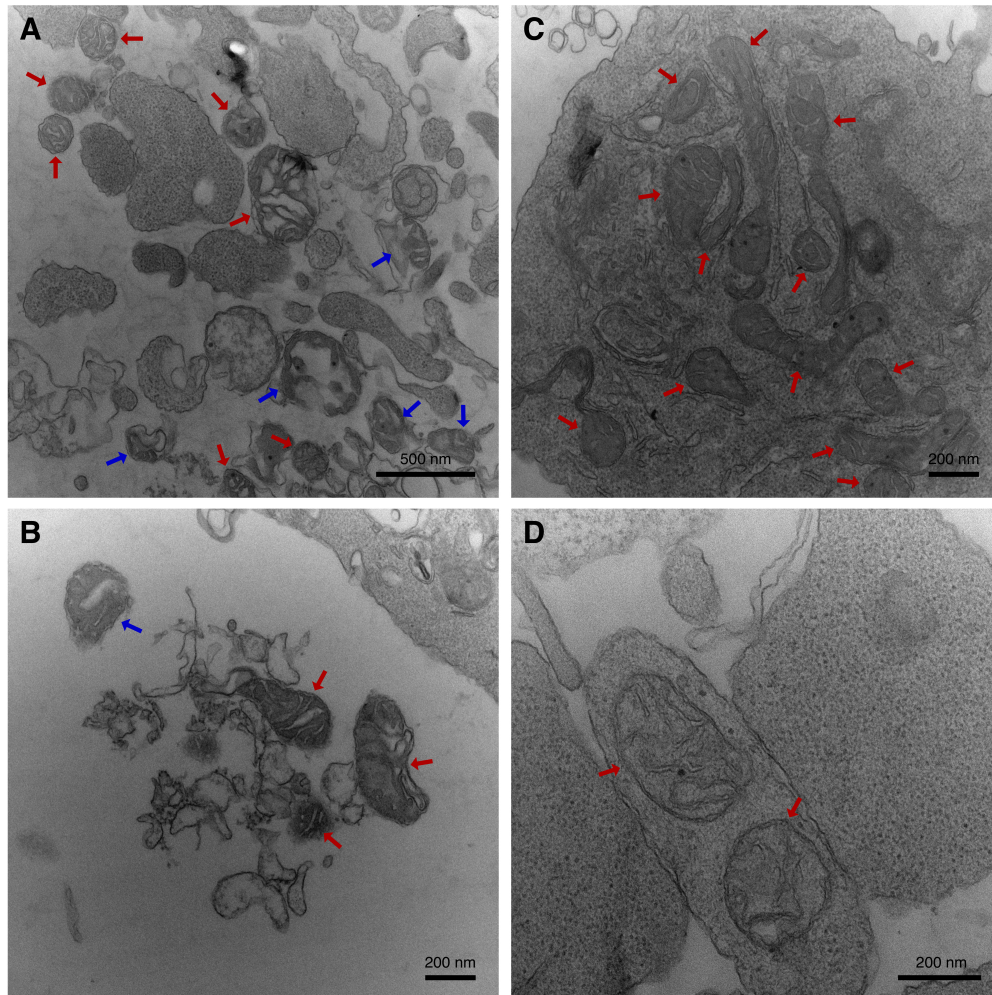


Figure 15: EM pictures of ultra-thin sections (200 nm) from para-formaldehyde and glutaraldehyde fixated and agarose embedded crude mitochondria pellets obtained by dounce homogenizer based isolation from differentiated LUHMES cells. Both pestle were used for homogenization with gentle strikes and reduced amount of strikes as well as higher centrifugation of the homogenate. **A** and **B** show isolated mitochondria (indicated by red arrows) which were to some degree destroyed (blue arrows) and a lot of cellular compartments/debris. **C** and **D** show mitochondria still surrounded by cytoplasm (be it in compartments as in **D** or more or less whole cells as in **C**). Interestingly those mitochondria differ greatly from each other and the ones in more or less whole cell bodies (**C**) seem to be elongated and resemble more the ones found in figure 12.

With additional informations obtained from the group of Werner Kühlbrandt at the Max Plank Institute of Biophysics a last dounce homogenizer based experiment was done with different buffer (MRBs, IBs and FB for the preparation of cryo EM grids). The cell suspension was rather harshly homogenized with the loosened pestle (A) for 75 strikes without generating an air bubble between pestle and suspension. The obtained homogenate was centrifuged at 2000 g for 5 min at 4°C, the supernatant separated from the pellet, the pellet resuspended and again homogenized 75 strikes with a pestle and centrifuged. The combined supernatants were centrifuged again at 2000 g for 5 min at 4°C and separated from the pellet. The supernatant was centrifuged at 12000 g for 10 min at 4°C and resuspended in 30 µL MRBs. The first 75 strikes thereby reduced the amount of living cells by 50%, which was again observed with Trypan Blue solution and counting chambers (Neubauer Improved) from Laboroptik. Interestingly the dead cells showed small, individual, intense blue compartments located at the cellular membranes of the dead cells (data not shown). These could be mitochondria, trapped in the dead cell body in a similar way as observed before with MitoTracker orange for dounce homogenized differentiated LUHMES cells (see figure 9). Ultimately, this remains unclear.

The dot-blot control as well as the on-grid 5 nm Au-bead (anti rabbit) labeled negative stain (UA) and the cryo EM results are shown in figure 16. The dot-blot shows strong signal for all fractions (too high concentrated samples, primary antibody from different batch taken) but none for the negative controls (figure 16  $\theta_1$  and  $\theta_2$  for MRBs and IBs). A positive control on the other hand ( $\theta_{positive}$ ) with 1:200 anti VDAC (rabbit) showed a strong response. The highest signals were obtained by the crude mitochondria fraction ( $\epsilon$ ) and the second pellet of unbroken cells and nuclei, obtained after the second homogenisation ( $\beta_2$ ). Supernatant of the second 2000 g centrifugation ( $\gamma$ ) and the 12000 g centrifugation ( $\delta$ ) showed slightly less intensity (but the presence of signal would suggest a loss of mitochondria during these steps) as well as the supernatant of the homogenisation steps ( $\beta^+$  and  $\beta_2^+$ ). However, since the signal was rather intense and for each (except the negative control) samples seen, a unspecific binding of the antibody to other proteins cannot be excluded.

As before the negative stain showed some possible mitochondria structures, but the on grid Au-bead (indicated with red arrows) did not seem to target any structure specifically, as for example shown in figure 16 **B**. Generally, the negative stain results showed similar structures as for all other samples with no significant alterations. The Cryo EM data on the other hand showed aside from some liposome-like vesicles a collection of structures that could be mitochondria as shown in figure 16 **C-E**. There are inner membranes for those structures that are folded and look like the crestaes of mitochondria. The thickness of the structures makes it difficult to see further details, but the membranes are well visible. Generally the structures were a little disordered, like for **D** and had part which were broken up or had different structures. They also resemble the swollen mitochondria in the fixated samples of figures 15 and 12 and therefore may be mitochondria. There were also accumulations of such structures found, as seen in figure 16 **E**. They seem to be consisting out of different substructures like the ones shown in **D**, which would mean that they are clustered mitochondria. This could be the case, since the pellet after centrifugation at 12000 g has to be loosened rather carefully to not destroy the obtained sample. The structure shown in **C** seem on the other hand to be the negative of **D**, concerning the thickness of the internal structures. Probably **C** contains simply some smaller vesicles (since all of the internal membranes visible look like separated, elongated vesicles and this structure was only found once). Aside from the spots where these structures were found the ice of the grid was again pretty thick.

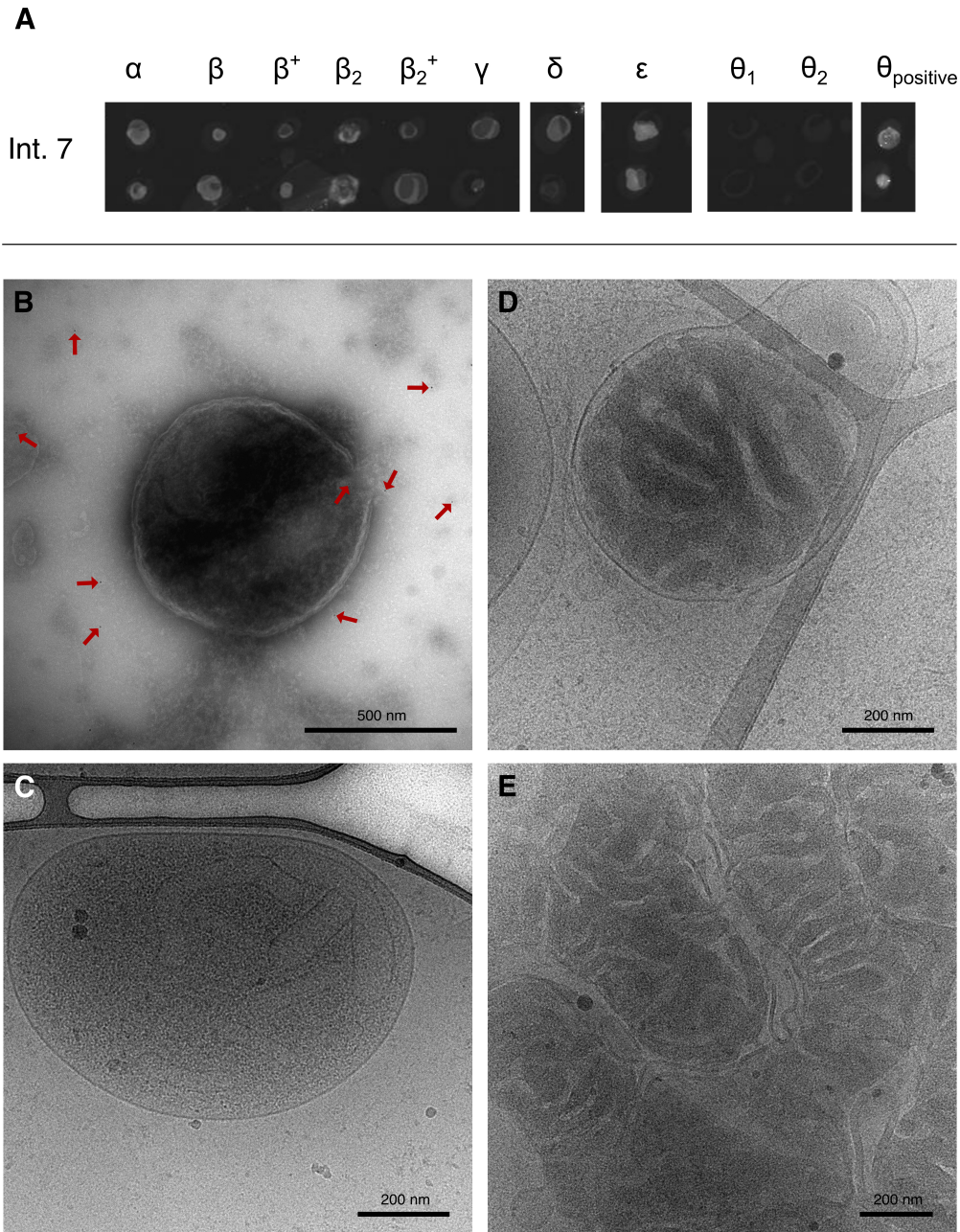


Figure 16: Dot-blot, cryo EM and Au-bead labelled negative stain (UA) EM pictures of the crude mitochondria fractions of dounce homogenizer based isolation from differentiated LUHES cells. Only loose (A) pestle and different set of buffers used as well as higher centrifugation of the homogenate. **A** shows the anti VDAC dot-blot results.  $\alpha$ : homogenate;  $\beta$ : pellet of unbroken cells and nuclei (first 75 strike homogenization);  $\beta^+$ : supernatant of pellet of unbroken cells and nuclei (first 75 strike homogenization);  $\beta_2$ : pellet of unbroken cells and nuclei (second 75 strike homogenization);  $\beta_2^+$ : supernatant of pellet of unbroken cells and nuclei (second 75 strike homogenization);  $\gamma$ : supernatant after second time 7000 g centrifugation of combined supernatant ( $\beta^+$  and  $\beta_2^+$ );  $\delta$ : supernatant of 12000 g centrifugation;  $\epsilon$ : crude mitochondria pellet after resuspension with MRBs;  $\theta_1$ : MRBs;  $\theta_1$ : IBs;  $\theta_{\text{positive}}$ : 1:200 anti VDAC (rabbit). Signal for all samples except negative controls  $\theta_1$  and  $\theta_2$ . Unspecific binding of antibody cannot be excluded. Nevertheless,  $\beta_2$  and  $\epsilon$  showed the strongest signals. **B** shows an on-grid 5 nm Au-bead (anti rabbit) labelled result. Although structures that could be mitochondria were found no specific targeting of any structure took place (Au beads indicated by red arrows). **C-E** shows the obtained cryo EM results. Although the ice was very thin some spots showed structures with a second internal membrane that seemed to have formed folded structures as mitochondrial cristae. Structures like **D** also seem to cluster together as seen for **E**, which might be due to the pelleting of the crude mitochondria sample.



Fixation of the same sample showed a wide variety of vesicular structures around the same size, as seen in figure 17 **A** and **B**. Some of them resemble mitochondria as they possess a folded inner membrane that reminds of the cristae. These structures are indicated by red arrows in figure 17, whereas the internal membranes are indicated by green arrows. Compared to other fixation results (figures 12 and 15) no intact cell sized structures are found anymore, indicating an effective rupture of the cells by nitrogen cavitation and differential centrifugation. It is to note that most of the mitochondria structures do not seem as swollen as the ones of the other fixations, however, they are not well structured and seem to be often damaged (ruptured as indicated by blue arrows in figure 17 **A**). This could be due to the homogenization or the buffer used or due to the process of fixation. Interestingly they do not seem to resemble the structures of the mitochondria found by cryo EM as much as the swollen fixated ones from figures 12 and 15. Additionally it is worth mentioning that the sample used for fixation wasn't fresh anymore but thawed for the second time, therefore freezing-thawing cycle damage could also be responsible for the structural damages. Nevertheless, these fixated results show some mitochondrial together with a large amount of other lipid structures.

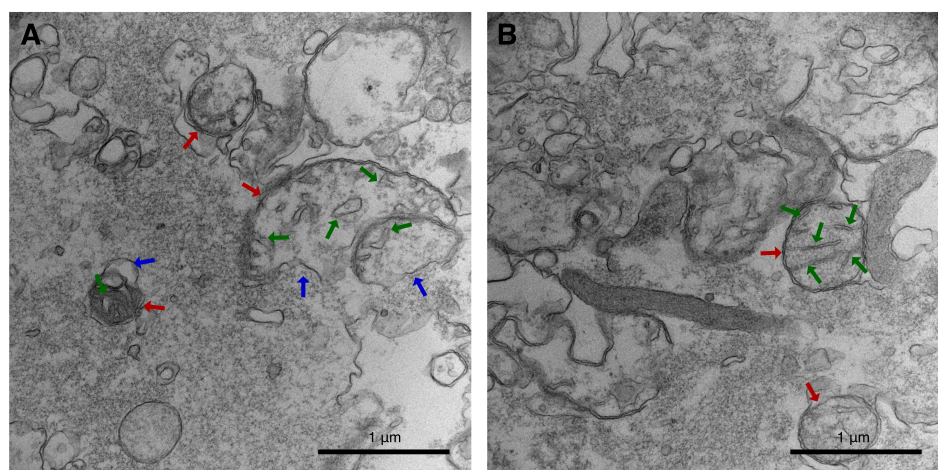


Figure 17: EM pictures of ultra-thin sections (200 nm) from para-formaldehyde and glutaraldehyde fixated and agarose embedded crude mitochondria pellets obtained by dounce homogenizer based isolation from differentiated LUHMES cells (pestle A). **A** and **B** showing overviews of lipid structures of which some resemble mitochondria, which are indicated by red arrows. The internal membrane with cristae-like structures is indicated by green arrows and ruptures are indicated by blue arrows in **A**.

Concerning the generation of thick ice and low contrast in cryo EM different ideas were considered. They went from different buffers (with or without mannitol) to different blotting methods (such as back-side blotting, so the sample has to be drawn through the grid), times (1.5-5 s with or without after blotting time of up to 3 s) and grids (quantifoil 3.5/1 or Lacey C only 300 mesh Cu). However, none of them seemed to have solved the problem of the thick ice. The best method in the end was the use of Lacey grids, a special freezing buffer with trehalose instead of mannitol and sucrose and a 3 µL sample drop. The blotting was done manually by gently pressing the blotting paper over half of the grid (to generate a gradient of thickness), waiting until the liquid border on the filter paper stopped and waiting from this moment on another 5 s before plunging.

## 5.4 Nitrogen Cavitation

Nitrogen cavitation was done using a 4635-39 cell disruption vessel from Parr. The vessel was cooled on ice and a magnetic stirrer was added. Two experiments with differentiated LUHMES cells were conducted at pressures of 1100 psi (sample one) and 1500 psi (sample two) for 30 min with magnetic stirring of 600 rpm (sample one) 900 rpm, respectively (sample two), using a IKA RCT basic IKAMAG safety controll magnetic stirrer. For sample one the normal buffers (SB, IB<sub>cells</sub> - 1 and MRB) were used, whereas for sample 2 the buffers based on the visit of the Max Plank institute were used (IBs, MRBs and FB for cryo EM). The cells were resuspended as before following the procedure shown in figure 3. In both cases a massive amount of foam was produced upon releasing the sample from the cavitation chamber, whereas the volume of the foam was considerably bigger than that of the solution, and the amount of living cells was in both cases reduced by >99%, as observed with Trypan Blue solution.

For the first nitrogen cavitation based homogenisation (sample one), the obtained foam/liquid homogenate was centrifuged at 1500 g for 5 min at 4°C to avoid cellular leftovers as observed for the dounce homogenizer experiments above. Interestingly there was no pellet visible and the foam did not disintegrate. A further centrifugation of 7000 g for 5 min at 4°C, however let the foam disappear and a pellet was visible. A further resuspension of the pellet and 800 g centrifugation for 5 min at 4°C revealed however a pellet, suggesting that a considerable amount of broken up cells and nuclei might be present in the foam. After a subsequent 1500 g centrifugation for 5 min at 4°C of the supernatant a second pellet of unbroken cells and nuclei appeared. Finally the supernatant was centrifuged at 12 000 g for 10 min at 4°C and the final crude mitochondria pellet was resuspended in MRB. A schematic of this changed procedure of differential centrifugation is shown in figure 18 A.

The dot-blot shown in figure 18 B was primarily used here to monitor the procedure by showing the presence of mitochondria (or VDAC, to be exact) in the different steps. For this, samples were taken for the liquid homogenate ( $\alpha$ ), the estimated position where the pellet after the first 1500 g centrifugation should have been (unbroken cells and nuclei; pellet was not seen) ( $\beta$ ), corresponding supernatant of this first 1500 g centrifugation was also taken ( $\beta^+$ ), supernatant after 7000 g centrifugation ( $\gamma$ ), the pellet after 800 g ( $\delta$ ) and the crude mitochondria fraction ( $\epsilon$ ). Additionally MRB as a negative sample ( $\theta$ ) was taken. In figure 18 A those samples are shown as well for clarification. Although in previous experiments the pellet obtained from unbroken cells and nuclei showed a significant signal (see figures 11, 13 and 16), the first pellet after centrifugation of the homogenate ( $\beta$ ), which was not visible, showed a very weak signal, whereas the supernatant ( $\beta^+$ ) showed a stronger signal. This clearly proves the absence of a pellet of unbroken cells or mitochondria containing cellular leftovers, as observed by the naked eye. However, due to the homogenisation such a pellet should be present to a certain degree. Interestingly, the 800 g centrifugation afterwards ( $\delta$ ; no foam anymore) clearly shows a presence of a pellet, as observed by the naked eye, and this pellet showed a strong signal. It should be noted that this dot-blot was done together with the dot-blot of the last dounce homogenizer based experiment (figure 16) and as previously mentioned an unspecific binding cannot be excluded. Nevertheless, the dot-blot shown in figure 18 A proves the appearance of a pellet only after the foam disappeared. This would indicate that the foam somehow suspends a portion of cellular fragments that could be easily spun down at 800 g but in the presence of foam it is not possible at 1500 g. This in return requires a change of the differential centrifugation protocol.

Negative stain (UA) results of the crude mitochondria pellet showed a lot of vesicular structures around 500 nm in size, which could be mitochondria, as visible in figure 19 A, where the cell debris is present but reduced compared to the negative stain results of dounce homogenizer

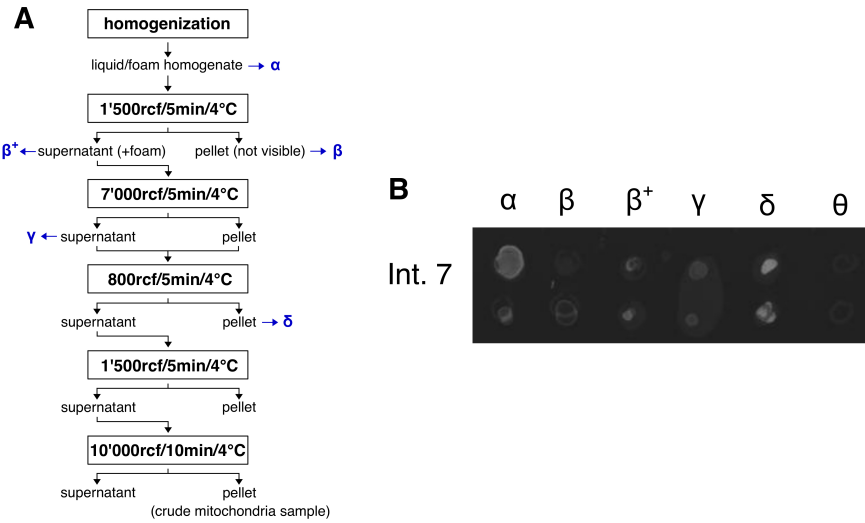


Figure 18: Schematic procedure (**A**) of differential centrifugation and obtained dot-blot (**B**) of nitrogen cavitation based homogenisation and differential centrifugation isolation of differentiated LUHMES cells (sample one). The protocol of differential centrifugation had to be changed as shown, mainly due to the foam formation and absence of cellular debris pellet. Positions of used samples for dot-blot are also shown in the schematic procedure in blue.  $\alpha$ : homogenate;  $\beta$ : the estimated position where the pellet after the first 1500 g centrifugation should have been (unbroken cells and nuclei; pellet was not seen);  $\beta^+$ : corresponding supernatant of this first 1500 g centrifugation;  $\gamma$ : supernatant after 7000 g centrifugation;  $\delta$ : pellet after 800 g centrifugation;  $\theta$ : MRB as negative control. Strangely pellet of cellular debris only appeared after foam disappeared (resuspended pellet obtained by 7000 g centrifugation). All sample except the negative control showed signals. Remarkably the pellet after 800 g centrifugation ( $\delta$ ) showed the highest concentration and  $\beta$  showed a very weak signal, indicating no pelleting in the first centrifugation step has taken place or at least not for labeled particles.

based results. The observed possible mitochondria structures were similar as the ones observed before for dounce homogenized samples. However, on-grid 5 nm Au-bead (anti rabbit) labelling showed no accumulation at these structures, as observed before for the dounce homogenized samples (data not shown). Additionally the Au-labelled grids were densely covered with sample and stain and sometimes hard to focus on. This is most likely an artefact of the on-grid staining procedure. Figure 19 **B-F** shows a selection of the obtained cryo EM results. Cellular debris and liposome-like vesicles (**B**) were visible as usual, but also some thicker vesicle, for which it is hard to obtain information about the inside (example shown in **C** and **D** with **E** and **F** as magnifications). It is possible to identify an outer and an inner membrane, as shown in **E** and **F** by red arrows. Also an internal structure could be visible, as indicated by blue arrows in **E** and **F**, however, the vesicle seem to be quite thick. It is possible that those are mitochondria which are still in good shape, what could explain the thickness of these structures. On the other hand it could also be that those are simply cellular compartments, filled with cytoplasm, such as those already seen in the fixated dounce homogenized sample (see figure 12). Nevertheless, they do not look similar to the structures found in figure 16 **D** and **E** but more like the one in figure 16 **C**.



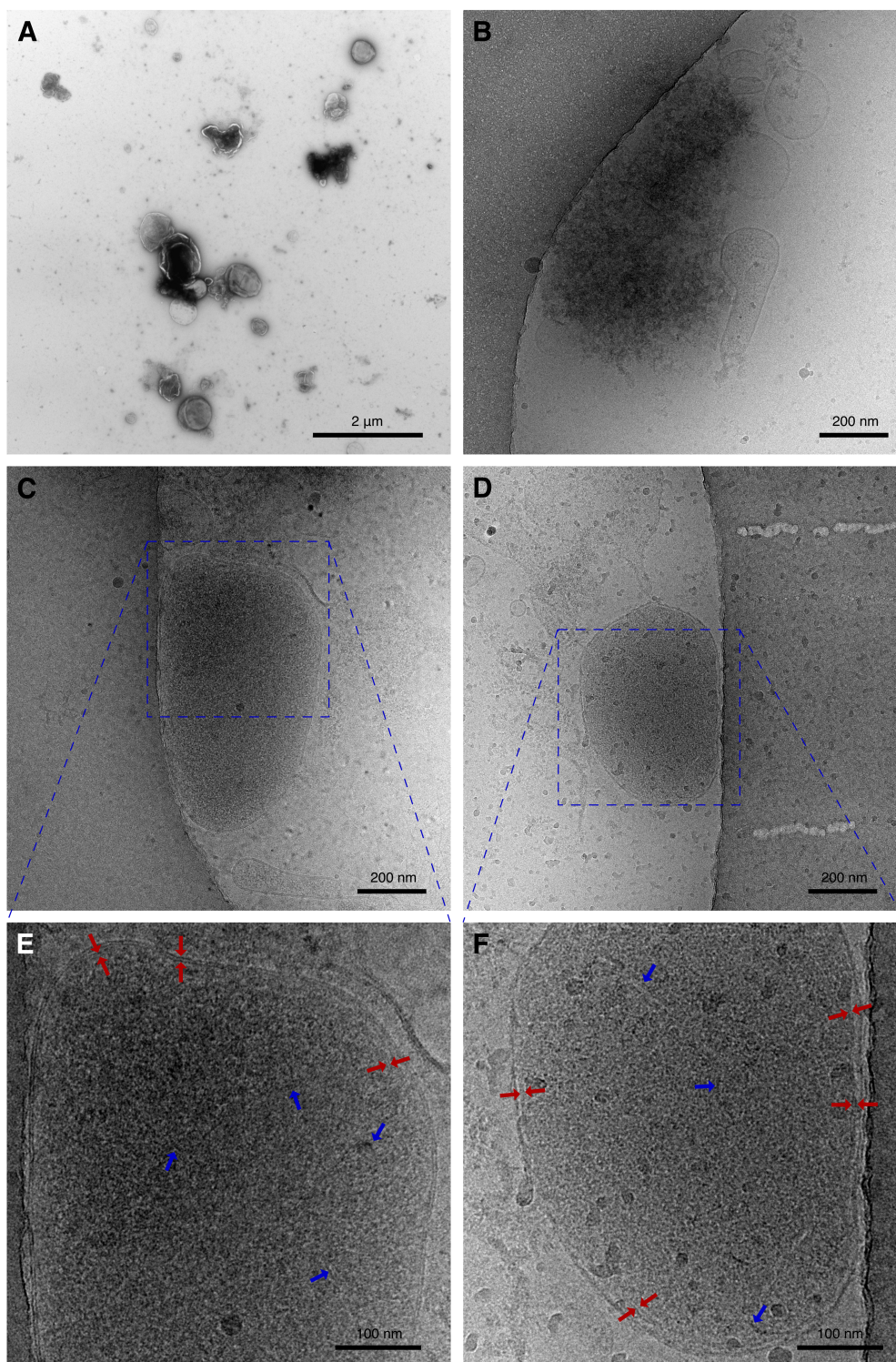


Figure 19: Cryo EM and UA negative stained EM pictures of the crude mitochondria fractions of nitrogen cavitation based isolation from differentiated LUHMES cells (sample one). **A** shows an exemple negative stain (UA) picture of the sample with differently sized vesicular structures. **B-F** show cryo EM results. In **B** the predominant structures such as cellular debris and liposome-like vesicles are seen, however, **C** and **D** show thicker structures with internal membranes (indicated by red arrows) and possible internal structures (indicated by blue arrows), which are especially well seen in the magnifications **E** and **F**. Those structures could be rather healthy and therefore thicker mitochondria.

For the second nitrogen cavitation based homogenisation (sample two), a 1500 g centrifugation for 5 min at 4° of the foam/liquid homogenate again didn't reveal any pellet of unbroken cells and nuclei and a large foam volume was again observed. The speculation that the BSA is responsible for the large foam production is demoted by the large foam production for sample one of the nitrogen cavitation experiments, where no BSA containing buffer (IB) was used. This time however, the foam/liquid solution was centrifuged a second time at 2000 g for 5 min at 4° (again no pellet was visible) and the liquid supernatant was centrifuged for 12 000 g for 10 min at 4°C to generate a crude mitochondria pellet. Again, the pellets were not visible until the last step. Either there is only very little cellular debris – which is not possible, since the amount of cellular debris/nuclei etc. should be bigger than the mitochondria output in the end – or the cellular debris is fractionated in very small parts or the foam is in some sort responsible. The schematic procedure as well as the samples taken for the dot-blot are shown in figure 20 A. The dot-blot following these different steps shows a signal in all fractions as shown in figure 20 B, except the negative control (MRBs). Since the dot-blot was made together with the one of the previous nitrogen cavitation (figure 18 B) and the last dounce homogenizer experiment (figure 16), the possibility of unspecific binding of the primary antibody cannot be excluded. This would also explain why all samples shown in 20 A showed a signal (except the control). Nevertheless one can see a bright signal for the final crude mitochondria pellet ( $\epsilon$ ) and basically no signal for the corresponding supernatant ( $\gamma$ ). Out of the other signals, especially the one for the estimated place of the pellet after the 2000 g centrifugation ( $\beta_2$ ) showed a higher signal than the samples before ( $\beta$  and  $\beta^+$ ) indicating some kind of pelleting. It is to note, that the foam sample ( $\beta_2^+$ ) also showed a signal, which means there are some proteins (if unspecific binding occurred with the antibody) or mitochondria (if specific binding happened) within the foam.

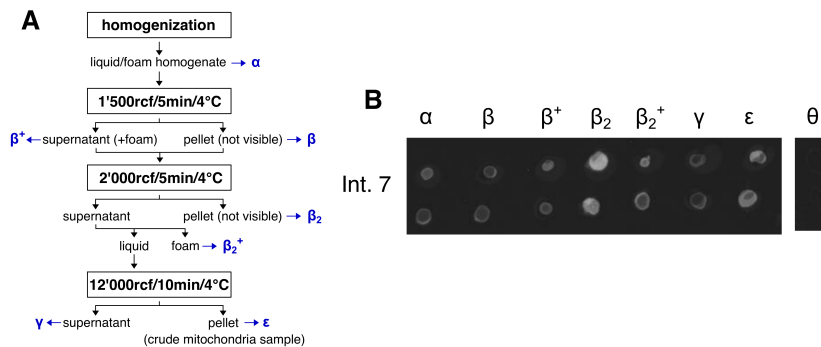


Figure 20: Schematic procedure (A) of differential centrifugation and obtained dot-blot (B) of nitrogen cavitation based homogenisation and differential centrifugation isolation of differentiated LUHMES cells (sample two). Protocol of differential centrifugation was changed as shown. Positions of used samples for dot-blot are also shown in the schematic procedure in blue.  $\alpha$ : homogenate;  $\beta$  estimated position where the pellet after the first 1500 g centrifugation should have been (unbroken cells and nuclei; pellet was not seen);  $\beta^+$ : corresponding supernatant of this first 1500 g centrifugation;  $\beta_2$ : estimated position where the pellet after the 2000 g centrifugation should have been (pellet was not seen);  $\beta_2^+$ : foam sample after 2000 g centrifugation;  $\gamma$ : supernatant after 12 000 g centrifugation;  $\epsilon$ : crude mitochondria fraction and  $\theta$ : MRBs as negative control. Signals visible for more or less every sample except negative control. Although no visible pellet was seen the strong signal for  $\beta_2$  suggests some kind of pelleting.  $\beta_2^+$  shows a certain signal for the foam, this means some targeted particles are located within the foam, caused by nitrogen cavitation.

Subsequent on-grid 5 nm Au-bead labelling (anti rabbit) of the crude mitochondria fraction showed no or very weak targeting of any observable structure. The structure in figure 21 **A** shows a disrupted vesicle with faint Au-bead targeting or aggregation (Au-beads indicated by red arrows). However, the Au-bead concentration is rather weak and could also be just coincidence.

At the same time, a larger amount of cellular debris and fewer vesicles than in sample one of the nitrogen cavitation experiments were found for the sample two (similar to the negative stain results from dounce homogenisation). The presence of larger contamination correlates with the absence of any visible pellet in the differential centrifugation steps.

The usage of PTA as negative stain showed similar results concerning the Au-labelling as the UA labelled ones, further supporting that the faint targeting in **A** was just a coincidence. However, for PTA the vesicles seemed sometimes better preserved and containing a wool-like interior (as shown in figure 20 **B** and **C**). Interestingly, on-grid 5 nm Au-bead labelling with protein A as secondary “antibody” resulted in a observable staining of certain vesicles, as shown in figure 20 **D** (indicated by red circles), but not cellular debris or all vesicles. This in return proves a certain selectivity and labelling of the targeted structures to be mitochondria. The obtained result here further supports the dot-blot findings of mitochondria presence in the crude mitochondria fraction.

Cryo EM results were again hard to obtain due to the thick ice and relatively low sample concentration in the observable holes. The structures visible were liposome and cellular debris as observed for the samples before. However, aside from those, seemingly thicker liposome-like structures of multiple 100 nm size as shown in figure 22 **A** were found. Upon closer examination (**B**) the central part of some of these structures harbour additional membranes (indicated by red arrows). These findings resemble the ones shown in figure 19 and very likely represent mitochondria. Again they do not resemble the structures found in figure 16 **D**, but could represent healthier mitochondria which are thicker and therefore do not allow such a clear view of their inside.



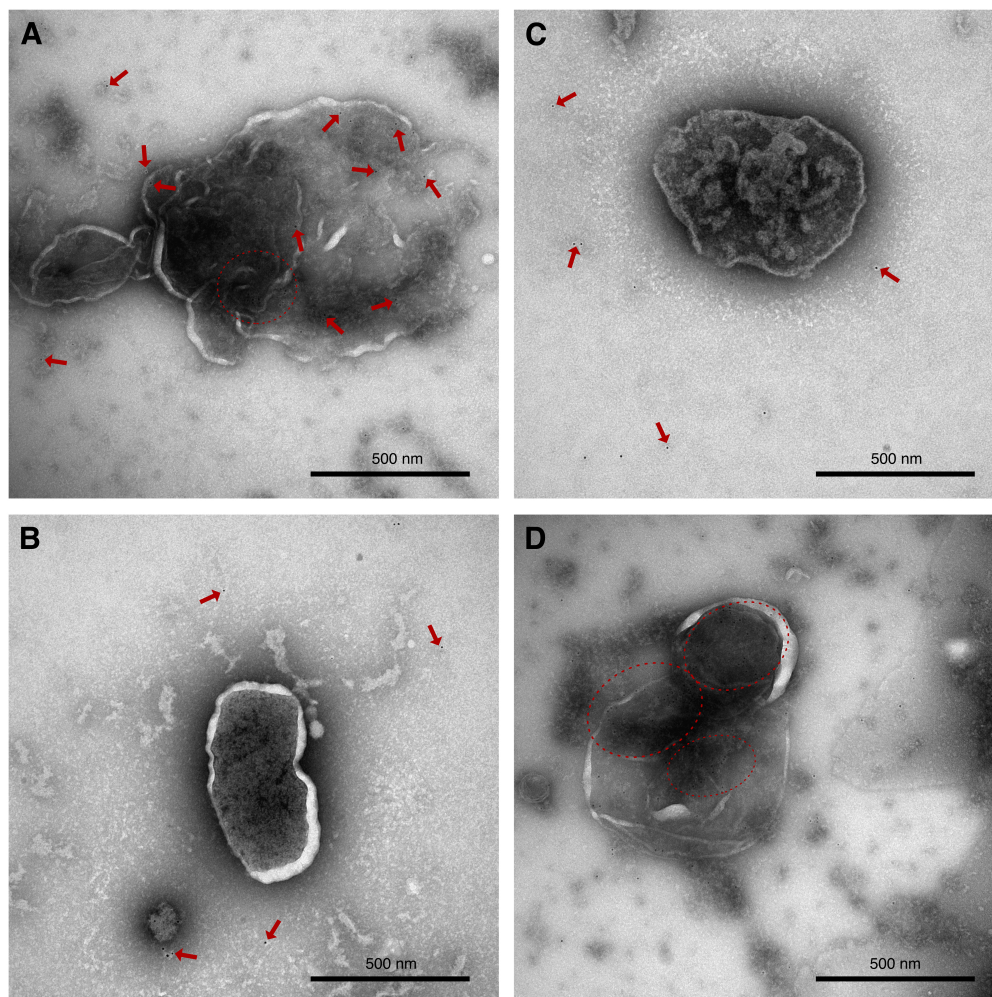


*Figure 21: On-grid 5 nm Au-bead (anti mouse and protein A) labelled negative stained (UA for **A** and **D**; PTA for **B** and **C**) EM pictures of the crude mitochondria fractions of nitrogen cavitation based isolation from differentiated LUHMES cells (sample two). **A-C** showing anti rabbit Au-bead labelling (indicated by red arrows). No or very weak significant targeting was observed here and the structures resemble the ones found for dounce homogenized samples. The use of PTA as negative stain in **B** and **C** showed a fuzzier interior of the observed structures than UA negative stained ones (**A**). Au-bead labeling with protein A as exemple shown in **D** yield a labelling of certain structures (indicated by red circles). However, since not all observed structures were labelled, the specificity of labelling indicated those structures as mitochondria.*

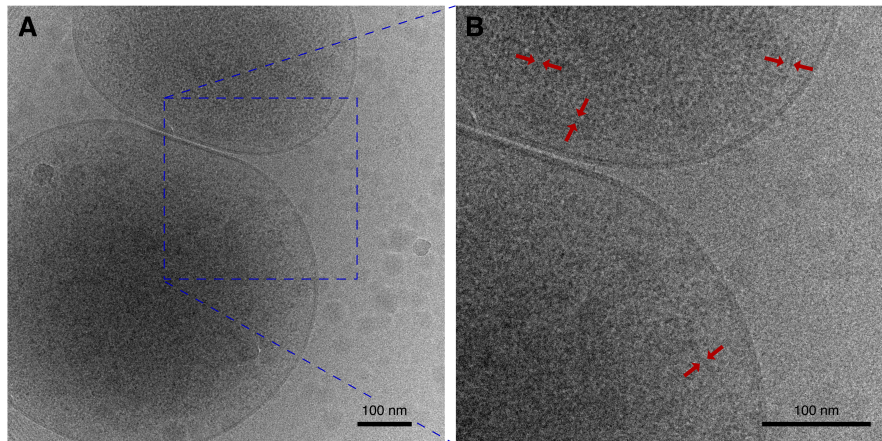


*Figure 22: Cryo EM pictures of the crude mitochondria fractions of nitrogen cavitation based isolation from differentiated LUHMES cells (sample two). **A** shows two liposome-like structures which have a thicker interior that doesn't allow a clear view. **B** shows a magnified view of **A**, where internal membrane structures were found (indicated with red arrows). These structures could represent the cristae and therefore identify the structures as mitochondria.*

Fixation of the same sample (sample 2) showed a wide variety of vesicular structures around the same size, as seen in figure 23 **A** and **B**. Some of them resemble the found cryo data shown in figure 22, as they possess a folded inner membrane that reminds of the cristae in mitochondria. These structures are indicated by red arrows in figure 23, whereas the internal membranes are indicated by green arrows. Compared to other fixation results (figures 12 and 15) no intact cell sized structures are found anymore, indicating an effective rupture of the cells by nitrogen cavitation and differential centrifugation, similar to the findings of figure 17. It is to note that most of the mitochondria structures do not seem as swollen as the ones of the other fixations, however, they are not well structured and seem to be often damaged (ruptured or with swollen parts, as seen in figure 23 **C**). This could be due to the homogenization or the buffer used or due to the process of fixation. Additionally it is worth mentioning that the sample used for fixation wasn't fresh anymore but thawed for the second time, therefore freezing-thawing cycle damage could also be responsible for the structural damages. Nevertheless, these fixated results resemble the ones found for 17 and show some mitochondrial structures together with a large amount of other lipid structures.



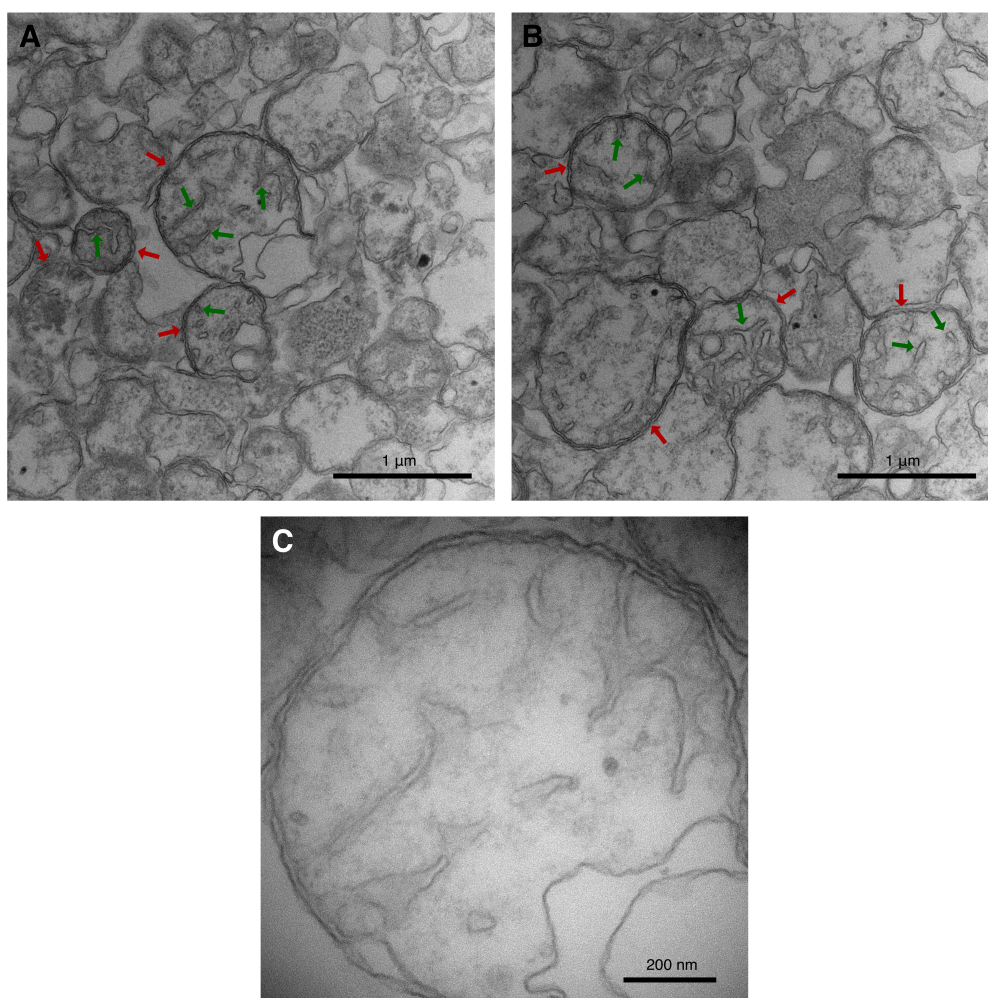


Figure 23: EM pictures of ultra-thin sections (200 nm) from para-formaldehyde and glutaraldehyde fixated and agarose embedded crude mitochondria pellets obtained by nitrogen cavitation based isolation from differentiated LUHMES cells (sample 2). **A** and **B** showing overviews of lipid structures of which some resemble mitochondria, which are indicated by red arrows. The Internal membranes with cristae-like structures are indicated by green arrows. **C** shows a more detailed view of such a structure, whereby the lower right corner seem to be disformed.

## 6 Discussion

One of the biggest problems during the experiments was the constant need of fresh crude/pure mitochondria samples to work with, since the isolated mitochondria lose their membrane potential over time if isolated and damages or structural changes can occur. A possible storage would be a drop-wise freezing of the sample in liquid nitrogen and storage at  $-80^{\circ}\text{C}$  as it is done by Niklas Klusch from the Max Plank Institute of Biophysics. However, in order to do so a higher amount of mitochondria (crude or purified) would be needed, which is easier to obtain from less demanding organisms like yeast or other single celled organism. However, a T175 cell culture flask of differentiated LUHMES cells contained between 400'000-800'000 healthy and living cells to work with (measured before homogenisation) and in this project it was usually worked with 1-2 T175 cell culture flasks for one experiment. Likely this amount of cells generated by far too less crude mitochondria sample for the Percoll purification, as shown for sonicated and dounce homogenizer based results in figure 4 C and D or mentioned in chapter 5.3 **Dounce Homogenisation**. Therefore, further purification with Percoll as suggested by Wieckowski et al. (2009)<sup>[46]</sup> was not longer pursued.

### 6.1 Increase in Cell Count

A higher amount of cells would have generated a bigger crude mitochondria pellet, which would in return have been helpful since it is possible to see by the naked eye that the obtained pellet is a mitochondrial pellet. Pellets with mitochondria appear brownish instead of white, however, with the small amount of cells used in this project the pellets were always white to yellowish. A higher concentration of the crude mitochondria fraction would have helped finding mitochondria in cryo EM. But for this Master's Thesis it was decided to use a smaller amount first, to evaluate the best method by changing the procedure until the outcome is satisfying to work with bigger amounts of cells. Looking back, this may have been misguided and bigger amounts of cells would have been needed from the start.

### 6.2 Resilience of Differentiated LUHMES Cells

Interestingly, for the comparison of HEK 293FT, SH-SY5Y, undifferentiated and differentiated LUHMES cells, the obtained results reveal some differences. Differentiated LUHMES cells appeared robuster than undifferentiated cells, as is made evident in the early sonication experiments. While undifferentiated cells died rather quickly, the differentiated cells seem to be more sturdy and need more pulses to die. At the same time HEK 293FT cells seem to be easier to homogenize than differentiated LUHMES cells. Their death-rate during sonication seems higher as well as during dounce pestle based homogenisation, compared to LUHMES cells at similar conditions. HEK 293FT cells seem much more sensible to pestle strikes than differentiated LUHMES cells, as at the same amount of pestle strikes, the ratio of surviving HEK 293FT cells to the amount of living cells before homogenisation is lower than the one for differentiated LUHMES cells. Generally, the differentiated LUHMES cells seem to be rather tough. While the protocol of Wieckowski et al. (2009)<sup>[46]</sup> recommended to damage 80-90% of the cells in his HeLa and MEF cell based protocol, up to 150-200 dounce homogenizer pestle strikes (tight or/and loose pestle) were needed to reach only around 70% damaged cells.

### 6.3 Adaptions of Protocol

Generally, the whole protocol of Wieckowski et al. (2009)<sup>[46]</sup> had to be adjusted. Already in the beginning some changes were made for the preparations of the cells before homogenisation, since elongating theses steps may result in an increased cell loss. However, during the experiments one of the most dramatic changes had to be done for the process of homogenisation itself. While for the first dounce based homogenisation results, the goal was to damage around 60-70% of the cells, the risk of overhomogenisation was drastically increased. This is most likely one of the reasons why no intact mitochondrial structures were found in the beginning. However, MitoTracker orange results, dot-blot results (figure 11; figure 13) and formaldehyde respectively glutaraldehyde fixated sample (figure 12) show a presence of mitochondria in the crude mitochondria sample. But at the same time fixation results (figure 12), negative stain results and even MitoTracker orange results (figure 9) show a massive amount of cellular debris as whole cells or nuclei, which should have been removed by differential centrifugation. Therefore the amount of structural intact and viable mitochondria in theses sample was too small to obtain satisfying results or cryo EM results at all. Additional experiments with reduced pestle strikes and reduced force yielded only a small reduction of living cells and large contaminations of cell debris in the crude mitochondria sample, as shown by additional fixation with para-formaldehyde and glutaraldehyde with agarose embedding (figure 15).

Although the number of strikes was reduced, the mitochondria still showed damages and increased swelling if they were isolated. A change of buffer to a higher concentration of sucrose and without mannitol as well as a massive increase of centrifugation force after homogenisation yield a better cryo result in the end. The fixated samples with new buffer and higher centrifugation force (figures 17 and 23) showed indeed a reduction of large cellular debris as whole cells and the mitochondrial structures appear to be in better shape (not swollen). However, they were still damaged, which could come from a longer storage with multiple thawing-freezing cycles of the sample (twice), the method of homogenisation or the fixation method. Additionally, there is still a considerable amount of membrane or vesicle debris visible. The rest of the obtained data for those samples, such as negative stain or Au-labelling, remained similar.

Therefore the buffers as well as the centrifugation force had to be adjusted. For the buffers the different groups in the literature generally employ similar substances with slight variations, one of which is the use of mannitol or just sucrose, where some groups seem to report differences while other do not.<sup>[27][45]</sup> While the pH-buffering (Tris-HCl/Tris-MOPS and HEPES) and the  $\text{Ca}^{2+}$  absorbing EGTA concentrations only vary slightly, the sucrose/mannitol concentration is probably the value that has to be adjusted, so the osmolarity is similar to the mitochondria environment. However, since this concentration is oscillating for different groups in the literature around 200-300 mM (even for same cell types as MEF cells)<sup>[27][46]</sup> it was decided to stick to the protocol until the last samples. This is mostly due to the fact that all other parameters were already slightly changed during the project. The usage of different methods, as MitoTracker orange, dot-blot and fixation, showed that the buffers are not maladjusted but might need some further adjusting to improve the result.

For the adjustments of the differential centrifugation protocol the main difference was in the increase in centrifugation force of the fresh homogenate. In literature theses value vary in a similar way as the amount of pestle strikes needed for homogenisation. Commonly used are 600 g<sup>[27][42][46]</sup>, 800 g<sup>[30]</sup>, 1000 g<sup>[51][53]</sup>, 1200 g<sup>[30]</sup>, 1300 g<sup>[45]</sup> and 1500 g<sup>[47]</sup> (also used by Niklas Klusch). The results shown here indicate that with 600 g and even 800 g too much cellular debris in form of whole cellular compartments and nuclei were in the crude mitochondria pellet. Upon increasing the force to 2000 g the samples mainly consisted out of similar sized lipid structures, mitochondria and cellular debris, as seen in a comparison of figures 15 and 17. Additional purifi-

cation with a Percoll gradient might be able to reduce the amount of lipid structures even further and increase the mitochondria density. However, for successfully further purify the crude mitochondria sample, the mitochondria need to be viable and without too much structural damage. Although there were no specific results in this project that indicate an improvement of the purity of the crude mitochondria fraction with increased centrifugation force, the results got better over the course of changes, whereby increasing the centrifugation force was one of those steps. Figure 24 shows the final protocol used for dounce homogeniser based isolation of mitochondria from differentiated LUHMES cells up to the crude mitochondria sample with the mentioned changes. This was the protocol used for the last mitochondria isolation mentioned in chapter 5.3 **Dounce Homogenisation** and represents the best protocol developed during this Master's Thesis.

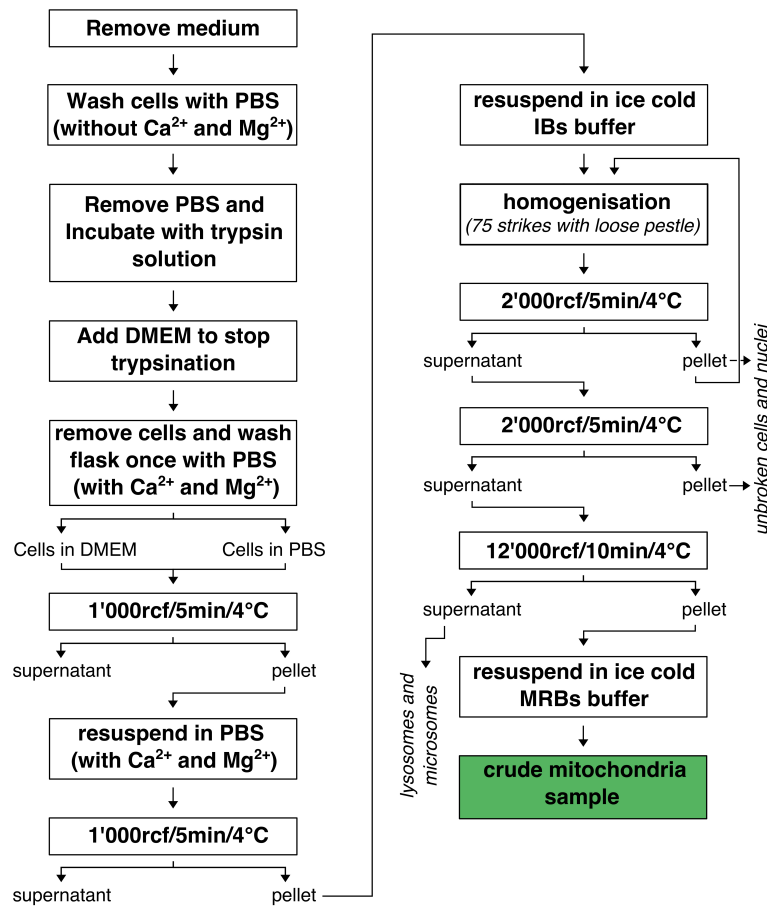


Figure 24: Schematic of the final protocol developed for mitochondria isolation from differentiated LUHMES cells based on dounce homogenisation. This protocol was developed based on the protocol of Wieckowski et al. (2009)<sup>[46]</sup> and contains all the mentioned changes to improve the results specifically for differentiated LUHMES cells. **rcf** stands for relative centrifugal force and can essentially be translated as g-force.

## 6.4 Nitrogen Cavitation and Dounce Homogenisation Show Success

Dounce pestle based homogenisation as well as nitrogen cavitation showed the best results. Potter-Elvehjem and sonication based homogenisation on the other hand bear too much risk of overhomogenisation. Although especially the Potter-Elvehjem based method should be conducted again with the improvements found during the dounce homogenizer based experiments for a final decision. The only result shown so far is that the amount of strikes to damage cells with a Potter-Elvehjem homogenizer is higher than with a dounce homogenizer. Together with the additional shear force (rotation) the higher amount of strikes can result in a huge increase of overhomogenisation. Therefore, the only conclusion concerning the comparison of the Potter-Elvehjem to the dounce homogenizer here is that the dounce homogenizer is more efficient and therefore better suited for smaller samples.

Similar to dounce pestle based homogenisation the nitrogen cavitation based homogenisation showed possible mitochondrial structures in cryo EM (figures 19 and 22). However, whereas the mitochondrial structures found by dounce homogenisation (figure 16) resemble the mitochondria from the fixated samples (figures 12 and 15) and seem to have some defects such as ruptured or swollen parts, the mitochondria structures obtained by nitrogen cavitation are delicate and the inner mitochondrial membrane is not as well visible as for the dounce homogenisation based mitochondrial structures. However, the fixation of the same sample (shown in figure 23) shows similar structures as the ones found by cryo EM, supporting the identification of those structures as mitochondria. As visible from figure 25, the mitochondrial structures obtained by dounce homogenisation (figure 16) look exactly like cryo EM pictures from Gold et al. (2017)<sup>[52]</sup> of mitochondria isolated from *D. Melanogaster* (figure 25 **A**) or results from Brandt et al. (2017)<sup>[30]</sup> for mitochondria isolated from mouse liver (**B** and **C**). The structure of mitochondria isolated by nitrogen cavitation (figures 19 and 22) on the other hand look more like the cryo EM results of isolated yeast mitochondria from Gold et al. (2017)<sup>[52]</sup> (figure 25 **D**). Interestingly, Brandt et al. (2017)<sup>[30]</sup> found by cryo EM aside from the mitochondria with clearly visible cristae (figure 25 **A**) also ones with less visible cristae for *D. Melanogaster*, as shown in figure 25 **D** and **F**. This means there are both mitochondrial structures in the same organism present, which further supports the statement that figures 19 and 22 show mitochondria.

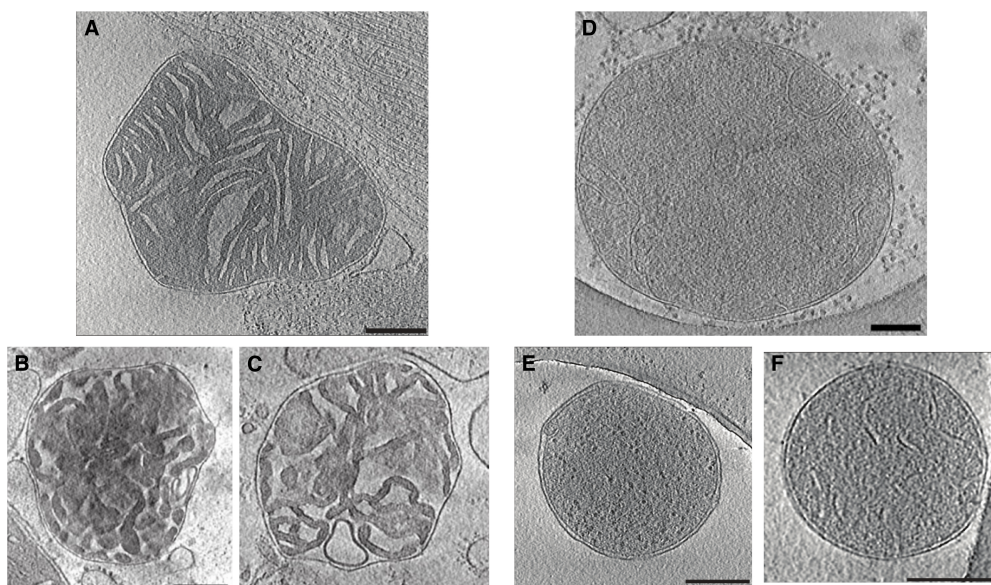


Figure 25: **A-C** are showing cryo EM pictures of mitochondria with well visible cristae. **A**: *D. Melanogaster* mitochondria by Brandt et al. (2017)<sup>[30]</sup>. Scale not shown. **B** and **C**: Mouse kidney mitochondria by Brandt et al. (2017)<sup>[30]</sup>. Scale bars, 250 nm. Showing mitochondria with morphological similarities to those in apoptotic cells. **D-F** show cryo EM pictures of mitochondria with less visible cristae. **D**: yeast mitochondria by Gold et al. (2017)<sup>[52]</sup>. Scale bar, 200 nm. **D** and **F**: *D. Melanogaster* mitochondria by Brandt et al. (2017)<sup>[30]</sup>. Scale not shown.

It should be mentioned that the cristae structure shown in figure 25 **B** resembles the morphology of a mitochondria in an apoptotic cell, as described by Brandt et al. (2017)<sup>[30]</sup>. Comparing the cristae structure to the structures found by cryo EM for the first batch of dounce homogenized HEK 293FT cells (figure 8 **D**) or the structures in figure 5 **E** and **F** or figure 7 **H** for Au-labelled sonicated differentiated LUHMES cells and tight (B) pestle only dounced homogenized differentiated LUHMES cells, respectively, a similarity is seen. Therefore it is possible that these structures represent disrupted mitochondria, which would also explain the visible Au-labelling, and therefore further indicate an overhomogenisation of those samples.

For the nitrogen cavitation the excessive foam production after release of the cell suspension is noteworthy. The presence of this foam however did not significantly disturb the outcome, since mitochondria structures were found regardless. However, dot-blot results show that a certain amount of mitochondria or cellular compartments that might include mitochondria or mitochondrial fragments is present within the foam. This also raises the question about structural damage due to the huge air exposure in the foam. For optimization the protocol this might need some additional adjustments. Nitrogen cavitation was more effective in reducing the amount of living cells than any other method while no repetitive force was exerted onto a single cell. It should be noted that only two experiments at different pressures (1100 psi and 1500 psi) were performed and no significant difference was observed.



## 6.5 Dounce Homogenisation shows large Variance

The force and amount of strikes of the pestle during homogenisation is the crux of the matter. In the literature the pestle, number of strokes and force exhibited onto the pestle vary greatly and depend heavily on the sample used. While some for example use a combination of pestle and syringe<sup>[42]</sup>, no difference was observed if just the pestle or a combination of pestle and syringe was used in this Master's Thesis. Some groups use only the tight (B) pestle or both (A and B)<sup>[45]</sup> or only the loose pestle (A)<sup>[30]</sup>. Different combinations of pestles, forces and strikes were used. The solution which produced the best result made use of the loose pestle (A) with 75 rather harsh strikes but without leaving the solution with the ball-tip of the pestle (no generation of air bubbles between pestle head and the homogenate). Afterwards the homogenate was centrifuged and the pellet loosened up and rehomogenised. It is worth mentioning that the use of the tight (B) pestle seemed to increase the risk of overhomogenisation for differentiated LUHMES cells, although suggested by the producer to be used for the final homogenisation.

## 6.6 PTA vs UA for Negative Stain

During the whole course of experiments the negative stain samples didn't vary much. Since it is impossible to see whole mitochondria with negative stain, due to the structural collapse during drying, this method was used to estimate the amount of cellular debris and possible mitochondrial structures. Indeed, larger amount of debris or larger vesicle (such as possible nuclei) could be seen and gave some information about the homogenisation and the purification by differential centrifugation. To minimize the structural collapse, PTA as negative stain was simultaneously used with UA. However, during most of the time there were staining artefacts from PTA or the stain was extremely dense. However, as seen in figure 21 the structures seem more fuzzy and stable with PTA in comparison to UA. Nevertheless, for the detection of mitochondria the different staining didn't do much difference.

## 6.7 On-Grid labelling shows little Results

The on-grid 5 nm gold labelling seemed somewhat tricky and didn't work most of the time. Some rather fuzzy structures for sonication or the first dounce based homogenisations of differentiated LUHMES cells show a labelling (figures 5 **E** and **F** and 7 **H**). This could indicate that those samples were overhomogenised as expected and the fuzzy structures are burst mitochondria. However, these structures do not look like disrupted mitochondria in fixated samples or show the remnant of a disrupted outer membrane. Additionally the absence of labelling of any other structures, even for later samples with less overhomogenisation, questions the use of this method to label mitochondria. Only labelling with protein A 5 nm Au-beads (figure 21) for a nitrogen cavitation homogenized sample worked and labelled specifically structures that could be mitochondria. It is worth mentioning that during this method often both sides of the grid were incubated (due to the preparation method on droplets) and therefore the staining as well as the sample concentration was dense for some parts. It is also possible that some of the beads were simply not visible although they decorated the sample, since they were either covered by stain or out of focus (on top of the structure). This method may be better suited for smaller vesicles or proteins than for whole mitochondria. The thin mitochondria concentration and large vesicle presence may also be problematic and a reason why no labelled mitochondria structure was found (except for the sample shown in figure 21).

## 6.8 Cryo Electron Microscopy

During the whole course of the project the production of suitable cryo grids was difficult to achieve. Most of the time the ice was too thick and even in the end only some spots were normally accessible. Different methods such as back-side-blotting or use of different grids (quantifoil 3.5/1 or Lacey C) or blotting times (up to 5 s + 2 s after blotting time) didn't show any progress. Although the mannitol presence in the buffer was counterproductive for the contrast of the obtained pictures, other buffer or grid-washing methods before plunging didn't work as anticipated. The best method in the end was developed after a visit of the group of Werner Kühlbrandt at the Max Planck Institute of Biophysics. A freezing buffer with trehalose was used together with Lacey C only 300 mesh Cu grids. The blotting was done manually by gently pressing the blotting paper over half of the grid (to generate a gradient of thickness), waiting until the liquid border on the filter paper stopped and waiting from this moment on another 5 s before plunging.

However, the ice was still mostly too thick but some spots were rather well accessible. It is to remark that the sample seemed from time to time rather sticky, which probably has something to do with cellular debris or leftover DNA, causing some kind of clustering. Due to the viscosity of the sample the blotting could get too inefficient, resulting in too thick ice. Additionally, healthy mitochondria can be rather thick and if they appear in a high concentration it is possible for them to block the electron beam and let the grid appear black. However, due to the low concentration of mitochondria in the samples presented in this Master's Thesis, it is doubtful that this was the reason. The low mitochondria concentration was also the reason why the sample was not further diluted to minimize the viscosity. Instead repetitive pipetting was used to dissolve the sample as gently as possible. It is also to mention that mitochondria have a tendency to stick to the carbon, making it even more difficult to find them in ice, which was another reason to employ Lacey grids.

## 6.9 Membrane Potential and Mitochondria Viability

Interestingly, one can see the drop of membrane potential as soon as the mitochondria are isolated in figure 9. MitoTracker orange is accumulated in the mitochondrial membrane due to its negative charge. Subsequently to a drop of the membrane potential, the attraction of MitoTracker to the mitochondria drops as well. As seen in figure 9 the mitochondria isolated do not glow as bright as the one still assembled in the dying cells or at places where the cells just burst (cytoplasmic environment). This has on one hand to do with the faster movement of free mitochondria but also show a decreased affinity of MitoTracker orange, most likely due to the membrane potential drop.

Nevertheless, since the MitoTracker is still visible in the crude mitochondria pellets, the mitochondria have to be relatively healthy. These observations are supported by the fixated samples (figures 12 and 15) where isolated mitochondria look more swollen or even disrupted than the ones in cytoplasmic environment. Additionally the cristae of the mitochondria seem to be rather disordered. This picture of reduced viability and disturbed structure can either be caused by the fixation process or by the isolation of the mitochondria.



The superstructures shown in cryo EM for figure 16 look similar to the swollen mitochondria. However, the cristae look fairly composed and the mitochondria appear to be healthier than the isolated specimens in the fixated sample. This is also supported by comparison with the literature (see figure 25). The cristae in the cryo EM results of figure 16 are parallel and not chaotic, like shown in figure 25 **B** and **C**. Although the mitochondria of the sample shown in figure 16 seem to cluster sometimes (**E**), which is likely a cause of the centrifugation of the crude mitochondria pellet, the cristae structure does not show strong sign of formation of circular compartments (as seen for the isolated mitochondria in fixative, shown in figure 12 or mentioned by Brandt et al. (2017)<sup>[30]</sup>) or chaotic structures in general. Therefore those isolated mitochondria seem rather healthy, although the cristae in comparison with the literature look a bit swollen. For the mitochondria from nitrogen cavitation (figures 19 and 22) a conclusion from the superstructure on the health of the mitochondria is more difficult to draw, especially since the inner membrane is not well visible.

Interestingly, the fixation of the samples shown in figures 17 and 23 show a strong resemblance. Compared to literature results of isolated mitochondria they do not resemble the ones found by Kristian et al. (2016)<sup>[49]</sup> for neurons and astrocytes isolated by nitrogen cavitation, which are more like the swollen ones shown in figures 12 or 15. However they do resemble the structures shown by Franko et al. (2013)<sup>[53]</sup> for isolated heart and brain mitochondria from mice. Since a slightly different method was used for fixation of the two samples shown in figures 17 and 23 than in figures 12 and 15, a difference in the observed mitochondria structure is possible, which is based on the fixation protocol. On the other hand the difference in the used buffers could have better preserved the structure of the mitochondria. Structural damage as shown in the figures (as disrupted mitochondria structures) are also found in results from Kristian et al. (2016)<sup>[49]</sup>, who also used nitrogen cavitation. These damages can come either from the process of homogenization or from the fixation of the sample. However, since the cryo results shown in figure 22 **D** also shows a similar local swelling as the structures shown in figure 23 **C** for the fixated sample, a damaging during the process of isolation seem at least for some part of the damaging responsible. The results show also a considerable amount of contamination of other lipid structures.

## 6.10 Magnetic Bead Isolation

The Isolation with magnetic beads did not work as planned. The homogenate formed a plug in the capillary and upon releasing a meshwork of membranes and vesicles was shown, however, no separation of mitochondria took place. The used setup however was not designed for such big samples, but more for separating proteins from a solution. Therefore the method itself, which was also used by Franco et al. (2013)<sup>[53]</sup> or in the isolation kit of invitrogen/Dynal, may work, but not with this magnet bead protein isolation setup.

## 7 Conclusion

Over the course of experiments two different methods to isolate mitochondria from differentiated LUHMES were developed. One method by using around 75 rather harsh strikes with the loose (A) pestle of a dounce homogenizer and differential centrifugation, as shown in figure 24, and another by nitrogen cavitation at different pressures. After several adjustments of the original protocol of Wieckowski et al. (2009)<sup>[46]</sup> over the course of experiments (including pestle usage, centrifugation force and buffers) cryo EM pictures showing mitochondrial structures were obtained in the end. Variable application of the pestle in terms of force and numbers of strikes generated slightly different results, whereas too many strikes led to overhomogenisation and too less force was not able to completely disrupt the cells or demanded a higher amount of strikes, increasing the risk of overhomogenisation. Although the tight pestle is recommended for final homogenisation, the best results were obtained for differentiated LUHMES cells by only using the loose pestle. The presence of mitochondria within the crude mitochondria sample was also verified by dot-blot against VDAC and MitoTracker orange.

Nitrogen cavitation led to a great amount of foam, which held some mitochondria or cellular compartment but didn't interfere to much with the final result. With this method a slightly different form of mitochondria were obtained. Nitrogen cavitation was by far the most efficient method of reducing the amount of living cells without increasing the risk of overhomogenisation. Potter-Elvehjem and sonication based homogenisation on the other hand yield a too high risk of overhomogenisation, be it due to the force used (sonicating damaged cells rather quickly) or number of strikes used (Potter-Elvehjem homogenizer).

Differentiated LUHMES were proven to be generally tougher than undifferentiated cells or HEK 293FT cells. A bigger amount of cells would have made the purification considerably easier and would have allowed an additional purification by Percoll gradient centrifugation. But the amount of the crude mitochondria sample at hand was too low to apply these methode. The obtained results for mitochondrial strcuture are in agreement with the literature, however, the results showed a drop in membrane potential as well as swelling and structural abnormalities of the mitochondria upon isolation. Therefore further adjustments of buffer and method may be needed.

The generation of cryo EM grids turned out to be rather troublesome, since the ice was most of the time too thick and the samples had a rather low concentration of mitochondria. This is on one part due to the viscosity of the sample and on the other hand due to the thickness of certain structures.

Although negative staining was used to estimate the cellular debris and amount of potential mitochondria like structures, the method was not directly applicable to recognize them. Additional on-grid 5 nm Au-bead labelling against VDAC was also not able to reliably identify mitochondria-like structures or such structures were not found or marked due to the low concentration of mitochondria within the crude mitochondria sample or the labelling method.

## 8 Outlook

With the two protocols to obtain crude mitochondria fractions from differentiated LUHMES cells further experiments and optimizations can be conducted. The nitrogen cavitation approach can be further investigated to optimize the settings and obtaining a more uniform protocol, since the two experiments shown in this thesis differ significantly in terms of pressure used (1100 psi or 1500 psi), buffers used (IB and MRB or IBs and MRBs) and differential centrifugation afterwards (different steps and g-forces).

A larger amount of cells can be purified by following the protocols, especially for the dounce homogenizer. With a larger amount of crude mitochondria fraction it should be easier to find mitochondria in cryo EM. At the same time further purification of the sample using a discontinuous Percoll gradient can be preformed. According to fixation results of the best obtained samples in this thesis, a considerable amount of contamination is still present in the crude mitochondria sample, therefore an additional purification is advisable. However, the use of a continuous Percoll gradient seemed rather unusual for the protocol used in this thesis. Therefore a discontinuous Percoll gradient as already used by different groups [45][49][50][51] and upon recommendation of Niklas Klusch from the Max Plank Institute of Biophysics would be the better choice.

Further the viability of the isolated mitochondria can be investigated in detail using either a clark type oxygen electrode as suggested by different groups [27][30][45][49][50][53][56][57] or the membrane potential sensitive dye TMRE as suggested by Lampl et al. (2013)[42] or TMRM as suggested by Nakamura et al. (2011)[14], which both work in a similar way as the MitoTracker orange. With these results the protocol can be further optimized.

Additionally, the total amount of mitochondria in the purified solution can be determined using either a Biuret[27] or the more sensitive Lowry based assay. [49][55] Furthermore, cryo tomography can be conducted to gain more insight about the structure of the isolated LUHMES mitochondria.[40]

Aside from the possible outlook concerning the pure mitochondria isolated from differentiated LUHMES cells, superstructure interaction experiments of the isolated mitochondria with  $\alpha$ -Syn oligomers or fibrils can be conducted. These experiment would give further insight about the influence of  $\alpha$ -Syn on the structure of substantia nigra like mitochondria in the absence of other cellular interactions. Also the possible formation of  $\alpha$ -Syn oligomers upon mitochondrial death, as suggested by Kumar et al. (2016)[18] can be mimicked by the addition of neurotoxins like MPP<sup>+</sup> to a  $\alpha$ -Syn monomer isolated mitochondria solution.

## References

- [1] Ana Navarro, Alberto Boveris, Manuel J. Báñez, María Jesús Sánchez-Pino, Carmen Gómez, Gerard Muntané, and Isidro Ferrer. Human brain cortex: mitochondrial oxidative damage and adaptive response in Parkinson disease and in dementia with Lewy bodies. *Free Radical Biology and Medicine*, 46(12):1574–1580, June 2009.
- [2] P. Blin, C. Dureau-Pournin, A. Foubert-Samier, A. Grolleau, E. Corbillon, J. Jové, R. Lassalle, P. Robinson, N. Poutignat, C. Droz-Perroteau, and N. Moore. Parkinson's disease incidence and prevalence assessment in France using the national healthcare insurance database. *European Journal of Neurology*, 22(3):464–471, March 2015.
- [3] O. Riedel, D. Bitters, U. Amann, E. Garbe, and I. Langner. Estimating the prevalence of Parkinson's disease (PD) and proportions of patients with associated dementia and depression among the older adults based on secondary claims data: Estimating the epidemiology of PD with secondary data. *International Journal of Geriatric Psychiatry*, 31(8):938–943, August 2016.
- [4] Ole-Bjørn Tysnes and Anette Storstein. Epidemiology of Parkinson's disease. *Journal of Neural Transmission*, 124(8):901–905, August 2017.
- [5] M. Nerius, A. Fink, and G. Doblhammer. Parkinson's disease in Germany: prevalence and incidence based on health claims data. *Acta Neurologica Scandinavica*, 136(5):386–392, November 2017.
- [6] Xiao-min Zhang, Ming Yin, and Min-hua Zhang. Cell-based assays for Parkinson's disease using differentiated human LUHMES cells. *Acta Pharmacologica Sinica*, 35(7):945–956, July 2014.
- [7] Francesca Longhena, Gaia Faustini, Cristina Missale, Marina Pizzi, PierFranco Spano, and Arianna Bellucci. The Contribution of  $\alpha$ -Synuclein Spreading to Parkinson's Disease Synaptopathy. *Neural Plasticity*, 2017:1–15, 2017.
- [8] Kalpita Banerjee, Maitrayee Sinha, Chi Le Lan Pham, Sirsendu Jana, Dalia Chanda, Roberto Cappai, and Sasanka Chakrabarti.  $\alpha$ -Synuclein induced membrane depolarization and loss of phosphorylation capacity of isolated rat brain mitochondria: Implications in Parkinson's disease. *FEBS Letters*, 584(8):1571–1576, April 2010.
- [9] P. M. Keeney. Parkinson's Disease Brain Mitochondrial Complex I Has Oxidatively Damaged Subunits and Is Functionally Impaired and Misassembled. *Journal of Neuroscience*, 26(19):5256–5264, May 2006.
- [10] Miquel Vila, David Ramonet, and Celine Perier. Mitochondrial alterations in Parkinson's disease: new clues: Mitochondrial alterations in Parkinson's disease. *Journal of Neurochemistry*, 107(2):317–328, August 2008.
- [11] H. Mori, T. Kondo, M. Yokochi, H. Matsumine, Y. Nakagawa-Hattori, T. Miyake, K. Suda, and Y. Mizuno. Pathologic and biochemical studies of juvenile parkinsonism linked to chromosome 6q. *Neurology*, 51(3):890–892, September 1998.
- [12] Ken Nakamura.  $\alpha$ -Synuclein and Mitochondria: Partners in Crime? *Neurotherapeutics*, 10(3):391–399, July 2013.

- [13] Stefan Schildknecht. Generation of genetically-modified human differentiated cells for toxicological tests and the study of neurodegenerative diseases. *ALTEX*, 30(4):427–444, 2013.
- [14] Ken Nakamura, Venu M. Nemani, Farnaz Azarbal, Gaia Skibinski, Jon M. Levy, Kiyoshi Egami, Larissa Munishkina, Jue Zhang, Brooke Gardner, Junko Wakabayashi, Hiromi Sesaki, Yifan Cheng, Steven Finkbeiner, Robert L. Nussbaum, Eliezer Masliah, and Robert H. Edwards. Direct Membrane Association Drives Mitochondrial Fission by the Parkinson Disease-associated Protein  $\alpha$ -Synuclein. *Journal of Biological Chemistry*, 286(23):20710–20726, June 2011.
- [15] M. H. Polymeropoulos. Mutation in the -Synuclein Gene Identified in Families with Parkinson’s Disease. *Science*, 276(5321):2045–2047, June 1997.
- [16] M. H. R. Ludtmann, P. R. Angelova, N. N. Ninkina, S. Gandhi, V. L. Buchman, and A. Y. Abramov. Monomeric Alpha-Synuclein Exerts a Physiological Role on Brain ATP Synthase. *Journal of Neuroscience*, 36(41):10510–10521, October 2016.
- [17] Tatiana K. Rostovtseva, Philip A. Gurnev, Olga Protchenko, David P. Hoogerheide, Thai Leong Yap, Caroline C. Philpott, Jennifer C. Lee, and Sergey M. Bezrukov.  $\alpha$ -Synuclein Shows High Affinity Interaction with Voltage-dependent Anion Channel, Suggesting Mechanisms of Mitochondrial Regulation and Toxicity in Parkinson Disease. *Journal of Biological Chemistry*, 290(30):18467–18477, July 2015.
- [18] Ashutosh Kumar, Douglas Ganini, and Ronald P. Mason. Role of cytochrome c in  $\alpha$ -synuclein radical formation: implications of  $\alpha$ -synuclein in neuronal death in Maneb- and paraquat-induced model of Parkinson’s disease. *Molecular Neurodegeneration*, 11(1), December 2016.
- [19] Stefanie Menges, Georgia Minakaki, Patrick M. Schaefer, Holger Meixner, Iryna Prots, Ursula Schlötzer-Schrehardt, Kristina Friedland, Beate Winner, Tiago F. Outeiro, Konstanze F. Winklhofer, Christine A. F. von Arnim, Wei Xiang, Jürgen Winkler, and Jochen Klucken. Alpha-synuclein prevents the formation of spherical mitochondria and apoptosis under oxidative stress. *Scientific Reports*, 7:42942, February 2017.
- [20] David S. Cassarino, Janice K. Parks, W.Davis Parker, and James P. Bennett. The parkinsonian neurotoxin MPP<sup>+</sup> opens the mitochondrial permeability transition pore and releases cytochrome c in isolated mitochondria via an oxidative mechanism. *Biochimica et Biophysica Acta (BBA) - Molecular Basis of Disease*, 1453(1):49–62, January 1999.
- [21] J.Timothy Greenamyre, Ranjita Betarbet, and Todd B Sherer. The rotenone model of Parkinson’s disease: genes, environment and mitochondria. *Parkinsonism & Related Disorders*, 9:59–64, August 2003.
- [22] T. P. Singer, R. R. Ramsay, K. McKeown, A. Trevor, and N. E. Castagnoli. Mechanism of the neurotoxicity of 1-methyl-4-phenylpyridinium (MPP<sup>+</sup>), the toxic bioactivation product of 1-methyl-4-phenyl-1,2,3,6-tetrahydropyridine (MPTP). *Toxicology*, 49(1):17–23, April 1988.
- [23] Julie Lotharius and Karen L. O’Malley. The Parkinsonism-inducing Drug 1-Methyl-4-phenylpyridinium Triggers Intracellular Dopamine Oxidation: A NOVEL MECHANISM OF TOXICITY. *Journal of Biological Chemistry*, 275(49):38581–38588, December 2000.
- [24] Mauro Degli Esposti. Inhibitors of NADH-ubiquinone reductase: an overview. *Biochimica et Biophysica Acta (BBA) - Bioenergetics*, 1364(2):222–235, May 1998.

- [25] Ranjita Betarbet, Todd B. Sherer, Gillian MacKenzie, Monica Garcia-Osuna, Alexander V. Panov, and J. Timothy Greenamyre. Chronic systemic pesticide exposure reproduces features of Parkinson's disease. *Nature Neuroscience*, 3(12):1301–1306, December 2000.
- [26] Andreas Bender, Kim J Krishnan, Christopher M Morris, Geoffrey A Taylor, Amy K Reeve, Robert H Perry, Evelyn Jaros, Joshua S Hersheson, Joanne Betts, Thomas Klopstock, Robert W Taylor, and Douglass M Turnbull. High levels of mitochondrial DNA deletions in substantia nigra neurons in aging and Parkinson disease. *Nature Genetics*, 38(5):515–517, May 2006.
- [27] Christian Frezza, Sara Cipolat, and Luca Scorrano. Organelle isolation: functional mitochondria from mouse liver, muscle and cultured fibroblasts. *Nature Protocols*, 2(2):287–295, February 2007.
- [28] T.H. Sanderson, S. Raghunayakula, and R. Kumar. Neuronal hypoxia disrupts mitochondrial fusion. *Neuroscience*, 301:71–78, August 2015.
- [29] Douglas C. Wallace. A Mitochondrial Paradigm of Metabolic and Degenerative Diseases, Aging, and Cancer: A Dawn for Evolutionary Medicine. *Annual Review of Genetics*, 39(1):359–407, December 2005.
- [30] Tobias Brandt, Arnaud Mourier, Luke S Tain, Linda Partridge, Nils-Göran Larsson, and Werner Kühlbrandt. Changes of mitochondrial ultrastructure and function during ageing in mice and *Drosophila*. *eLife*, 6, July 2017.
- [31] M. Gu, J. M. Cooper, J. W. Taanman, and A. H. V. Schapira. Mitochondrial DNA transmission of the mitochondrial defect in Parkinson's disease. *Annals of Neurology*, 44(2):177–186, August 1998.
- [32] Patricia A. Trimmer, M. Kathleen Borland, Paula M. Keeney, James P. Bennett, and W. Davis Parker. Parkinson's disease transgenic mitochondrial cybrids generate Lewy inclusion bodies: Lewy inclusions in PD cybrids. *Journal of Neurochemistry*, 88(4):800–812, January 2004.
- [33] Wen-Wei Li, Ru Yang, Jing-Chun Guo, Hui-Min Ren, Xi-Liang Zha, Jie-Shi Cheng, and Ding-Fang Cai. Localization of  $\alpha$ -synuclein to mitochondria within midbrain of mice. page 4, 2007.
- [34] Latha Devi, Vijayendran Raghavendran, Badanavalu M. Prabhu, Narayan G. Avadhani, and Hindupur K. Anandatheerthavarada. Mitochondrial Import and Accumulation of  $\alpha$ -Synuclein Impair Complex I in Human Dopaminergic Neuronal Cultures and Parkinson Disease Brain. *Journal of Biological Chemistry*, 283(14):9089–9100, April 2008.
- [35] Candace M. Pfeifferkorn, Zhiping Jiang, and Jennifer C. Lee. Biophysics of  $\alpha$ -synuclein membrane interactions. *Biochimica et Biophysica Acta (BBA) - Biomembranes*, 1818(2):162–171, February 2012.
- [36] William Dauer, Nikolai Kholodilov, Miquel Vila, Anne-Cecile Trillat, Rose Goodchild, Kristin E. Larsen, Roland Staal, Kim Tieu, Yvonne Schmitz, Chao Annie Yuan, Marcelo Rocha, Vernice Jackson-Lewis, Steven Hersch, David Sulzer, Serge Przedborski, Robert Burke, and Rene Hen. Resistance of  $\alpha$ -synuclein null mice to the parkinsonian neurotoxin MPTP. *Proceedings of the National Academy of Sciences*, 99(22):14524–14529, October 2002.

- [37] Peter Klivenyi, Donald Siwek, Gabrielle Gardian, Lichuan Yang, Anatoly Starkov, Carine Cleren, Robert J. Ferrante, Neil W. Kowall, Asa Abeliovich, and M. Flint Beal. Mice lacking alpha-synuclein are resistant to mitochondrial toxins. *Neurobiology of Disease*, 21(3):541–548, March 2006.
- [38] Hsiuchen Chen, J. Michael McCaffery, and David C. Chan. Mitochondrial Fusion Protects against Neurodegeneration in the Cerebellum. *Cell*, 130(3):548–562, August 2007.
- [39] L. J. Martin. Parkinson’s Disease -Synuclein Transgenic Mice Develop Neuronal Mitochondrial Degeneration and Cell Death. *Journal of Neuroscience*, 26(1):41–50, January 2006.
- [40] K. M. Davies, C. Anselmi, I. Wittig, J. D. Faraldo-Gomez, and W. Kuhlbrandt. Structure of the yeast F1Fo-ATP synthase dimer and its role in shaping the mitochondrial cristae. *Proceedings of the National Academy of Sciences*, 109(34):13602–13607, August 2012.
- [41] Herman van der Putten, Karl-Heinz Wiederhold, Alphonse Probst, Samuel Barbieri, Claudia Mistl, Simone Danner, Sabine Kauffmann, Katja Hofele, Will P. J. M. Spooren, Markus A. Ruegg, Shuo Lin, Pico Caroni, Bernd Sommer, Markus Tolnay, and Graeme Bilbe. Neuropathology in Mice Expressing Human  $\alpha$ -Synuclein. *Journal of Neuroscience*, 20(16):6021–6029, August 2000.
- [42] Thomas Lampl, Jo A. Crum, Taylor A. Davis, Carol Milligan, and Victoria Del Gaizo Moore. Isolation and Functional Analysis of Mitochondria from Cultured Cells and Mouse Tissue. *Journal of Visualized Experiments*, (97), March 2015.
- [43] Andrey V Kuznetsov, Vladimir Veksler, Frank N Gellerich, Valdus Saks, Raimund Margreiter, and Wolfram S Kunz. Analysis of mitochondrial function in situ in permeabilized muscle fibers, tissues and cells. *Nature Protocols*, 3(6):965–976, June 2008.
- [44] Hue-Tran Hornig-Do, Gritt Günther, Maria Bust, Patricia Lehnartz, Andreas Bosio, and Rudolf J. Wiesner. Isolation of functional pure mitochondria by superparamagnetic microbeads. *Analytical Biochemistry*, 389(1):1–5, June 2009.
- [45] Neil R Sims and Michelle F Anderson. Isolation of mitochondria from rat brain using Percoll density gradient centrifugation. *Nature Protocols*, 3(7):1228–1239, July 2008.
- [46] Mariusz R Wieckowski, Carlotta Giorgi, Magdalena Lebiecinska, Jerzy Duszynski, and Paolo Pinton. Isolation of mitochondria-associated membranes and mitochondria from animal tissues and cells. *Nature Protocols*, 4(11):1582–1590, November 2009.
- [47] Chris Meisinger, Thomas Sommer, and Nikolaus Pfanner. Purification of *Saccharomyces cerevisiae* Mitochondria Devoid of Microsomal and Cytosolic Contaminations. *Analytical Biochemistry*, 287(2):339–342, December 2000.
- [48] Alexander Hahn, Kristian Parey, Maike Bublitz, Deryck J. Mills, Volker Zickermann, Janet Vonck, Werner Kuhlbrandt, and Thomas Meier. Structure of a Complete ATP Synthase Dimer Reveals the Molecular Basis of Inner Mitochondrial Membrane Morphology. *Molecular Cell*, 63(3):445–456, August 2016.
- [49] Tibor Kristián, Irene B. Hopkins, Mary C. McKenna, and Gary Fiskum. Isolation of mitochondria with high respiratory control from primary cultures of neurons and astrocytes using nitrogen cavitation. *Journal of Neuroscience Methods*, 152(1-2):136–143, April 2006.

- [50] Maile R. Brown, Patrick G. Sullivan, and James W. Geddes. Synaptic Mitochondria Are More Susceptible to  $\text{Ca}^{2+}$  Overload than Nonsynaptic Mitochondria. *Journal of Biological Chemistry*, 281(17):11658–11668, April 2006.
- [51] Brian Storrie and Edward Amadden. [16] Isolation of subcellular organelles. In Murray P. Deutscher, editor, *Methods in Enzymology*, volume 182 of *Guide to Protein Purification*, pages 203–225. Academic Press, January 1990.
- [52] Vicki AM Gold, Piotr Chroscicki, Piotr Bragoszewski, and Agnieszka Chacinska. Visualization of cytosolic ribosomes on the surface of mitochondria by electron cryo-tomography. *EMBO reports*, 18(10):1786–1800, October 2017.
- [53] Andras Franko, Olivier R. Baris, Eva Bergschneider, Christine von Toerne, Stefanie M. Hauck, Michaela Aichler, Axel K. Walch, Wolfgang Wurst, Rudolf J. Wiesner, Ian C. D. Johnston, and Martin Hrabě de Angelis. Efficient Isolation of Pure and Functional Mitochondria from Mouse Tissues Using Automated Tissue Disruption and Enrichment with Anti-TOM22 Magnetic Beads. *PLoS ONE*, 8(12):e82392, December 2013.
- [54] Pavel F Pavlov, Charlotta Rudhe, Shashi Bhushan, and Elzbieta Glaser. In Vitro and In Vivo Protein Import Into Plant Mitochondria. page 18.
- [55] Pedram Azimzadeh, Hamid Asadzadeh Aghdaei, Peyman Tarban, and Mohammad Mahdi Akhondi. Comparison of three methods for mitochondria isolation from the human liver cell line (HepG2). page 9, 2016.
- [56] Roberta A. Gottlieb and Souichi Adachi. Nitrogen Cavitation for Cell Disruption to Obtain Mitochondria from Cultured Cells. In *Methods in Enzymology*, volume 322, pages 213–221. Elsevier, 2000.
- [57] Vera S. Gross, Heather K. Greenberg, Sergei V. Baranov, Greta M. Carlson, Irina G. Stavrovskaya, Alexander V. Lazarev, and Bruce S. Kristal. Isolation of functional mitochondria from rat kidney and skeletal muscle without manual homogenization. *Analytical Biochemistry*, 418(2):213–223, November 2011.





## Erklärung zur wissenschaftlichen Redlichkeit

(beinhaltet Erklärung zu Plagiat und Betrug)

~~Bachelorarbeit~~ / Masterarbeit (nicht Zutreffendes bitte streichen)

Titel der Arbeit (Druckschrift):

Structural Analysis of Mitochondria in the Context of Parkinson's Disease

Name, Vorname (Druckschrift): Lattner, Patrick

Matrikelnummer: 11-061-090

Hiermit erkläre ich, dass mir bei der Abfassung dieser Arbeit nur die darin angegebene Hilfe zuteil wurde und dass ich sie nur mit den in der Arbeit angegebenen Hilfsmitteln verfasst habe.

Ich habe sämtliche verwendeten Quellen erwähnt und gemäss anerkannten wissenschaftlichen Regeln zitiert.

Diese Erklärung wird ergänzt durch eine separat abgeschlossene Vereinbarung bezüglich der Veröffentlichung oder öffentlichen Zugänglichkeit dieser Arbeit.

☐ ja ☒ nein

Ort, Datum: Ormingen, 30.04.2018

Unterschrift:

Dieses Blatt ist in die Bachelor-, resp. Masterarbeit einzufügen.

# CIRRICULUM VITAE

---

**Patrick Lattner**

---

Address: Zuzgerstrasse 10, 4463 Buus  
Telephone: +41 (0)61 843 94 90  
Mobile: +41 (0)79 664 58 71  
E-mail: patrick.lattner@stud.unibas.ch

---



---

**Education:**

---

08/2007 – 12/2010 grammar school Liestal: Matura profile B biology/chemistry  
08/2011 – 07/2015 Bachelor of Science in Nanosciences (B Sc), University Basel

---

---

**Military Education:**

---

03/2011 – 04/2011 Rekrutenschule 50-1, Lyss  
04/2011 – 06/2011 Atomic biological und chemical defence (ABC) Unteroffiziersschule 58-1, Spiez  
06/2011 Promotion to corporal ABC defence force

---

---

**Professional Experience:**

---

10/2016 – 02/2017 University Basel, Biozentrum, Roderick Lims group, project work: „Complex formation of the nuclear pore membrane proteins Pom121 and Ndc1, proteoliposome formation and nuclear transport receptor binding capability“, investigating the two trans-membrane proteins Pom121 and Ndc1 by using in vitro assays based on proteoliposomes to gain further insight in the pre-pore formation of nuclear pore complexes (NPCs). Methods used for detection: Fluorescence correlation spectroscopy, transmission electron microscopy and immunoblotting (western).  
02/2016 – 08/2016 University Basel, department of Physics, Nanolino group, project work: „Formation and analysis of nanostructures by unbalanced magnetron sputtering“, manufacturing of spike like nano structures on metal surfaces to generate an auto sterile surface (based on obtained results now currently in work with Straumann company)  
07/2010 – 08/2010 Bau- und Verkehrsdepartement Basel Stadt, temporary job as city-gardener

---

---

**Languages:**

---

German: native language  
English: written and verbal good  
French: basic knowledge

---

---

**Special Abilities:**

---

- youth leader; reformierte Kirchgemeinde Buus-Maisprach
- Rotary youth leadership awards (RYLA)
- Atomic biological und chemical defence corporal of the swiss army
- course Businessplan, Business Model Canvas und Co. professionell gemacht; Business Tools AG

---

**Hobbies:**

---

travelling, judo, brewing mead (honey wine) and berry wine, drawing, cooking, photography

---

**References:**

---

Prof. Ernst Meyer	Head of the Nanolino group Department of Physics, university Basel ernst.meyer@unibas.ch Tel +41 (0)61 267 37 24
Dr. Laurent Marot	Postdoc, PhD in physics Department of Physics, university Basel laurent.marot@unibas.ch Tel +41 (0)61 267 37 20
Lucas Moser	PhD student, Master in physics Department of Physics, university Basel lucas.moser@unibas.ch Tel +41 (0)61 267 27 25
Simon Leuenberger	Leiter Kreis Kleinbasel Str. Leiter Abt. Grünflächenunterhalt Stadtgärtnerei Basel Stadt simon.leuenberger@bs.ch Tel +41 (0)61 695 91 01
Radhakrishnan Panatala	Postdoc, PhD in biology Biozentrum, university Basel r.panatala@unibas.ch Tel +41 (0)61 207 22 60